Thermo-Hydro-Mechanical properties of MX-80

Results from advanced laboratory tests

Ann Dueck and Ulf Nilsson, Clay Technology AB

December 2010

SKB

Thermo-Hydro-Mechanical properties of MX-80

Results from advanced laboratory tests

Ann Dueck and Ulf Nilsson, Clay Technology AB

December 2010

Abstract

General

Highly compacted bentonite is proposed as the buffer material in the Swedish concept for disposal of nuclear waste. The saturated homogenized bentonite is expected to fully act as a buffer material between the waste canister and the surrounding bedrock. Material models describing the thermo-hydro-mechanical (THM) behaviour of the buffer material have been created with the purpose to simulate and predict the behaviour in a repository both before and after water saturation. The material models of water saturated and water unsaturated buffer material are complicated and contain a number of parameters that need to be determined.

The present report is a compilation of results concerning thermo-hydro-mechanical laboratory tests on saturated and unsaturated buffer material. The main purpose of the report is to supply modelling groups with available results for improving models and determine parameters that can be used for the THM modelling of the behaviour of the buffer.

Retention curves

The relation between water content and relative humidity has been determined in a number of test series for some specific conditions, e.g. different initial water contents. Two methods have been used; the sorption balance method and a method with jars as desiccators. The majority of the results were derived from tests where *RH* was controlled and the response of the bentonite samples was measured. The results are given as water content versus relative humidity in diagrams and in tabular form.

Volume change

The volume change of water unsaturated bentonite specimens has been investigated by compression tests and swelling/shrinkage tests for some specific stress and moisture paths. The constant relative humidity was generated by the vapour equilibrium technique combined with an air circulation system. Measured stresses, deformation and relative humidity are presented versus time in diagrams and the final values at different stages are also presented in tabular form.

Moisture transport

The moisture transport in bentonite specimens has been investigated in tests where specimens with different initial states were exposed to different gradients of *RH* and where the corresponding gradients of water content, at transient conditions, were determined. The constant relative humidity was generated by the vapour equilibrium technique combined with an air circulation system. The results are presented, in diagrams and in tabular form, as gradients of relative humidity and corresponding gradients of water content. The axial stresses are also presented.

Moisture redistribution

Redistribution of moisture was investigated by studying unsaturated specimens exposed to temperature gradients under constant volume conditions and without supply of additional water.

The results are given in diagrams as gradients in water content, density, void ratio and degree of saturation. The gradients are given both as absolute values and normalized values. For modelling purpose the resulting gradients in water content and density are also given as changes from the initial state.

Triaxial tests

Two triaxial tests were run on water saturated bentonite specimens. Since the influence of stress history was studied, the results in terms of effective average stress and deviator stress are compared to results from previous published tests.

Sammanfattning

Allmänt

Högkompakterad bentonit har föreslagits som buffertmaterial i det svenska konceptet för slutförvar av använt kärnbränsle. Den vattenmättade homogeniserade bentoniten förväntas verka som en buffert mellan kapseln med det använda kärnbränslet och det omgivande berget. Materialmodeller som beskriver buffertmaterialets termohydromekaniska (THM) uppförande har tagits fram för att kunna simulera och prediktera uppförandet både före och efter vattenmättnad. Materialmodellerna av vattenmättat och vatten-omättat buffertmaterial är komplicerade och innehåller ett antal parametrar som måste bestämmas.

Denna rapport är en sammanställning av resultat från termohydromekaniska laboratorieförsök på mättat och omättat buffertmaterial. Huvudsyftet med rapporten är att förse modelleringsgrupper med användbara resultat som kan användas för att förbättra modellerna och bestämma parametrar som kan användas för THM modellering av buffertens uppförande.

Vattenhållningskurvor

Relationen mellan vattenkvot och relativ fuktighet har bestämts i ett antal försöksserier för några speci-fika förhållanden t.ex. olika initialvattenkvoter. Två metoder har använts för bestämningen; en metod med sorptionsvåg och en metod med glasburkar. Majoriteten av resultaten kommer från försök där *RH* hållits konstant och responsen hos bentoniten mäts. Resultatet ges som vattenkvot mot relativ fuktighet i både diagram- och tabellform.

Volymförändring

Volymförändringen hos vattenomättade bentonitprover har undersökts med kompressionsförsök och svällning/krympningsförsök för några specifika spännings- och fuktvägar. Konstant relativ fuktighet har genererats genom att cirkulera luft, med ett bestämt ångtryck från jämvikt med olika saltlösningar, genom provutrustningen och därmed förbi proverna. Uppmätta spänningar, deformationer och relativ fuktighet presenteras mot tid i diagramform och slutvärden för de olika stegen presenteras även i tabellform.

Fukttransport

Fukttransporten i bentonitprover har undersökts med försök där prover med olika initialtillstånd har exponerats för olika gradienter i relativ fuktighet och där motsvarande gradienter i vattenkvot, under transienta förhållanden, mäts upp. Konstant relativ fuktighet har genererats genom att cirkulera luft, med ett bestämt ångtryck från jämvikt med olika salt lösningar, förbi provernas ändytor. Resultatet presenteras i diagram- och tabellform som gradienter i relativ fuktighet med tillhörande gradienter i vattenkvot. De axiella spänningarna presenteras också.

Omfördelning av fukt

Omfördelning av fukt har undersökts genom att utsätta omättade bentonitprover för en temperaturgradient då volymen hållits konstant och då inget ytterligare vatten varit tillgängligt. Resultatet ges i diagram-form som gradienter i vattenkvot, densitet, portal och vattenmättnadsgrad. Gradienterna ges både som absolutvärden och normaliserade värden och för att underlätta jämförelser med modelleringsresultat ges resultatet även som ändringar från initialtillståndet.

Triaxialförsök

Två triaxialförsök har utförts på vattenmättade prover. För att studera inverkan av spänningshistoria har resultatet i termer av medelspänning och deviatorspänning jämförts med tidigare publicerade försöksresultat.

Contents

1 Introduction

1.1 General

The present report is a compilation of results concerning thermo-hydro-mechanical laboratory tests on saturated and unsaturated bentonite buffer material. The main purpose is to supply modelling groups with available results for improving models and determine parameters that can be used for the thermo-hydro-mechanical (THM) modelling of the behaviour of the buffer in the Swedish concept for disposal of nuclear waste.

1.2 Background

Highly compacted bentonite is proposed as the buffer material in the Swedish concept for disposal of nuclear waste. The saturated homogenized bentonite is expected to fully act as a buffer material. Material models describing the thermo-hydro-mechanical behaviour of the buffer have been created with the purpose to simulate and predict the behaviour in a repository both before and after water saturation. The material models of saturated and unsaturated buffer are complicated and contain a number of parameters that need to be determined. For this reason a number of advanced laboratory tests to determine such parameters have been performed and are described in this report.

1.3 Content of the report

The main part of the laboratory study was performed during 2005–2007 and is reported here as a part of a continuous work concerning the behaviour of unsaturated bentonite. This part of the study is a continuation of the laboratory study presented by Dueck (2004) where some of the tests performed in the present study were initiated. These laboratory tests concern retention curves, volume change properties and moisture transport.

Test series concerning water redistribution in unsaturated specimens due to temperature gradients were performed during 2009. These tests are a continuation of tests presented by Börgesson (2001).

A limited series of triaxial tests on saturated specimens was performed before 1999 in a project concerning influence of stress paths and time. These triaxial test results are also presented.

The detailed results are presented in the appendices.

2 Material and base variables

2.1 Material

The buffer material used for the tests is a sodium dominated bentonite known as MX-80. MX-80 is the quality symbol of a bentonite from Wyoming, which is commercially produced by American Colloid Co. Mineralogy and sealing properties of MX-80 were reported by Karnland et al. (2006).

The water content of MX-80 under laboratory conditions is about 10%. Higher water content was achieved by mixing the bentonite and the required amount of de-ionized water. The water mixed bentonite was homogenized for at least 24 hours in closed containers before testing.

A particle density of $\rho_s = 2.78$ Mg/m^3 and a water density of $\rho_w = 1.0$ Mg/m^3 were used for evaluation of void ratio and degree of saturation from measured variables (see e.g. Börgesson et al. 1988 and 1995).

2.2 Base variables

2.2.1 Water content and bulk density

The base variables water content w, void ratio e and degree of saturation S_r were determined according to Equations 2-1 to 2-3 where ρ is the bulk density, m_{tot} is the total weight and m_s is the dry mass of a sample.

$$w = \frac{m_{tot} - m_s}{m_s} \ (\%) \qquad\qquad (2\text{-}1)$$

$$e = \frac{\rho_s}{\rho}(1 + w/100) - 1 \qquad\qquad (2\text{-}2)$$

$$S_r = \frac{\rho_s \cdot w}{\rho_w \cdot e} (\%) \qquad\qquad (2\text{-}3)$$

The dry mass was obtained from drying the wet sample at 105°C for 24 h. The density was calculated from the total mass of the sample and a volume determined by weighing the sample above and submerged into paraffin oil. The dry density was calculated from w and ρ.

2.2.2 Relative humidity and suction

The relative humidity RH was measured by capacitive sensors. The sensors were calibrated above saturated salt solutions attached to a calibrator. The calibrator was also used for the measurement of RH above bentonite samples.

The relative humidity is defined according to Equation 2-4. From the relative humidity, the corresponding suction can be determined according to Equation 2-5 (Fredlund and Rahardjo 1993).

$$RH = 100 \cdot \frac{p}{p_s} (\%) \qquad\qquad (2\text{-}4)$$

where

p = partial pressure of pore-water vapour (kPa)

p_s = saturation pressure of water vapour over a flat surface of pure water at the same temperature (kPa).

$$\psi = -\frac{R \cdot T}{v_{w0} \cdot \omega_v} \ln(\frac{p}{p_s})$$

(2-5)

where

ψ = suction (kPa)

T = absolute temperature (K)

R = universal gas constant (8.31432 J/(mol K))

v_{w0} = specific volume of water ($1/\rho_w$ m³/kg)

ω_v = molecular mass of water vapour (18 kg/kmol).

2.2.3 Stress and strain

The stress on a specimen was calculated from measured load and the area of the piston used for transmitting the load from the specimen to the load cell, cf. Figure 3-17. Both radial and axial load were measured and radial stress P_{radial} and axial stress P_{axial} calculated. The results are also presented as the average stress P_{avr} which is calculated according to Equation 2-6.

$P_{avr} = (P_{axial} + 2 \cdot P_{radial})/3$

(2-6)

Strain was calculated as engineering strain according to Equation 2-7 where Δl is the deformation and l_0 the initial length. The deformation was measured by displacement transducers.

$$\varepsilon = \frac{\Delta l}{l_0} \, (\%)$$

(2-7)

3 Laboratory tests on unsaturated MX-80

3.1 General

Different test types were used in order to study four different properties of unsaturated MX-80. The tests are presented in separate sections. The presentation contains results from measurements of:

- water retention
- volume change
- moisture transport
- moisture redistribution.

3.2 Retention curves

3.2.1 Method and equipment

Retention curves of MX-80 have been investigated and reported by Dueck (2004, 2008) where the important influence of the initial water content was described. Two different methods were used: a method with glass jars as desiccators and a sorption balance. Those two methods were also used in the present study.

The method using glass jars is described by Wadsö et al. (2004). The method involves placing a specimen with the weight of approximately 10 g in a glass jar above the surface of salt solution. The salt solution generates a relative humidity in the jar where the bentonite sample is hanging from the lid of the jar. The specimen is left in the generated relative humidity until equilibrium or almost equilibrium is achieved.

For the sorption balance method, a specimen of approximately 15 mg is used. The specimen is initially dried in nitrogen gas and then exposed to a continuous flow of air with a specified relative humidity. The relative humidity is increased in steps from $RH = 0\%$ to about 95% and then decreased back to 0%. The specimen is placed on a micro balance and weighed continuously. The sorption balance measurements were made by Lars Wadsö at the Division of Building Materials at Lund University.

The retention curve determined with the initial water content of 0% is called the basic retention curve, while curves determined from initial water contents deviating from 0% are called specific retention curves. The continuous curve including both absorption and desorption, starting with $w_{ini} = 0\%$ and determined with a sorption balance is often called the sorption isotherm. The term isotherm is used to emphasise the constant temperature conditions.

3.2.2 Preparation of specimen and test procedure

For the method using jars, one specimen was prepared for each relative humidity. The MX-80 bentonite was prepared at the chosen initial water content. Each specimen was placed in a metal cage inside a jar, which was placed in an oven with constant temperature. At regular intervals the specimen was weighed by hanging it below a balance without removing it from the jar. When the test was finished the water content of each specimen was determined according to Section 2.2.1.

For the sorption balance method one specimen was prepared for the total retention curve including both absorption and desorption. The test started with a dry specimen placed on a micro balance which was weighed continuously at constant temperature.

3.2.3 Test program

The test series performed to determine water retention properties are presented in Table 3-1 and Table 3-2 where the approximate values of the initial water content w_{ini}, temperature T and relative humidity RH used, are shown. The names of each series, written in the first column of the tables, represent *serial number_initial water content_temperature*. Eight test series were conducted with the glass jars and two test series with the sorption balance.

Table 3-1. Test series for the determination of retention curves with glass jars.

Name in Figures	Serial number raw data	Initial water content w_{ini} (%)	Temperature T (°C)	Relative Humidity RH (%)
1_0_20	CT_1_0	0	20[1]±1	11,33,59,75,85,93,98
2_0_53	CT_2_0	0	53±0.1	11,30,51,74,81,93
3_10_20	CT_3_10	10	20[1]±1	11,33,59,75,85,93,98
4_10_53	CT_4_10	10	53±0.1	11,30,51,74,81,93
5_64_20	CT_5_60	64	20[1]±1	0,11,33,59,75,85,93,98
6_64_53	CT_6_60	64	53±0.1	0,11,30,51,74,81,93
7_0_26	CT_7_0	0	26±0.1	0,11,33,57,75,84,93,97
8_0_10	LTH_8_0	0	10±0.2	0,11,33,62,76,87,93,98

[1] Approximate value of room temperature.

Table 3-2. Test series for the determination of retention curves with sorption balance method.

Name in Figures	Initial water content w_{ini} (%)	Temperature T (°C)	Relative Humidity RH (%)
SB_0_20	0	20	0,10,20,30,40,50,60,70,80,90,95
SB_0_53	0	53	0,10,20,30,40,50,60,70,80,90,95

The measurements with glass jars were done at eight different RH (0%, 11%, 33%, 59%, 75%, 85%, 93% and 98% at 20°C) using molecular sieve for 0%, an unsaturated NaCl solution for 93% and saturated salt solutions (LiCl, MgCl$_2$, NaBr, NaCl, KCl, K$_2$SO$_4$) for the others. The relative humidity is represented by values tabulated by Greenspan (1977) or, in the case of unsaturated NaCl solution, calculated from vapour pressures given by Clarke and Glew (1985). All eight RH values were not present in each series. At 53°C $RH = 98\%$ was not used and $RH = 0\%$ was only used in the series with an initial water content of 64% and in the series at 26°C and 10°C.

3.2.4 Test results

The resulting retention curves are presented below. Figure 3-1 to Figure 3-3 show results at 20°C and Figure 3-4 to Figure 3-8 show results at other temperatures. The results are presented as final water content versus relative humidity used. The labels for series from the glass jars include *serial number_ initial water content (%)_temperature (°C)*. The labels for the series from the sorption balance include *SB_initial water content (%)_temperature (°C)*. All results from the glass jars are presented in Appendix 1.

Figure 3-1 shows results from the sorption balance method. The results from this study (test series SB_0_20) are shown with two curves from the literature. Figure 3-2 shows retention curves from the jars and from the sorption balance methods at 20°C, all from the present study. The retention curve from the jars is represented by an absorption curve from $w_{ini} = 0\%$ and a desorption curve from $w_{ini} = 64\%$.

The results from the sorption balance method show good repeatability. Moderate agreement at absorption is observed with the results from the method using jars. The maximum water content influences the desorption portion of the curves.

Figure 3-3 shows results only from the method with jars, from this and from a previous study. The basic retention curve (starting from $w_{ini} = 0\%$) is shown with specific retention curves (starting from w_{ini} deviating from 0). Arrows show the moisture paths. Figure 3-3 illustrates the importance of using a retention curve with the correct initial condition.

In Appendix 1 an equation is suggested for the resulting curves at 20°C with a set of constants for each of the initial water contents 0%, 10%, 17.5%, 27% and 64%, respectively.
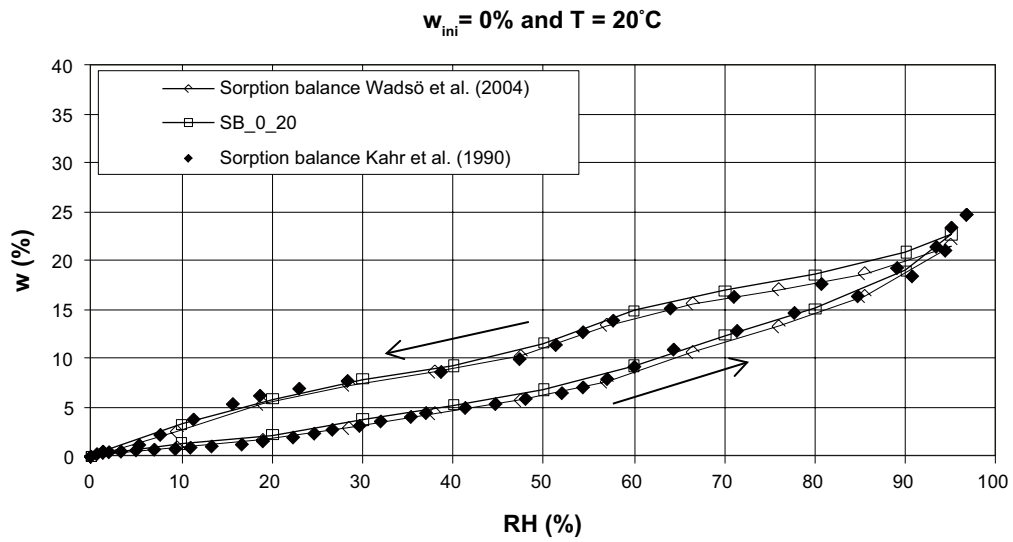
w_ini= 0% and T = 20°C

Figure 3-1. *Retention curves determined with the sorption balance method. The result SB_0_20 are presented together with results from Wadsö et al. (2004) and Kahr et al. (1990).*
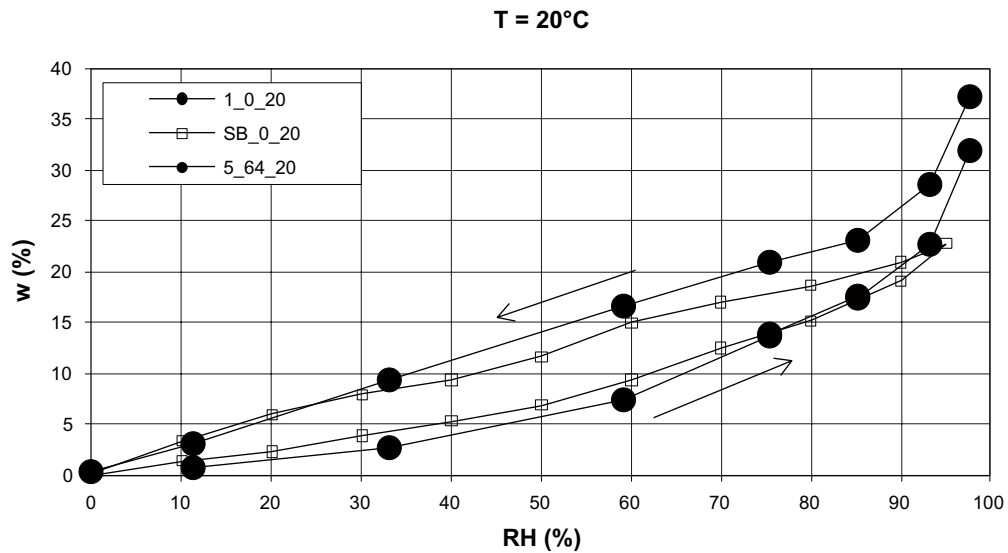
T = 20°C

Figure 3-2. *Retention curves at 20°C determined with the sorption balance (SB_0_20, which is also shown in Figure 3-1) and jar method with w_ini= 0% and 64% from this study.*

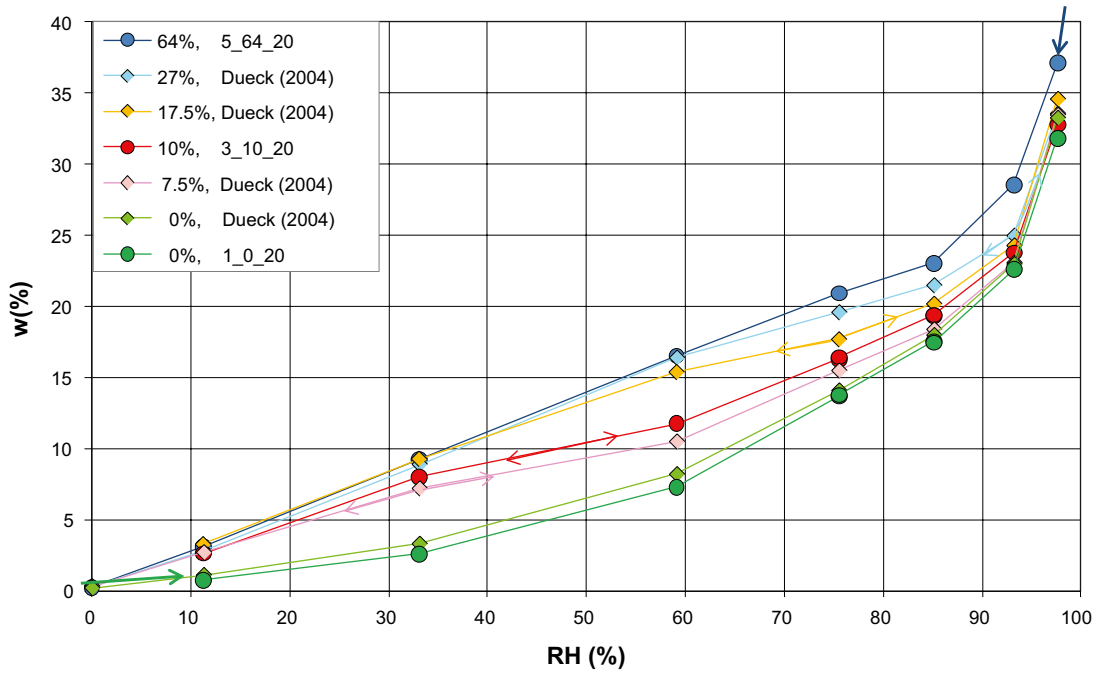**Figure 3-3.** *Retention curves determined with jars starting from different initial water contents. The labels show the initial water content w_{ini} for all specimens. For the results that originate from this study, the label for the test series also includes 'name_w_{ini}_temperature' otherwise a reference is given in the label.*

Retention curves at different temperatures are shown below. Figure 3-4 shows results from the sorption balance method only, at 20°C and 50°C. Figure 3-5, Figure 3-6 and Figure 3-7 show corresponding results from the jar method with the initial water contents of 0%, 10, and 64%, respectively. Figure 3-8 show comparable results from both methods.

An increase in temperature yields an increase in *RH* when the water content are kept constant according to the sorption balance method and the desorption curve from the jar method. However, this is not the case for the absorption curve determined by the jar method.
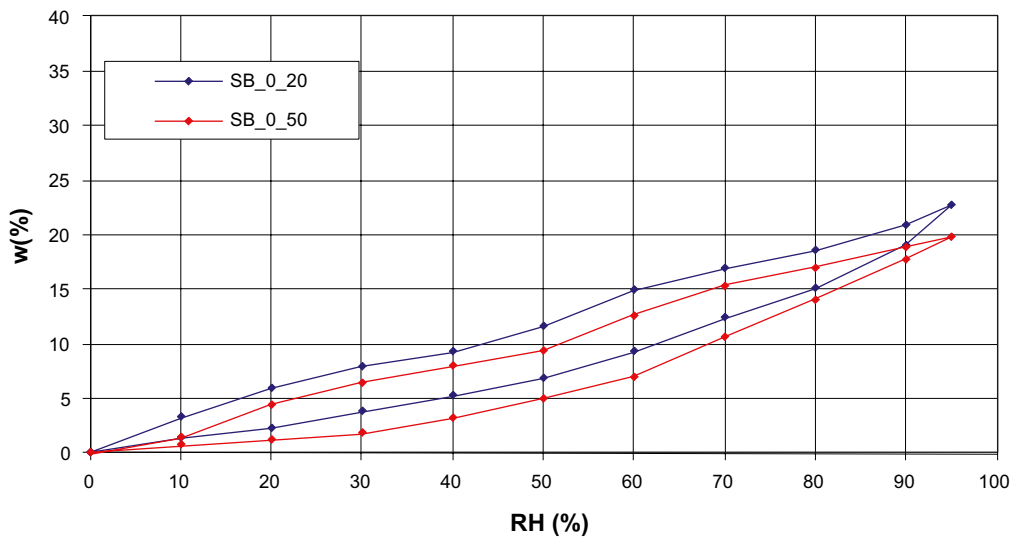

Figure 3-4. *Retention curves at 20 and 50°C determined with the sorption balance method and w_{ini}= 0%. The same specimen was used for both curves.*
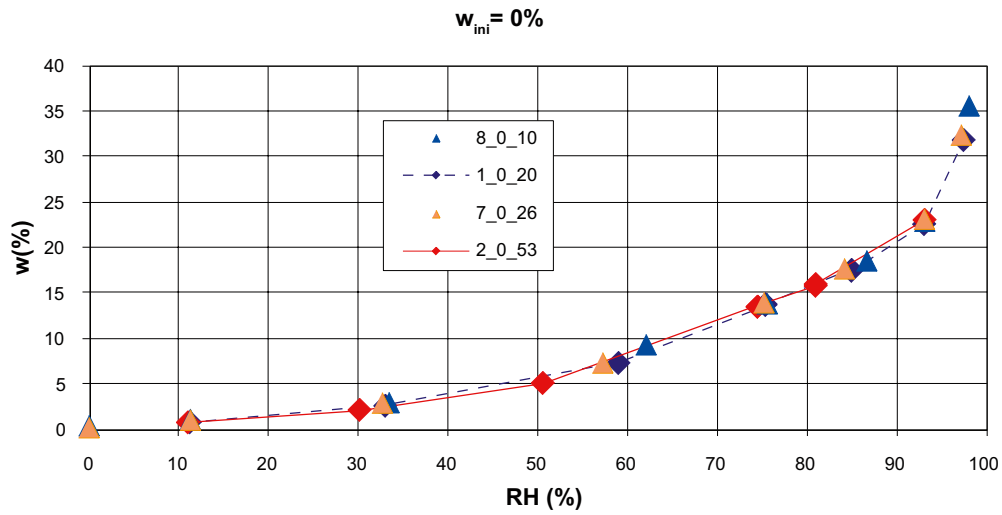
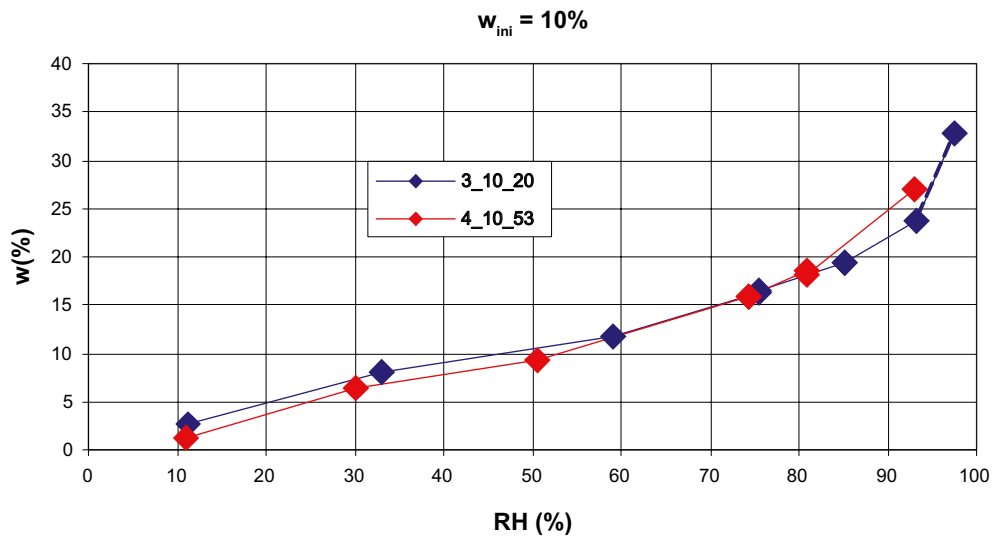**Figure 3-5.** *Retention curves at 10°C, 20°C, 26°C, and 53°C determined with the jar method and w_{ini} = 0%.*

Figure 3-6. *Retention curves at 20°C and 53°C determined with the jar method and w_{ini} = 10%.*
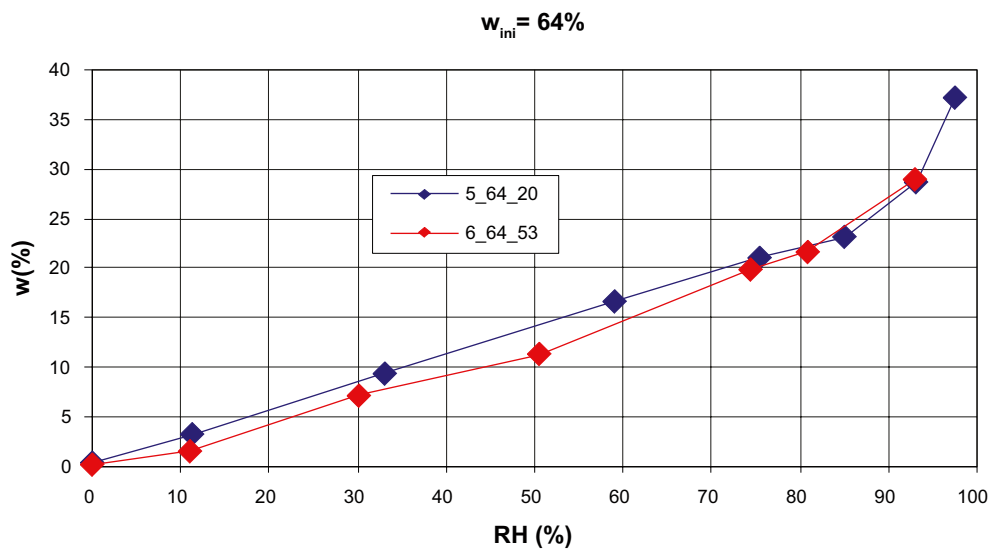

Figure 3-7. *Retention curves at 20°C and 53°C determined with the jar method and w_{ini} = 64%.*
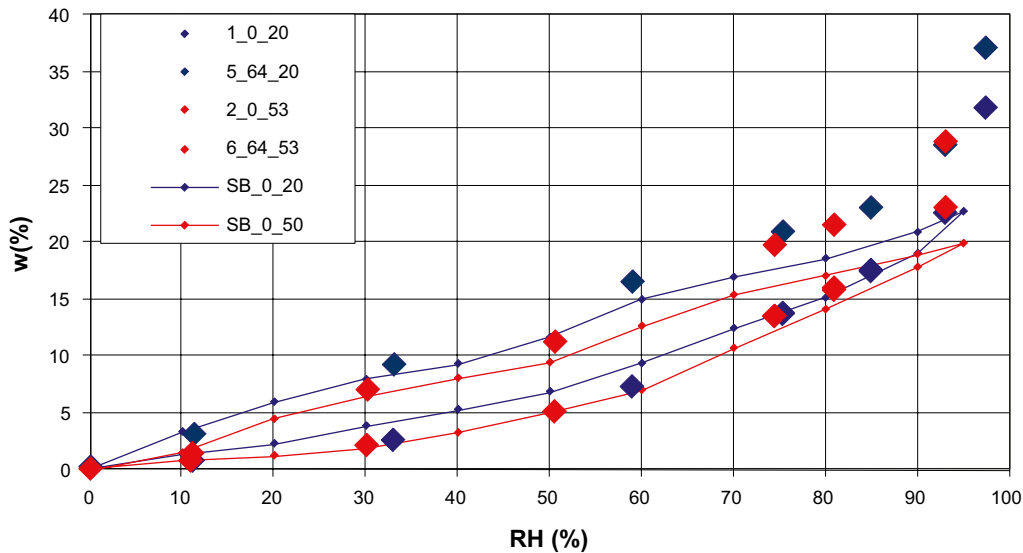
Figure 3-8. *Retention curves at 20°C and 50°C (53°C) determined with the sorption balance and jar method. The results from jars started from w_{ini} = 0% and w_{ini} = 64%.*

The rate of absorption at different temperatures and relative humidity in the jars are shown below where Figure 3-9 to Figure 3-12 show results starting from the initial water content of 0%, Figure 3-13 and Figure 3-14 from the initial water content of 10% and finally Figure 3-15 and Figure 3-16 show results starting from the initial water content of 64%.

The increase in water content seems to be more rapid at higher temperature and at lower relative humidity. A useful criterion for the termination of a test is Ω in Equation 3-1 (Wadsö et al. 2004) where m (g) is the mass and t (s) is time.

$$\Omega = \frac{dm}{dt} \cdot \frac{(RH_{final} - RH_{initial})/100}{m(t) - m_{initial}} \text{ (1/s)} \tag{3-1}$$

Wadsö et al. (2004) suggest that Ω should be less than $5\cdot10^{-9}$ s^{-1}. This was achieved in almost all of the tests performed in jars. The final values of Ω for each specimen are shown in Appendix 1.
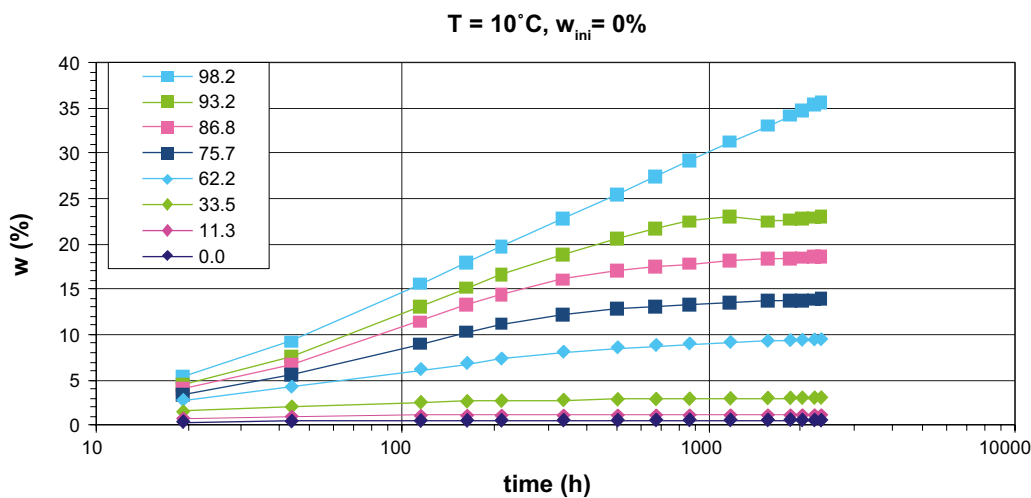

Figure 3-9. *Increase in water content vs. time at 10°C and different RH from w_{ini} = 0%.*
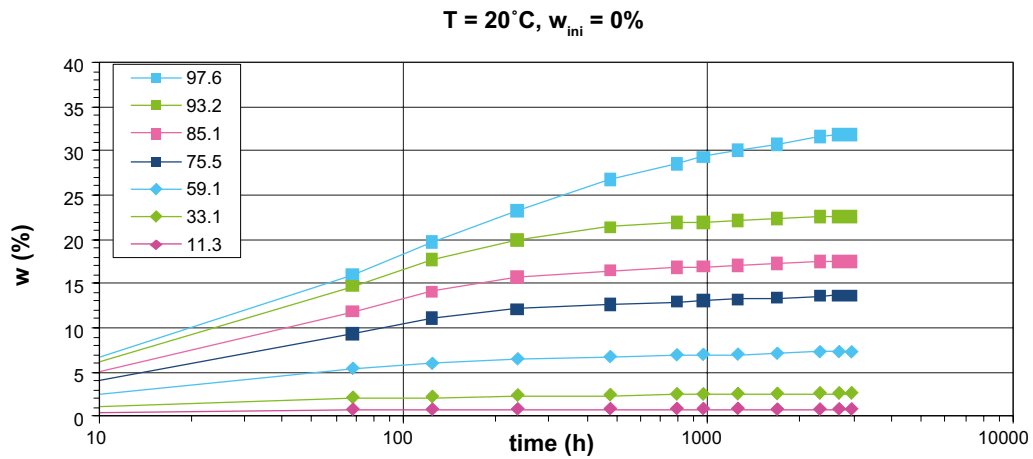
Figure 3-10. *Increase in water content vs. time at 20°C and different RH from $w_{ini} = 0\%$.*

Figure 3-11. *Increase in water content vs. time at 26°C and different RH from $w_{ini} = 0\%$.*

Figure 3-12. *Increase in water content vs. time at 53°C and different RH from $w_{ini} = 0\%$.*

Figure 3-13. *Change in water content vs. time at 20°C and different RH from w_{ini} = 10%.*

Figure 3-14. *Change in water content vs. time at 53°C and different RH from w_{ini} = 10%.*

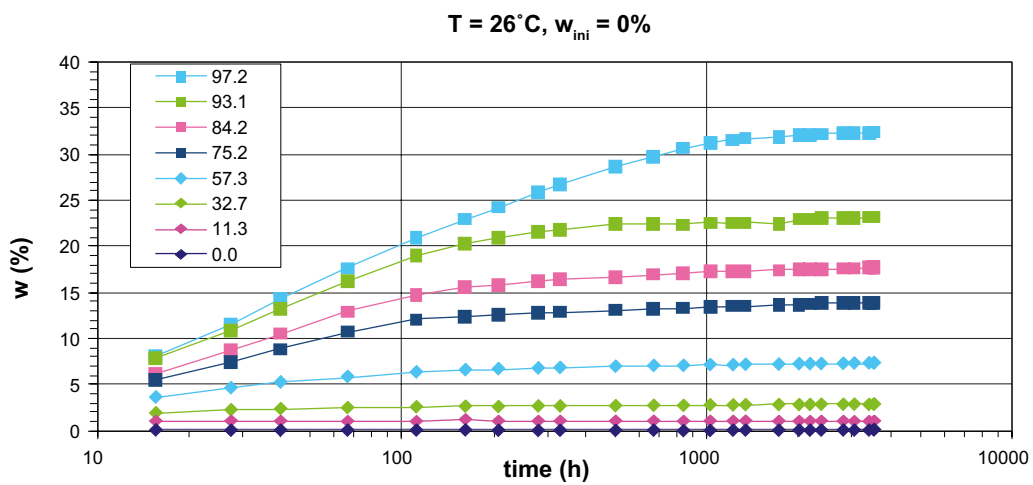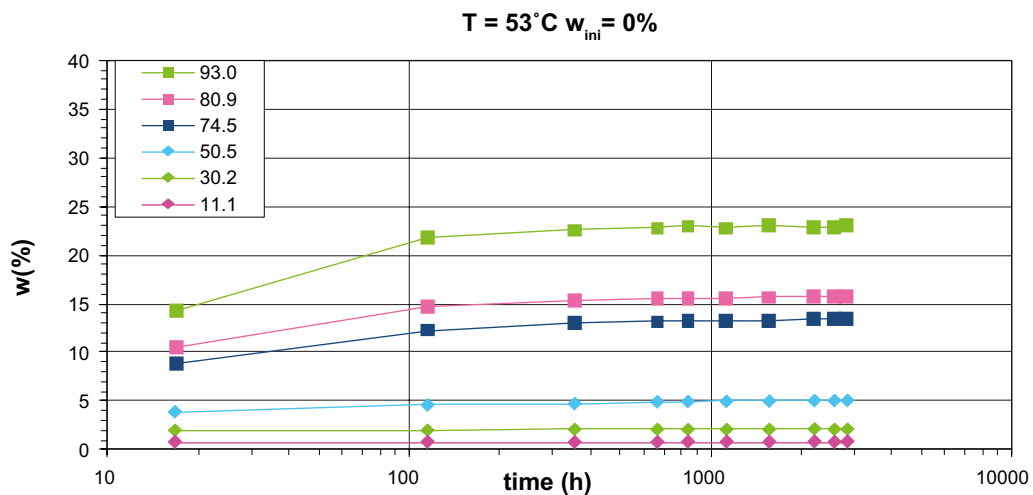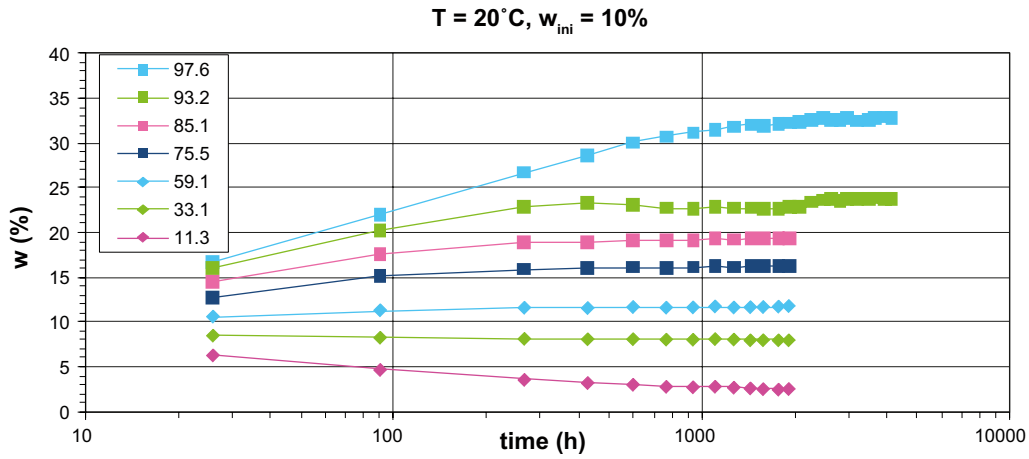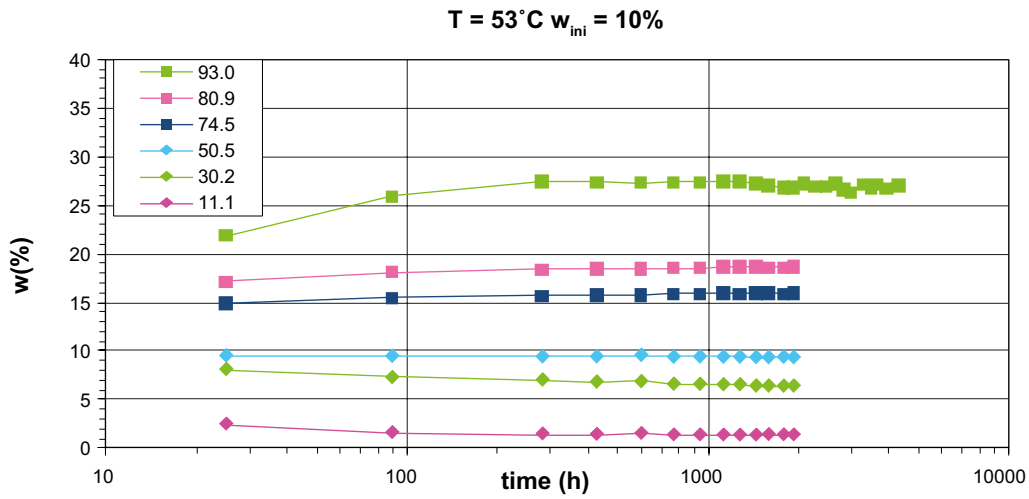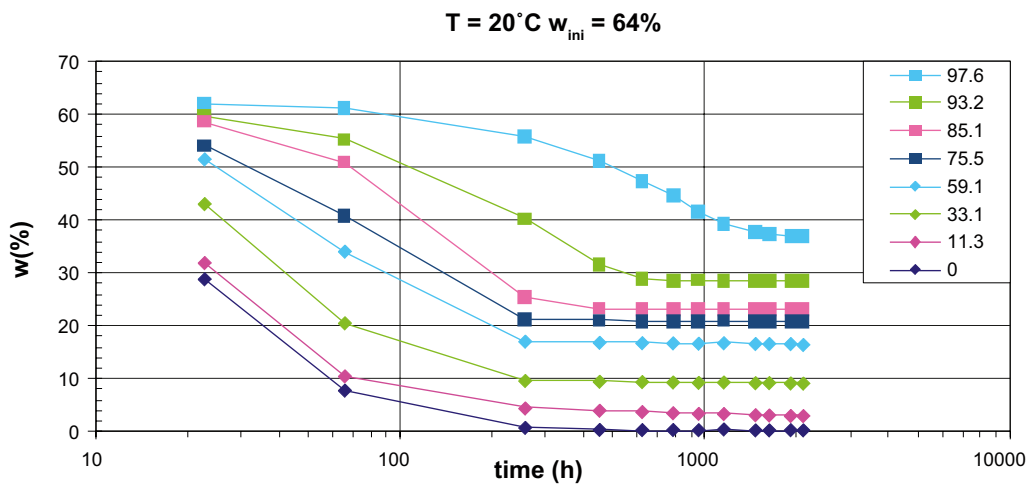**Figure 3-15.** *Decrease in water content vs. time at 20°C and different RH from w_{ini} = 64%.*
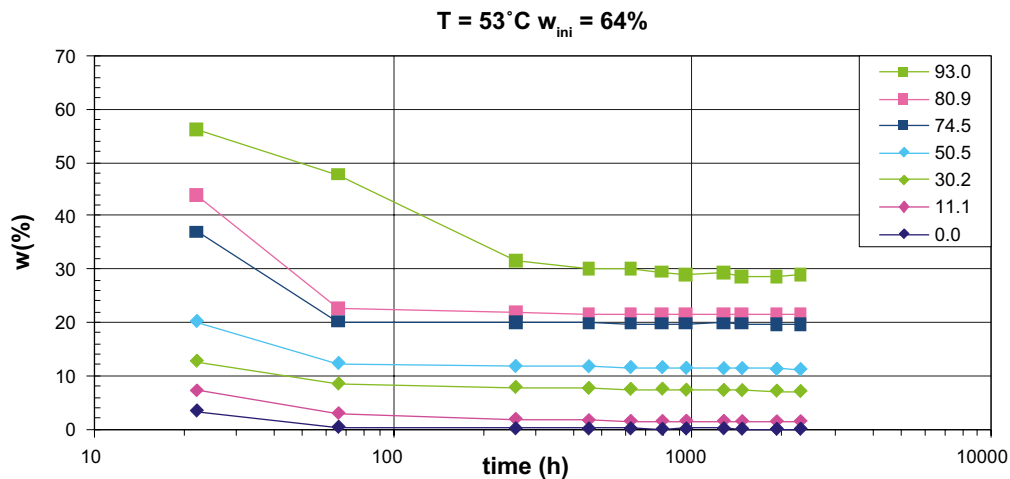
Figure 3-16. *Decrease in water content vs. time at 53°C and different RH from $w_{ini} = 64\%$.*

3.2.5 Comments

In general the test results will be used for checking and calibrating a material model. However, the following observations could be made:

- The results from the sorption balance method show good repeatability.

- Moderate agreement during absorption is observed between the results from the sorption balance and the jar method. At desorption the maximum water content influences the curves.

- The change to a new equilibrium in water content is more rapid the higher temperature and the lower relative humidity according to the measurements in jars.

- Different influence of temperature is seen in the results from the different test techniques but all methods except absorption with the jar technique indicate an increased *RH* with approximately 5% at an increased temperature from 20°C to 50°C.

Some comments regarding the testing time and the influence of temperature on measured *RH* are presented below.

Testing time

In the test with jars there is a change in water content after long equilibration times. This slow water uptake was analysed to get an idea of the time dependency of the water uptake of the bentonite. The measured results were compared to results from a model of diffusion in air. The model and the comparison are presented in Appendix 1. It seems as one controlling factor of the water uptake is the transport of water through the air filled gap between the surface of the salt solution and the bentonite surface. Thus, the diffusion used in the method with jars involves a slow transport of moisture in the air. However, the testing time has been the same or longer than is required according to the model of diffusion in air. Still after sufficient time for diffusion there is a change in the measured water content especially at high *RH*, which indicates a time dependence of the water uptake in the bentonite. This may be caused by the large swelling of the bentonite at high *RH*.

The results at increased temperature were also analysed with the diffusion model. The results were well captured in that the final water content was reached earlier at higher temperature. This also implies that at higher temperature shorter time is needed to reach correct *RH* at the surface of the specimen.

Influence of temperature on measured RH

The results reported in this chapter were derived from tests where *RH* was settled and controlled and the response of the bentonite samples was measured. The influence of temperature on *RH*, where *RH* was controlled by the bentonite sample while the response of the *RH*-sensor was measured, was also studied.

The series was limited and the result is shown in Appendix 1. The results show that influence of temperature on measured *RH* seems to coincide well with the temperature influence of the desorption part of the retention curves.

3.3 Volume change

3.3.1 Method and equipment

The volume change properties were investigated with an oedometer designed for this purpose. The equipment is shown with a sketch in Figure 3-17 and a photo in Figure 3-18. With this equipment it was possible to apply a constant axial load and a constant suction to a specimen. The load and suction were measured continuously as well as the deformation of the specimen. The load was applied with the equipment shown in Figure 3-19 and Figure 3-20. The applied load (in terms of stress) was in the range of 0 to 20 MPa and the applied suction (in terms of relative humidity) was in the range of 75% to 98%. After the tests, the water content and bulk density of the specimens were determined.

The equipment consisted of a steel ring around the specimen with filters on both sides. A piston and a force transducer were placed vertically above the specimen. A piston and a force transducer were also placed in the radial direction with the piston going through the steel ring. The constant suction was generated by the vapour equilibrium technique, where saturated salt solutions generated a specified relative humidity. The specimens were exposed to the humidified air by a circulation system where air was pumped from the box with the saturated salt solution to the steel rings which enclosed each specimen. The air passed through grooves above and below the filter stones.

When the vapour equilibrium technique is used it is important to prevent temperature gradients over the equipment, including the compartment with the salt solution. This is especially important if the relative humidity tabulated for the salt used would be used. In this project the equipment was placed in laboratory room climate and it was expected that a temperature gradient would appear over the equipment since each device included several parts (e.g. pump, tubes, oedometer and load frame). Consequently, the relative humidity was measured at the periphery of the specimen half way between the filters. The measured value was considered to be the representative *RH,* used in the evaluation.
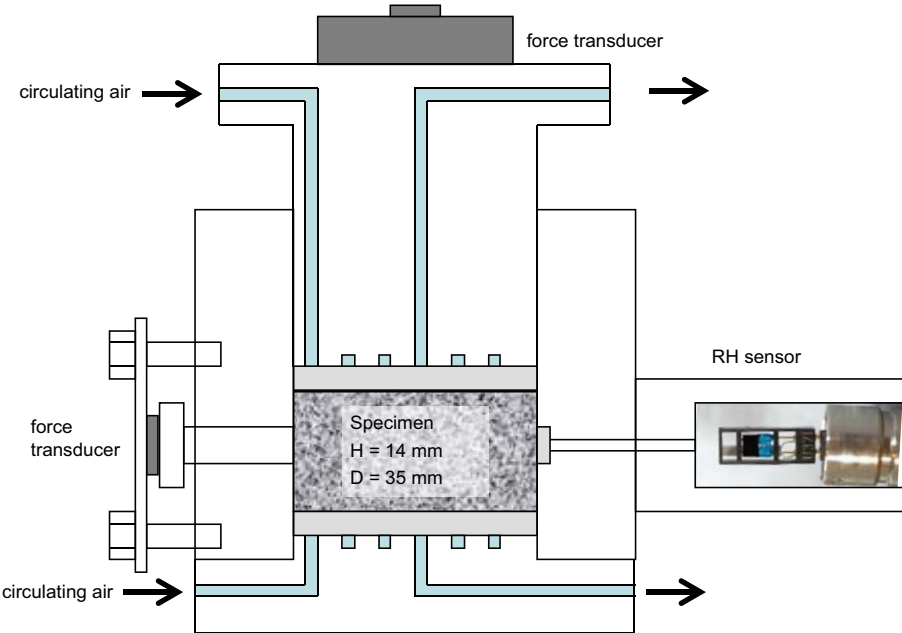

Figure 3-17. *Device used for the oedometer tests.*

Figure 3-18. *Device used for the oedometer tests. The oedometer is equipped with a deformation sensor, a force transducer and an RH sensor.*

Figure 3-19. *Maximal loading applied on one of the loading frames.*

Figure 3-20. *A pressure cylinder was used as loading device for application of high load.*

3.3.2 Preparation of specimens and test procedure

For all tests cylindrical specimens were prepared in a compaction device by compressing MX-80 bentonite to a diameter of 35 mm and an initial height of 14 mm. The bentonite had an initial water content of 10% and an initial void ratio of 0.6 was the target. After compaction, the specimens were unloaded and placed in the test device (Figure 3-17). Two types of tests were performed:

- Type 1: Compression tests with constant suction (OCS)
- Type 2: Swelling/shrinkage tests with constant load (SCL).

The stress and moisture paths for both test types are illustrated in Figure 3-21 and Figure 3-22 as relative humidity RH versus axial stress P_a. The OCS-type of test involved a stepwise change of load at constant values of suction, or RH. The SCL-type of test involved stepwise change of suction, or RH, at a constant axial load. The compaction is marked and represents a compaction pressure of 33 MPa at the relative humidity corresponding to the retention curve, i.e. $RH = 43\%$. During the tests the load, relative humidity and deformation were continuously measured.

The stress and moisture paths contained four levels of axial stress; 0.1 MPa, 1 MPa, 9 MPa and 20 MPa and three levels of relative humidity; 75%, 85% and 98%. The relative humidity was generated by use of the saturated salt solutions; NaCl, KCl and K_2SO_4. After the test the density and water content were determined according to Section 2.2.1.

Figure 3-21. *Axial stress and moisture paths for the OCS-type of test. Arrows show paths and solid circles show the final conditions of the tests, labelled to the right. The unfilled circle marks the compaction of the specimens.*
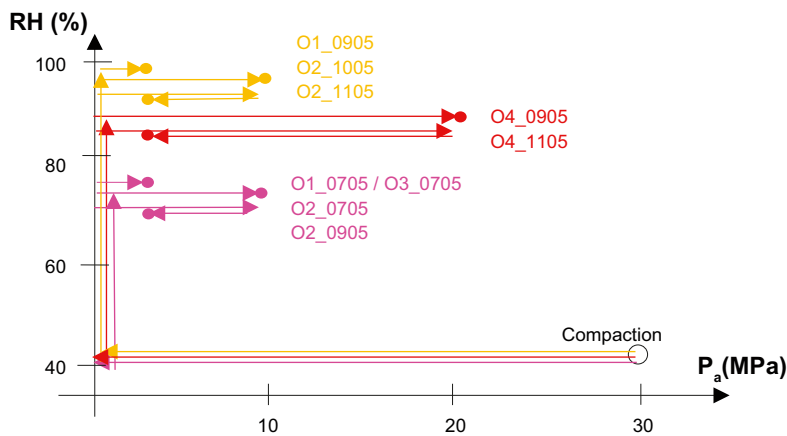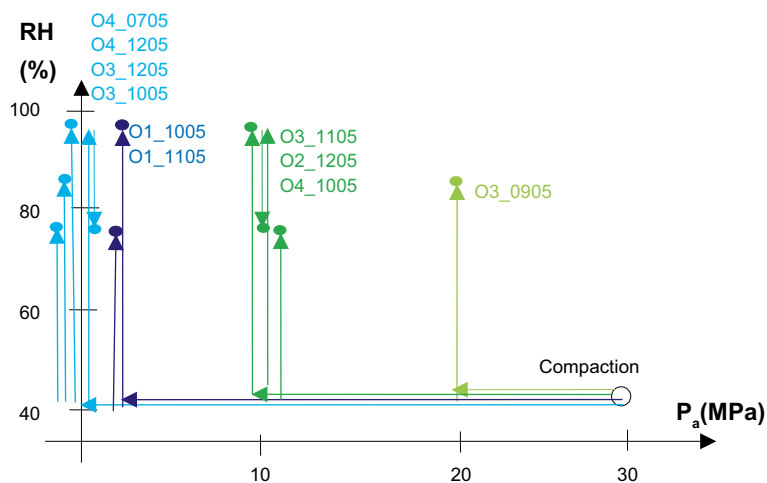

Figure 3-22. *Axial stress and moisture paths for the SCL- type of test. Arrows show paths and solid circles show the final conditions of the tests, labelled above the paths. The unfilled circle marks the compaction of specimens.*

3.3.3 Test program

The test program for the OCS-type and SCL-type of test are shown in Table 3-3 and Table 3-4. The stress and moisture paths were also shown as stress and moisture paths in Figure 3-21 and Figure 3-22, respectively. The label of each test includes *the name of the used oedometer (O1–O4)_the month and the year for the test (mmyy)*.

Table 3-3. Test plan for the compression tests (OCS).

Label	Step	*RH* set by a saturated salt solution (%)	P_a (MPa)	Remarks
O1_0705	1	(43)[1]	33	start
	2	(43)[1]	0.1	
	3	75	0.1	
	4	75	1	end
O1_0905	1	(43)[1]	33	start
	2	(43)[1]	0.1	
	3	98	0.1	
	4	98	1	end
O2_0705	1	(43)[1]	33	start
	2	(43)[1]	0.1	
	3	75	0.1	
	4	75	9	end
O2_0905	1	(43)[1]	33	start
	2	(43)[1]	0.1	
	3	75	0.1	
	4	75	1	
	5	75	9	
	6	75	1	end
O2_1005	1	(43)[1]	33	start
	2	(43)[1]	0.1	
	3	98	0.1	
	4	98	1	
	5	98	9	end
O2_1105	1	(43)[1]	33	start
	2	(43)[1]	0.1	
	3	98	0.1	
	4	98	1	
	5	98	9	
	6	98	1	end
O3_0705	1	(43)[1]	33	start
	2	(43)[1]	0.1	
	3	75	0.1	
	4	75	1	end
O4_0905	1	(43)[1]	33	start
	2	(43)[1]	0.1	
	3	85	0.1	
	4	85	1	
	5	85	9	
	6	85	20	end
O4_1105	1	(43)[1]	33	start
	2	(43)[1]	0.1	
	3	85	0.1	
	4	85	1	
	5	85	9	
	6	85	20	
	7	85	9	
	8	85	1	end

[1] *RH* not set by a salt solution but given by the retention curve at *w* = 10%.

Table 3-4 Test plan for the swelling/shrinkage tests (SCL).

Name	Step	RH set by saturated salt solution (%)	P_a (MPa)	Remarks
O1_1005	1	(43)[1]	33	start
	2	(43)[1]	1	
	3	75	1	end
O1_1105	1	(43)[1]	33	start
	2	(43)[1]	1	
	3	98	1	end
O2_1205	1	(43)[1]	33	start
	2	(43)[1]	9	
	3	98	9	
	4	75	9	end
O3_0905	1	(43)[1]	33	start
	2	(43)[1]	20	
	3	85	20	end
O3_1005	1	(43)[1]	33	start
	2	(43)[1]	0.1	
	3	98	0.1	
	4	75	0.1	end
O3_1105	1	(43)[1]	33	start
	2	(43)[1]	9	
	3	98	9	end
O3_1205	1	(43)[1]	33	start
	2	(43)[1]	0.1	
	3	98	0.1	end
O4_0705	1	(43)[1]	33	start
	2	(43)[1]	0.1	
	3	75	0.1	end
O4_1005	1	(43)[1]	33	start
	2	(43)[1]	9	
	3	75	9	end
O4_1205	1	(43)[1]	33	start
	2	(43)[1]	0.1	
	3	85	0.1	end

[1] RH not set by salt solution but given by the retention curve at w = 10%.

3.3.4 Test results

Compression tests (OCS)

The test results from the compression tests with constant suction, OCS-type, are plotted in diagrams exemplified by Figure 3-23 and Figure 3-24 where the radial and axial stresses, the deformation and the measured relative humidity are plotted versus time. In Figure 3-25 the axial stress P_{ax} and the average stress P_{avr} are plotted vs. the specific volume (1+e). The states and load steps, also marked in the figures, represent the following:

0. Compaction of the specimen and assembly of the equipment.

1. The initial state of the test. Equilibrium with a small axial stress of approximately 0.1-0.2 MPa and with zero radial stress. The initial void ratio is calculated from the full diameter of the ring. The air with controlled relative humidity RH_{const} is applied, which causes swelling and increase in the radial stress.

2. End of the equilibration phase after application of the RH_{const}. Application of a step of axial load $P_{ax,step}$.

3. Equilibrium with $P_{ax\,step}$. New step of axial load.

4. New equilibriums and new step of axial load.

5. Final equilibrium and end of the test. The final water content and density are determined.

For specimen O2_0905 the applied relative humidity was RH_{const} = 75% and the steps of the applied axial stress were $P_{ax,step}$ = 1, 9, 1 MPa. Different numbers of steps were used in different tests and both increases and decreases occurred.
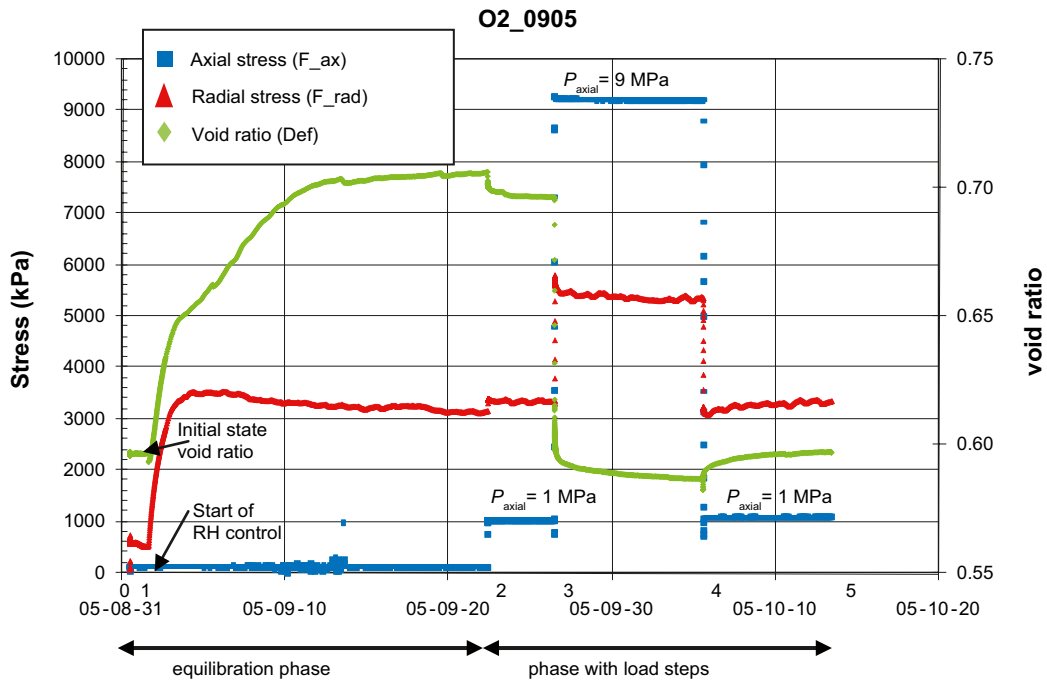
O2_0905

Figure 3-23. *Axial stress (F_ax), radial stress (F_rad) and void ratio (Def) plotted versus date for specimen O2_0905 with RH = 75%. The numbers refer to compaction (0), application of RH control (1), increase or decrease in axial load (2-4) and end of the test (5).*
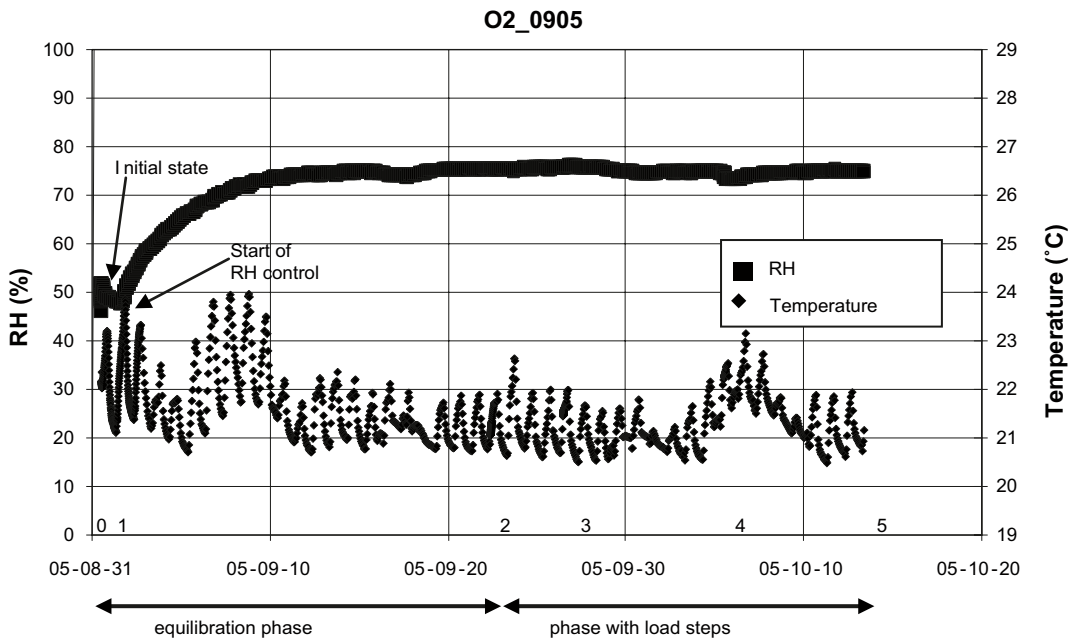
O2_0905

Figure 3-24. *Measured relative humidity and temperature plotted versus date for specimen O2_0905. The numbers refer to compaction (0), application of RH control (1), increase or decrease in axial load (2-4) and end of the test (5).*

O2_0905
stress (kPa)

Figure 3-25. The axial stress and average stress plotted versus specific volume 1+e for specimen O2_0905. The numbers refer to compaction (0), application of RH control (1), increase or decrease in axial load (2-4) and end of the test (5).
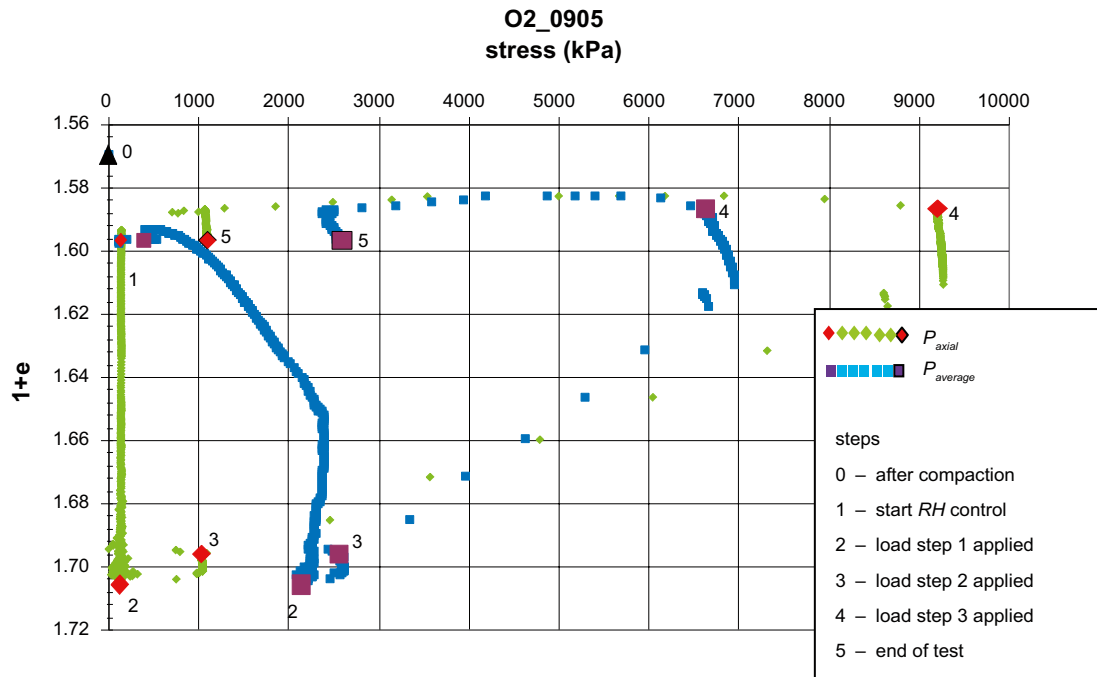
The test results from all compression tests are presented in Appendix 2 where the results are presented in diagrams as continuous measurements of stresses, relative humidity and void ratio versus time, and in tabular form with final values of each load step.

The results from this type of test are compiled as axial stress versus void ratio in Figure 3-26 and average stress versus void ratio in Figure 3-27 with the measured *RH* shown in the list of labels. The difference between the diagrams is that the radial stress is included in the average stress according to Equation 2-6 in Figure 3-27, which increases markedly during swelling caused by the high constant *RH* applied.

Figure 3-27 shows that the initial swelling is greater with higher RH_{const}. At equilibrium, after the swelling, the radial stresses of all specimens are larger than the axial stresses which are approximately 0.2 MPa for all tests. The radial stresses are approximately 5 to 25 times larger than the axial stresses at this step, cf. Appendix 2. Figure 3-27 also shows that all slopes ($\Delta e/\Delta \log P_{avr}$) are similar after the first swelling.

Swelling/shrinkage tests (SCL)

The test results from the swelling/shrinkage tests with constant load, SCL-type, are plotted in diagrams exemplified by Figure 3-28 and Figure 3-29 where the radial and axial stresses, deformation, and the measured relative humidity are plotted versus date. In Figure 3-30 the axial stress P_{ax} and the average stress P_{avr} are plotted versus specific volume (1+*e*). The states and load steps, also marked in the figures, represent the following:

0. Compaction of the specimen and assembly of the equipment.

1. The initial state of the test. The constant axial stress $P_{ax,const}$ was previously applied which causes increase in radial stress and decrease in volume but equilibrium is not yet established. The initial void ratio is calculated from the full diameter of the ring.

2. Equilibrium with the $P_{ax,const}$. Application of a step of RH_{step}.

3. Equilibrium with RH_{step} and application of a new step.

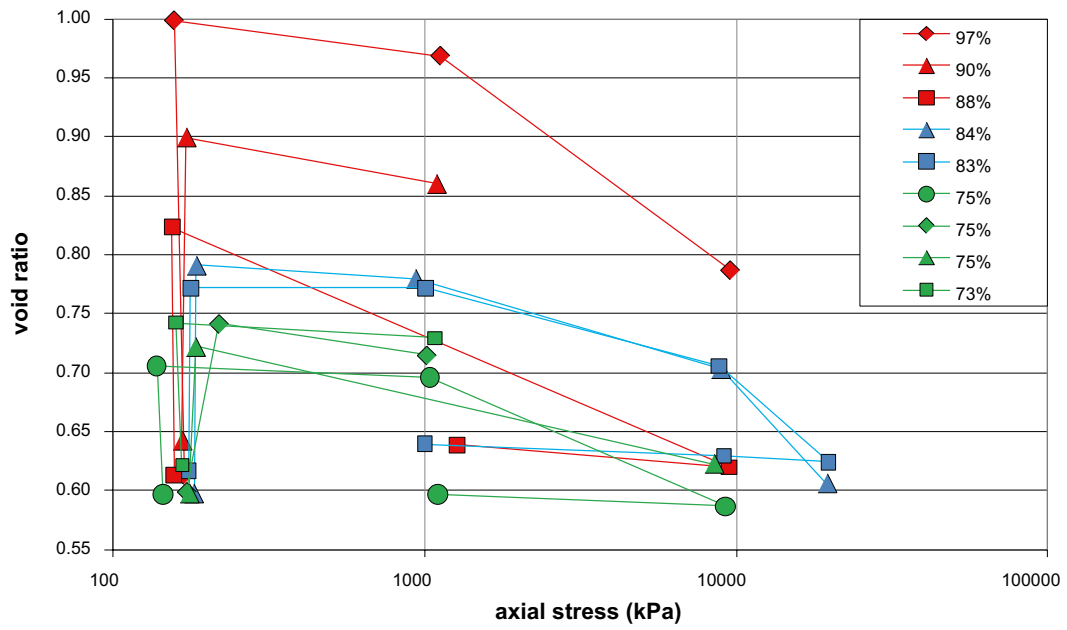4. Termination of the test. The final water content and density are determined.

Figure 3-26. *Axial applied stress versus void ratio. The labels show the approximate values of measured RH.*
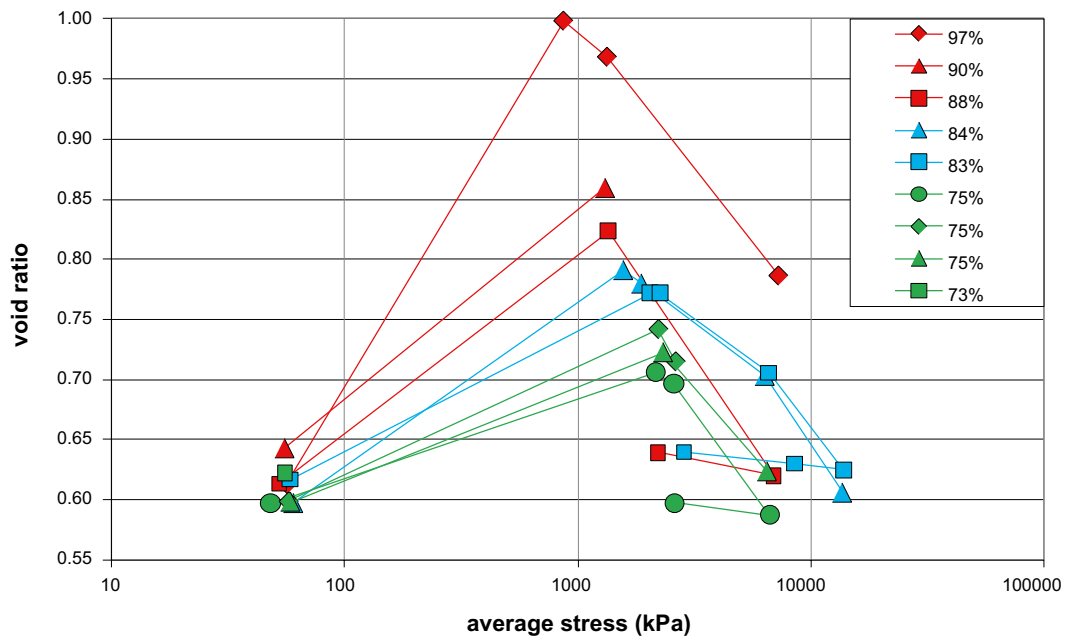

Figure 3-27. *Average applied stress versus void ratio. The labels show the approximate value of measured RH.*
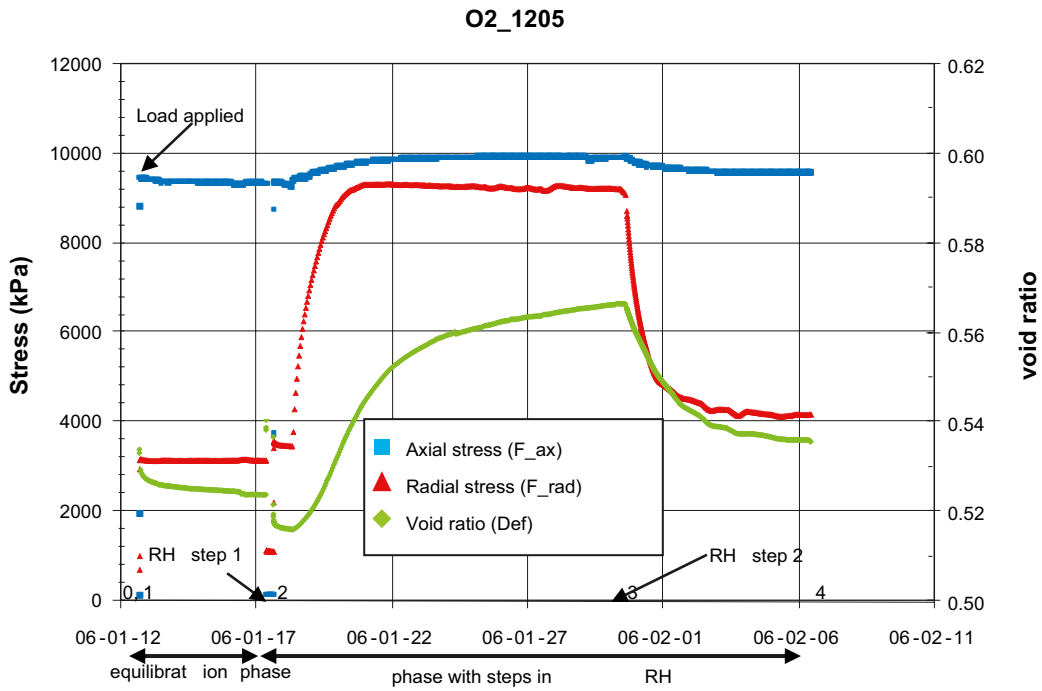
O2_1205

Figure 3-28. *Axial stress (F_ax), radial stress (F_rad) and deformation (Def) versus date for an SCL test on specimen O2_1205. The numbers refer to compaction and application of axial load (0–1), application of RH control in two steps (2–3) and termination of the test (4).*

O2_1205

Figure 3-29. *Measured relative humidity and temperature versus date for specimen O2_1205. The numbers refer to compaction and application of axial load (0–1), application of RH control in two steps (2–3) and termination of the test (4).*

Figure 3-30. *The axial stress and average stress plotted versus specific volume 1+e for specimen O2_1205. The numbers refer to compaction and application of axial load (0–1), application of RH control in two steps (2–3) and termination of the test (4).*
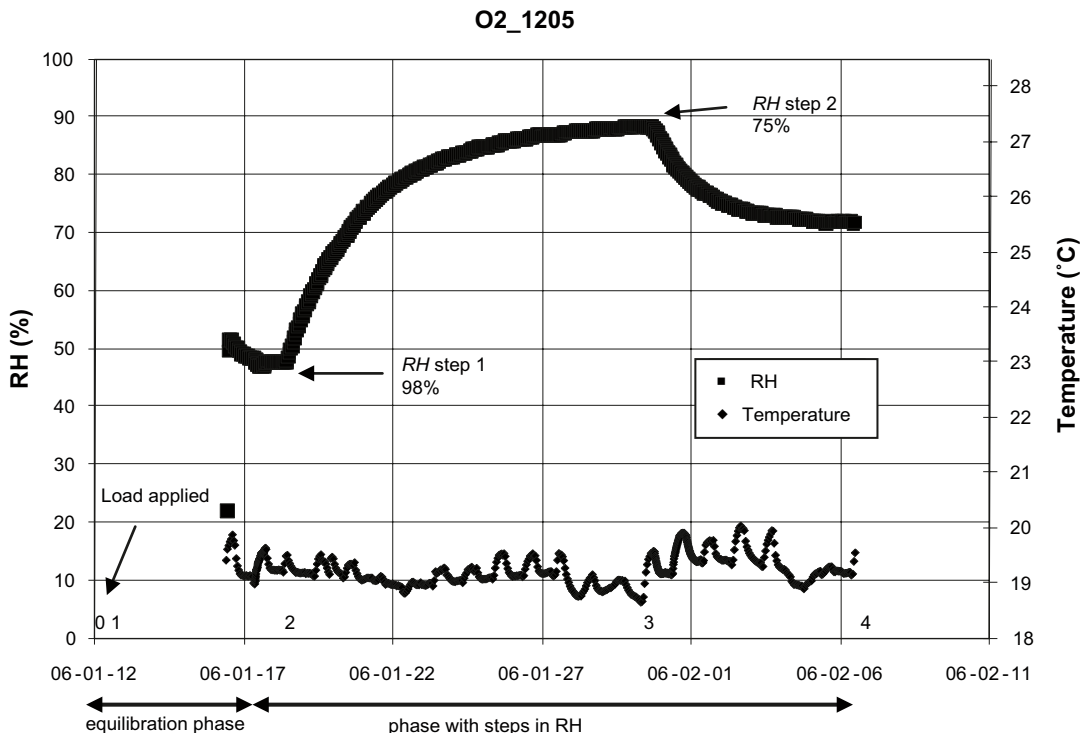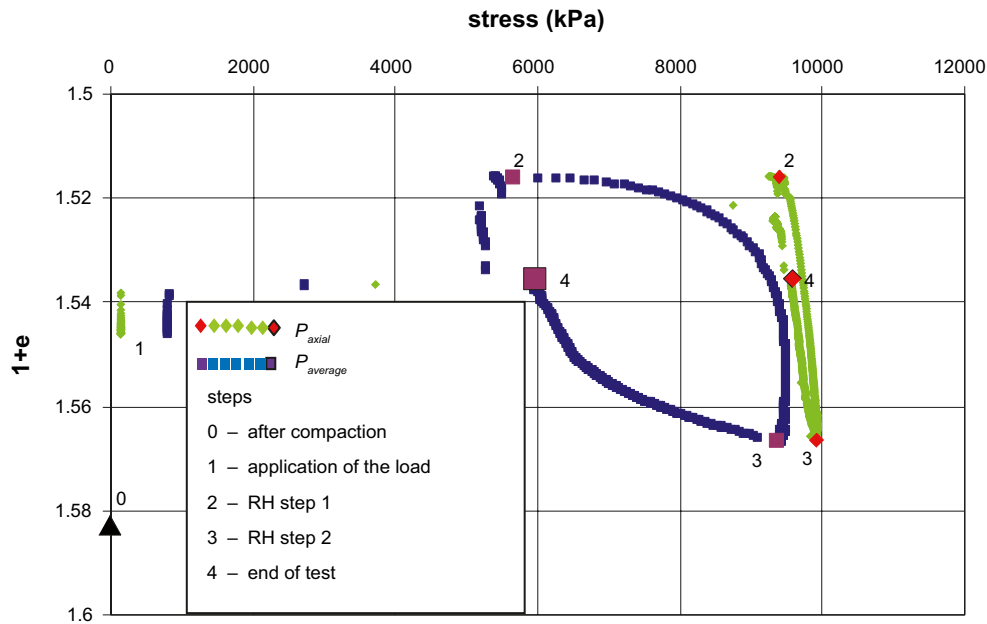
For specimen O2_1205 the the target values of the applied constant axial stress was $P_{ax,const}$ = 9 MPa and of the steps of RH_{step} = 98% and 75%. The actual axial stress was higher and the actual relative humidity was lower. All specimens were exposed to one increase in *RH* and some specimens were also exposed to one decrease.

The test results from all swelling/shrinkage tests are presented in Appendix 2 where the results are presented in diagrams as continuous measurements of stresses, relative humidity and void ratio versus time and in tabular form with final values of each load step.

In Figure 3-31 the results from the tests of this type are compiled as void ratio versus suction where suction is calculated from measured *RH*. The colours green, blue and red represent the approximate average stresses 2 MPa, 10 MPa and 20 MPa, respectively. If the axial stress is considered instead of the average stress the colours would represent almost the same stresses except the light green makers which would represent 0.2 MPa. The initial state of the specimens, at suction of approximately 100 MPa, represents the compacted specimens with the initial water content 10% and with the constant axial stress applied. Results from the SCL-type and OCS-type of tests are marked with diamonds and squares, respectively.

Figure 3-31 shows that the slope (Δe/Δlogψ) decreases with increased stress, i.e. the larger stress the lower swelling for the same decrease of suction. In addition, the stress measurements showed that the radial and axial stresses were almost the same in all tests except those with the smallest axial stress.

3.3.5 Comments

Since the main purpose of the compression and swelling/shrinkage tests was to evaluate and improve existing HM models and parameters for unsaturated bentonite the results from these tests are extensively presented in diagrams and tables in Appendix 2. However, the following observations could be made regarding volume change and stresses of specimens with a limited cross sectional area and influenced by a change of *RH* and stress:

- at a small constant axial stress of 0.2 MPa the swelling was larger the larger the applied *RH*.
- at a specific increase of *RH* the swelling was lower the larger the applied axial stress.
- at an increase of *RH* the radial and axial stresses were of the same order except in those cases with a small axial stress where the radial stresses were many times as large as the axial stresses.
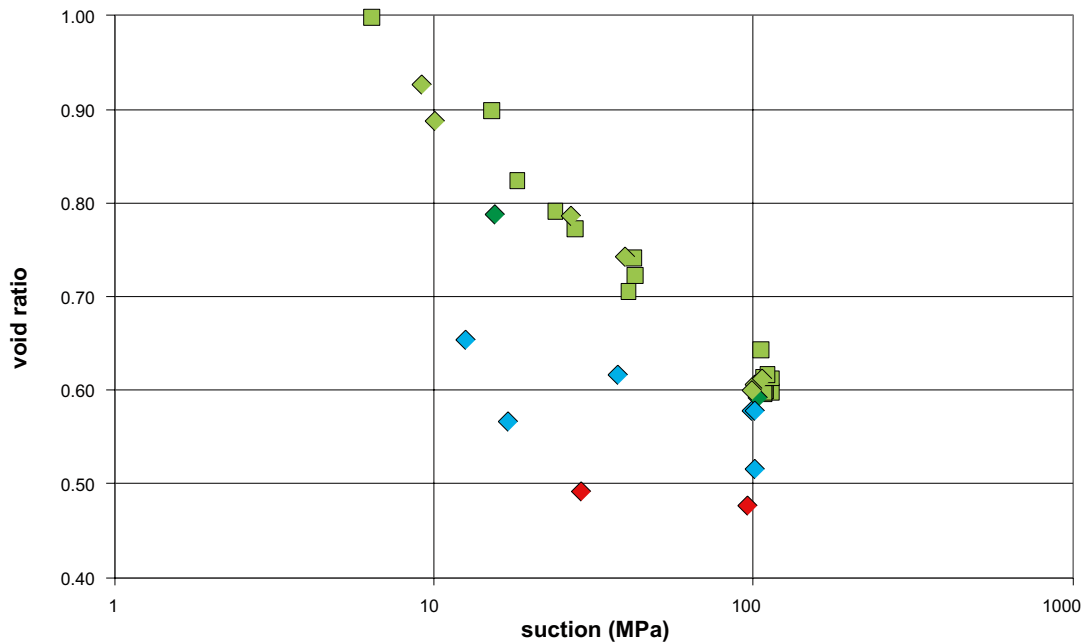
Figure 3-31. *Void ratio versus suction from the SCL-type (diamonds) and the OCS-type (squares) of test. All specimens start from suction of approximately 100 MPa. Suction is calculated from measured RH. The colours green, blue and red represent the approximate average stress 2 MPa, 10 MPa and 20 MPa, respectively.*

A model including two equations which relate the variables stress, relative humidity and degree of saturation or water content and void ratio were presented by Dueck (2004) and Dueck and Börgesson (2007). In the present investigation the tests included change in volume and since the model was mainly based on results from constant volume tests it was of interest to compare the test results with the calculation results from the model. In Appendix 2 the model is described and the comparison between test results and calculations is shown. Good agreement is shown between measurements and the results calculated by the model also after volume change.

The final values of a load step, here called equilibrium, were evaluated when only small changes were seen in the measured variables. The changes that continued to occur after long testing times can be evaluated from the diagrams in Appendix 2. Regarding the error in measured values evaluated from the calibration or the check of transducers after the tests was the following: for relative humidity the error was about 1%, for axial stresses the error was less than 2% except O3_1005 and O3_1205 where the initial axial stresses were approximately 100 kPa instead of 150 kPa. The error in the measured radial stress was less than 4% in all tests (except for O3_1205 where it was 11%). In terms of deformation, the error was less than 1%. In two tests, O1_0705 and O1_1005, the radial stresses applied at mounting were of the same size or larger than the final values and in those cases the radial stresses were considered as uncertain and are consequently not shown in Figure 3-27 and Figure 3-31.

3.4 Moisture transport

3.4.1 Method and equipment

Moisture transport tests were done in order to study the moisture transport process at a transient state. The set-up is shown in Figure 3-32. A constant relative humidity was applied at the top of three pressure cells with the vapour equilibrium technique described in Section 3.3.1. The specimens were kept at a constant volume condition and the axial force from all three specimens was measured. The lower drainage of the cell was sealed and the relative humidity was measured at three levels in one of the cells.
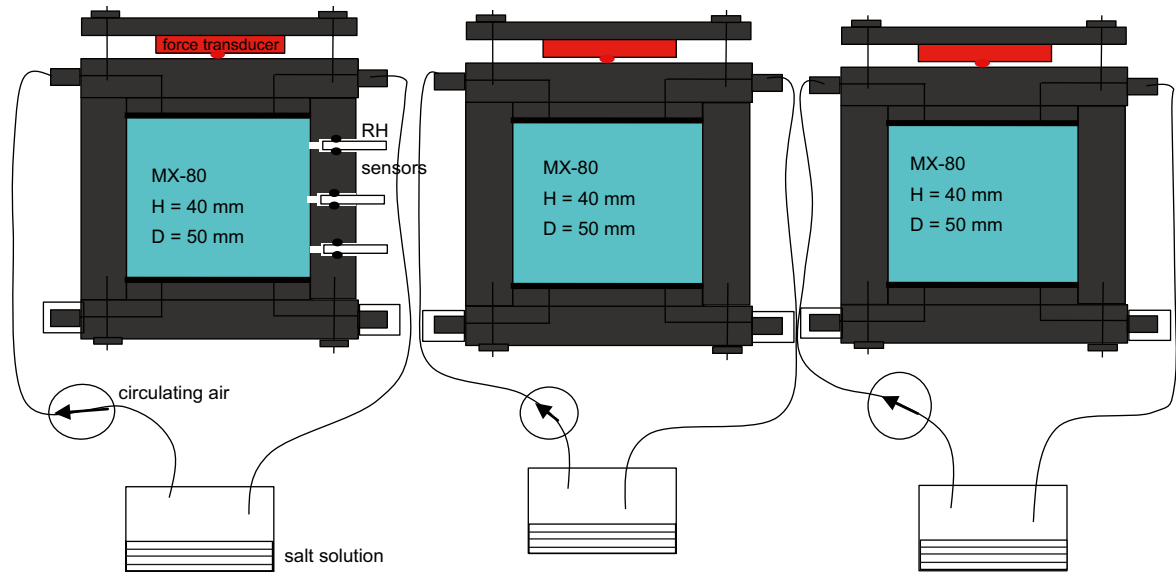
Figure 3-32. Set up of the tests used for studying the moisture transport process.

3.4.2 Preparation of specimens and test procedure

Three specimens with the same initial condition were prepared for each series. Cylindrical specimens with a diameter of 50 mm and a height of 40 mm were prepared by compressing MX-80 bentonite directly into each of the three test cells to ensure contact between the specimen and the wall of the test cell. Two different initial water contents w_{ini} were used in the series; 9.5% and 16.5%. With a target void ratio of 0.6, compaction pressures between 30 MPa and 40 MPa were used.

The three specimens with the same initial conditions were run parallel to each other and the prescribed relative humidity RH_a was applied at the same time. The three specimens were interrupted after different periods of time. The specimen with RH measurements was the last to be finished. After each test the gradient of water content and density were determined over the specimen height and the gradient of water content was coupled to the gradient of measured relative humidity present at the actual sampling time.

3.4.3 Test program

Table 3-5 shows the test plan where each test, e.g. TR 4, included three specimens with identical initial condition but interrupted after different periods of time, in this case after 171, 319 and 463 hours, respectively.

3.4.4 Test results

The main part of the results is presented in Figure 3-33 to Figure 3-36 as gradients of relative humidity and water content over the specimen height. The type of marker shows the initial water content where diamonds and squares represent 9.4% and 16.5%, respectively and the size of the markers shows the time elapsed with the larger markers representing the longer time. The labels show: *the name of the test_initial water content_time in hours*. The results are presented in tabular form in Appendix 3.

Table 3-5. Test plan for the moisture transport tests (TR).

$RH_{applied}$ (%)	w_{ini} = 9.4%	w_{ini} = 16.5%
85	TR 3	TR 4 and TR 5
98	TR 7	TR 6
Water	TR 1 and TR 2	

RH = 85%

Figure 3-33. *Measured RH in tests TR_3 and TR_4 as a function of the distance to the constant RH boundary at different times. (Labels show name of the test_ $w_{ini}(\%)$_time(h)). The RH value at the wet end was controlled but not measured.*

RH = 85%

Figure 3-34. *Distribution of water content in tests TR_3, TR_4 and TR_ 5 as a function of the distance to the constant RH boundary at different times. (Labels show name of the test_ $w_{ini}(\%)$_time(h)).*
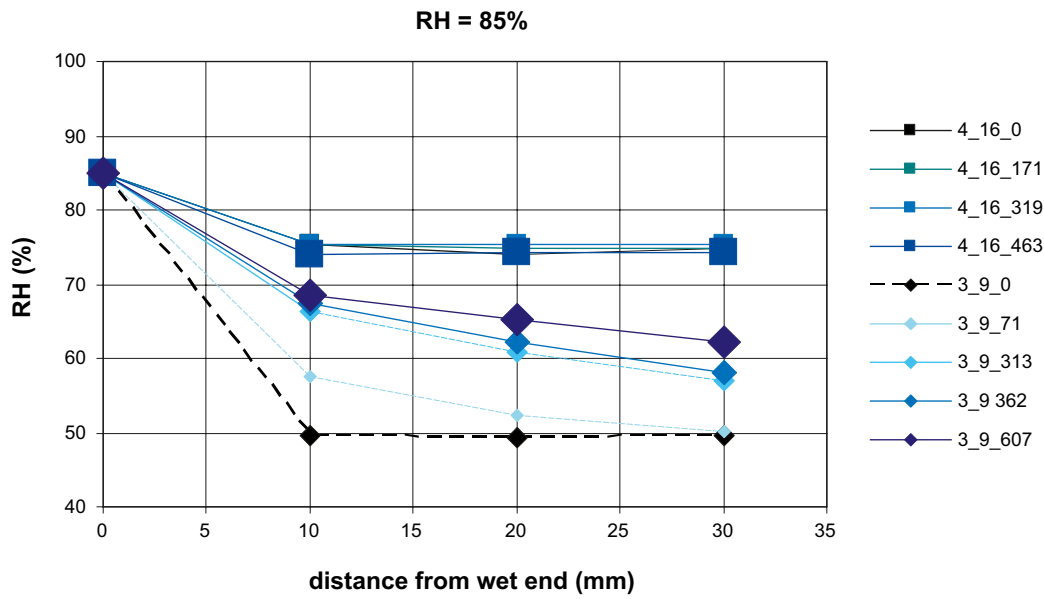
Figure 3-35. *Measured RH in tests TR_6 and TR_7 as a function of the distance to the constant RH boundary at different times. (Labels show name of the test_ $w_{ini}(\%)$_time(h)). The RH value at the wet end was controlled but not measured.*
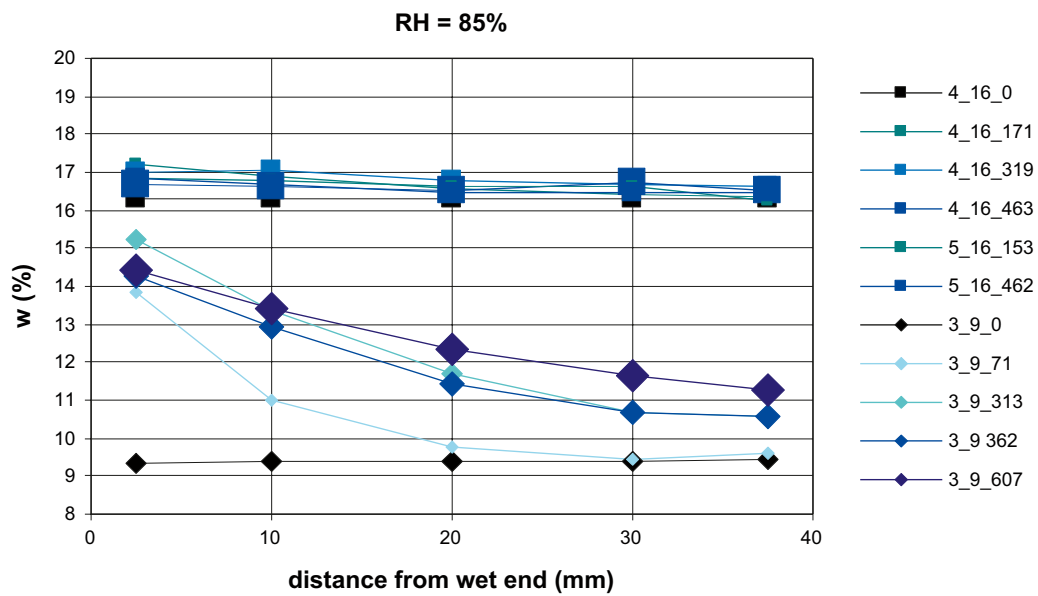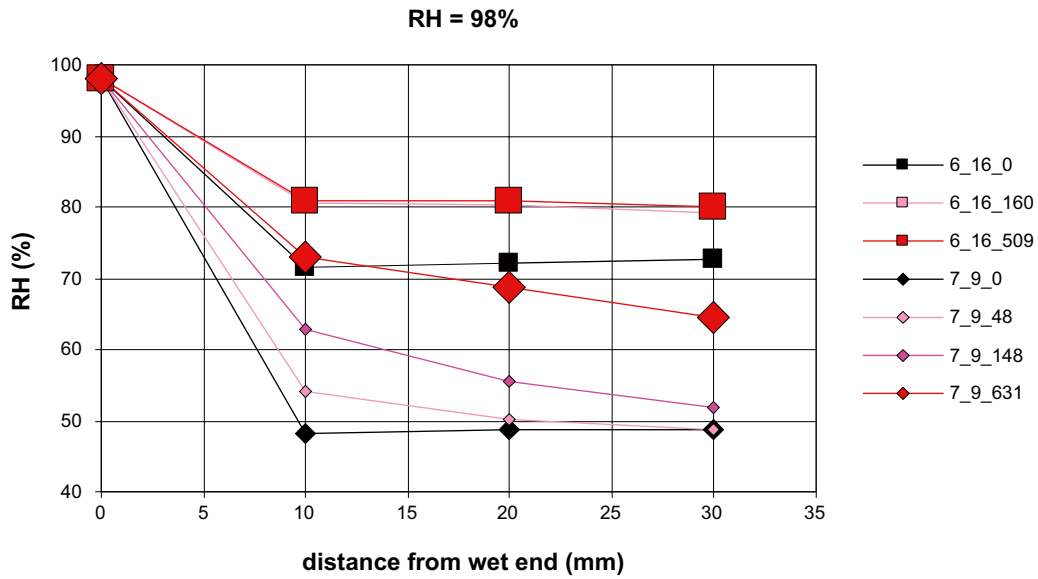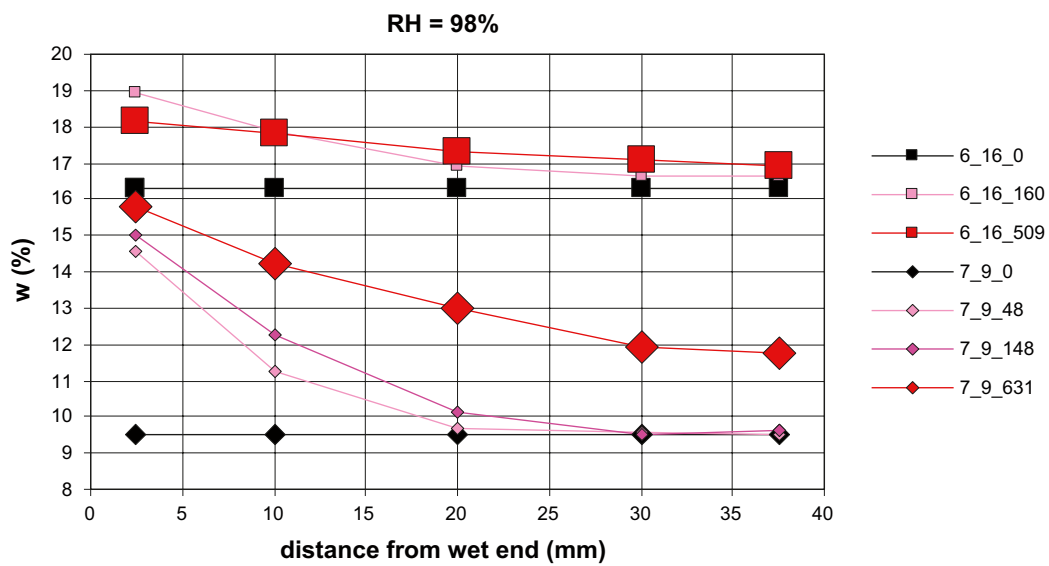

Figure 3-36. *Distribution of water content from tests TR_6 and TR_7 as a function of the distance to the constant RH boundary at different times. (Labels show name of the test_ $w_{ini}(\%)$_time(h)).*

In all four diagrams black points represent the initial states in terms of initial water content and relative humidity corresponding to the retention curve in Section 3.2.4. The blue and red colours represent tests with the applied relative humidity 85% and 98%, respectively.

The void ratio was initially approximately 0.6 and the intention was to keep the volume constant. However, small swelling occurred which was evaluated after removal of the specimen. The increase in void ratio was in all tests less than 0.08.

The constant *RH* was applied at the top of the specimens by the vapour equilibrium technique. The *RH* values at the wet ends in Figure 3-33 and Figure 3-35 are the tabulated values according to the used salt while the other *RH* values were measured. The actual *RH* values at the wet ends deviate presumably from the tabulated values since a temperature gradient could easily have been present between different parts of the equipment as discussed in Section 3.3.1. This is further commented on in Section 3.4.5.

The results are also shown as measured water content versus measured relative humidity in Figure 3-37 and Figure 3-38 for the initial water contents 9.4% and 16.5%, respectively. For comparison purposes the retention curves for the initial water contents 10% (label 3_10_20) and 17.5% (Dueck 2004) are shown.

All specimens were influence by stresses. Initially the specimens were compacted axially into the device with an axial stress of approximately 33 MPa. After the compaction the axial stress was removed, the specimens sealed and the constant *RH* applied at the boundary. During the water uptake an increase in axial swelling pressure was measured in all tests. The axial swelling pressures are shown in Appendix 3.

In another device, which was used at the beginning of the series and later modified, free water was applied at the bottom of the specimens. *RH* was only measured at one level and the distribution of water content was determined twice, i.e. from two specimens. The test results are shown in Figure 3-39 and Figure 3-40. The time t = 574 hours used in the label of specimen 1_9_574 is a corrected time since a couple of days was subtracted from the total time. During this time period no water was drawn into the specimen and no change of *RH* was measured. After flushing the filters an increase of *RH* was measured again.

In Figure 3-41 the results from Figure 3-37, Figure 3-39 and Figure 3-40 are shown. All specimens in this diagram started from the same initial water content. The initial state of specimen 1, 1_9_0, deviates from the initial states of the other tests in that this point is located on the retention curve, marked with an arrow. As mentioned above this test was performed in another device and the specimen was not compacted into the device as was the case for the other specimens. This means that initially no stress influenced this specimen.

Figure 3-37. *Final water content versus measured RH for specimens with an initial water content of $w_i \approx 9\%$. The number of hours is reflected by the size and darkness of the markers and unfilled markers represent the initial state. Two retention curves with $w_{ini} = 10\%$ (solid line) and $w_{ini} = 17.5\%$ (broken line) are shown.*
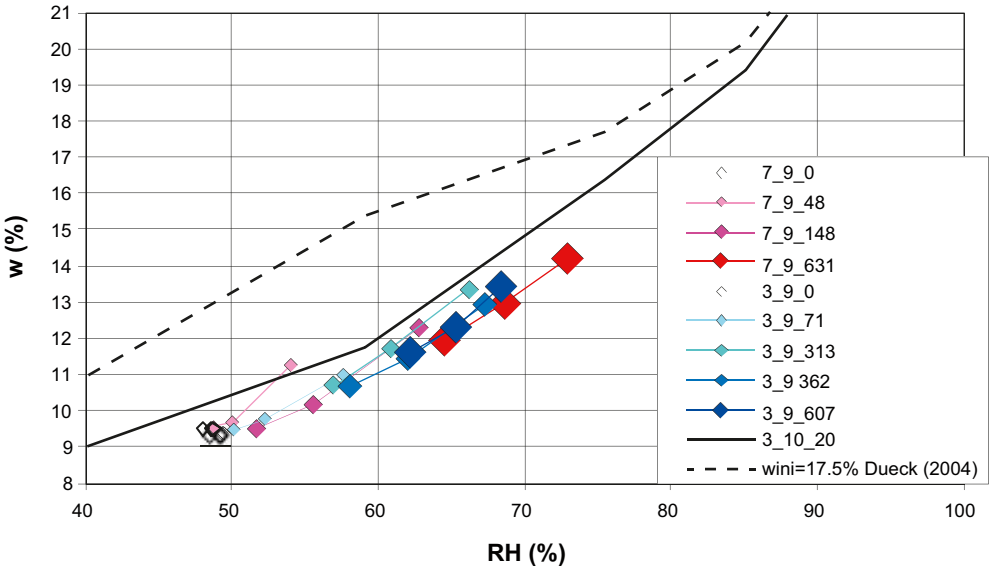
Figure 3-38. *Final water content versus measured RH for specimens with an initial water content of $w_i \approx 16\%$. The number of hours is reflected by the size and darkness of the markers and unfilled markers represent the initial state. Two retention curves with $w_{ini} = 10\%$ (solid line) and $w_{ini} = 17.5\%$ (broken line) are shown.*
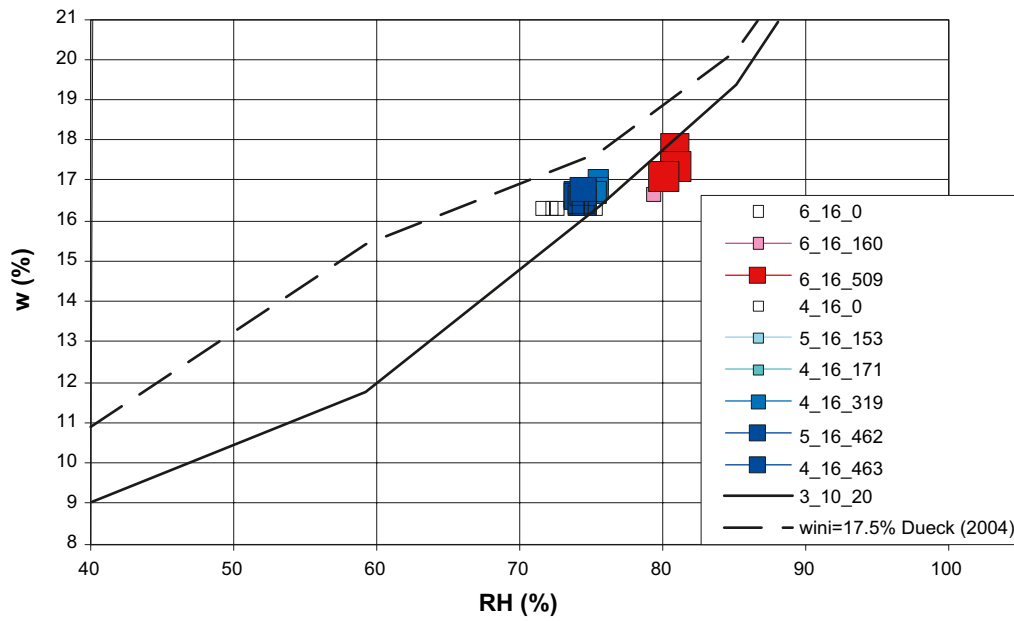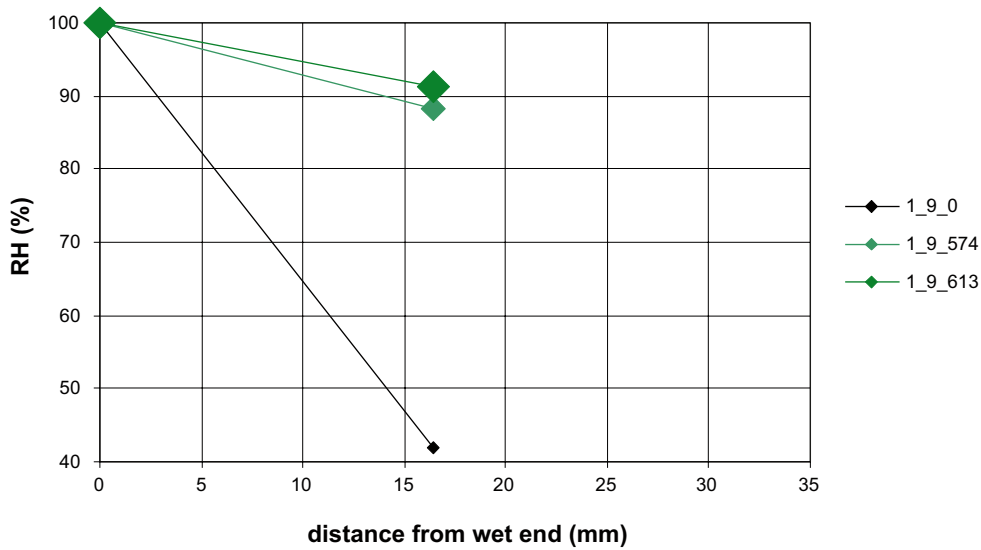

Figure 3-39. *Measured RH from tests TR_1 and TR_2. (Labels show name of the test_ $w_{ini}(\%)$_time(h)).*
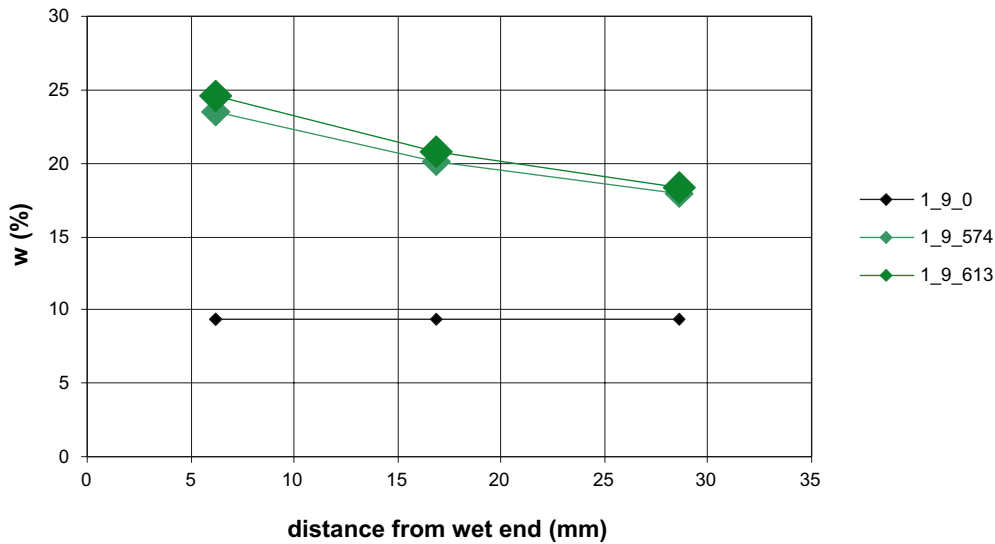
Figure 3-40. *Distribution of water content as a function of the distance to the water supply from tests TR_1 and TR_2. (Labels show name of the test_ w_{ini}(%)_time(h)).*
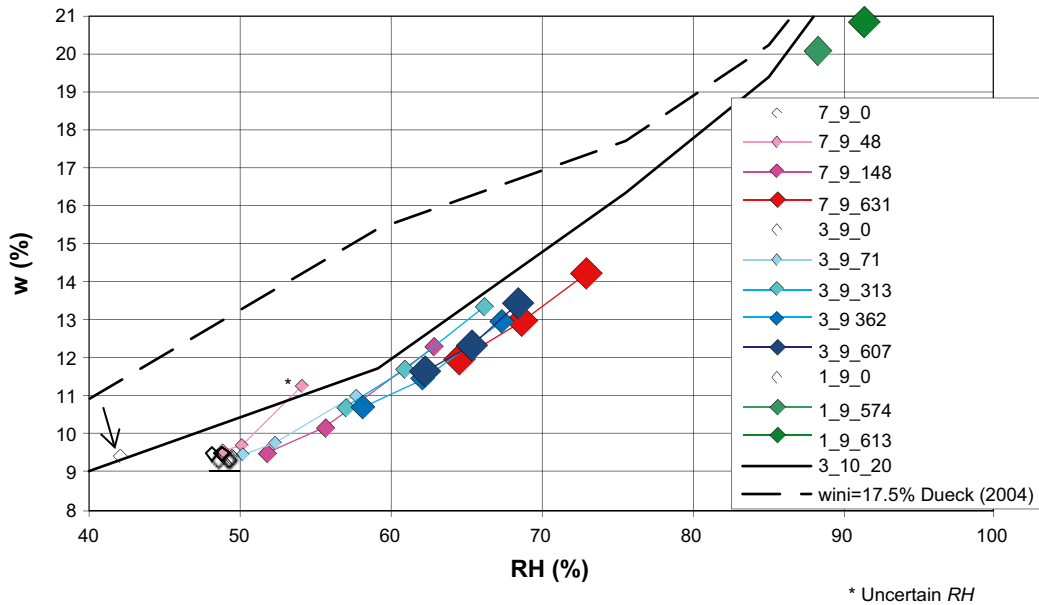

* Uncertain *RH*

Figure 3-41. *Measured RH vs. water content for specimens with an initial water content of $w_i \approx 9\%$. The number of hours is reflected by the size and darkness of the markers and unfilled markers represent the initial state. Two retention curves representing $w_{ini} = 10\%$ (solid line) and $w_{ini} = 17.5\%$ (broken line) are shown.*

3.4.5   Comments

The main purpose of the moisture transport tests was to evaluate and improve existing HM models for unsaturated bentonite. The results from the tests are therefore presented in tabular form in Appendix 3. The test results are presented as distribution of water content and relative humidity after different testing time and exposure to different gradients in relative humidity. Also the swelling pressure is shown.

In Figure 3-41 the moisture states are located on the right hand side of the retention curve for $w_i = 10\%$. This is logical since the relative humidity was measured when boundary stress influenced the specimens.

Boundary stress was also present initially since the specimens were compacted directly into the device and was influenced by the remaining initial radial stress at start. After the start of the test, axial stress rapidly increased from zero when the air circulation was started. It should also be noted that the initial water content was approximately 9% which most probable gives a retention curve adjusted to the right compared to the retention curve for $w_i = 10\%$.

Two points are located on the retention curve. One represents the initial state of the only specimen not compacted into the device and consequently not influence by boundary stress at start, marked with an arrow in Figure 3-41. The second point represents a determination of water content which was made on a specimen in pieces, marked with an asterisk in Figure 3-41. The position where the water content was present is uncertain and might in this case not coincide with the position of the corresponding RH measured at a fixed position.

The suction control in the moisture transport tests was generated by the vapour equilibrium technique combined with an air circulation system where humidified air was transported from the saturated salt solution to the filters at the end surfaces of the specimens. The test results indicate that the RH at the end surface of the specimens was not always constant during the test period. The indications are represented by two cases where an increase in water content is followed by a decrease nearest the wet end, cf. Figure 3-34 in test 3 after t = 313 hours (3_9_313) and Figure 3-36 in test 6 after t = 160 hours (6_16_160).

Presence of a temperature gradient over the equipment could be a possible source of error but this should have resulted in a low but constant value over time. Another reason could be that a too low air circulation rate was chosen. If the moisture transport into and in the bentonite is faster than the supply of moisture in the air circulation system the RH value at the wet end of the specimen could not be kept at the constant predetermined value. The air circulation rate used was 1 l/min.

The basic retention curve, describing the relation between RH and water content w starting from dry material and determined on free swelling specimens, is a basic property. However, for the modelling of the process of saturation, the relation between RH and w should be determined under constrained conditions e.g. constant volume condition. The test results from the moisture transport tests represent such data.

3.5 Moisture redistribution

3.5.1 Method and equipment

Redistribution of moisture was investigated by studying unsaturated specimens exposed to a temperature gradient under constant volume conditions and without supply of additional water. The specimens were heated from the bottom and cooled at the top.

The set-up consisted of an electric hotplate on which the test cell was placed, see Figure 3-42. On top of the cell aluminium cooling flanges, cooled by a fan, were fastened to dissipate heat. Since the temperature gradient should be linear, the circumference of the test cell was insulated to minimize the radial convective heat dissipation. Both heating and cooling was controlled by two on/off regulators (PID-type) using thermocouples inserted in the upper and lower plate respectively (shown with arrows in Figure 3-42).

Since the thermocouples used for the temperature control were placed some distance from the specimen the temperature was also measured at the bentonite surfaces during some tests. These measurements were made by foil Pt100 sensors inserted on the end surfaces of the bentonite, see Figure 3-43.

3.5.2 Preparation of specimen and test procedure

Cylindrical specimens with a diameter of 50 mm and a height of 50 mm were prepared by compressing MX-80 bentonite directly into the test cell to ensure contact between the specimen and the wall of the test cell. It was also of importance to have an initially homogeneous distribution of density over the specimen height and this was achieved by compressing the specimen from two directions. Several tests were made to optimize the compaction technique and the most homogenous specimen was achieved when the compaction was made in increments, equal on both sides.
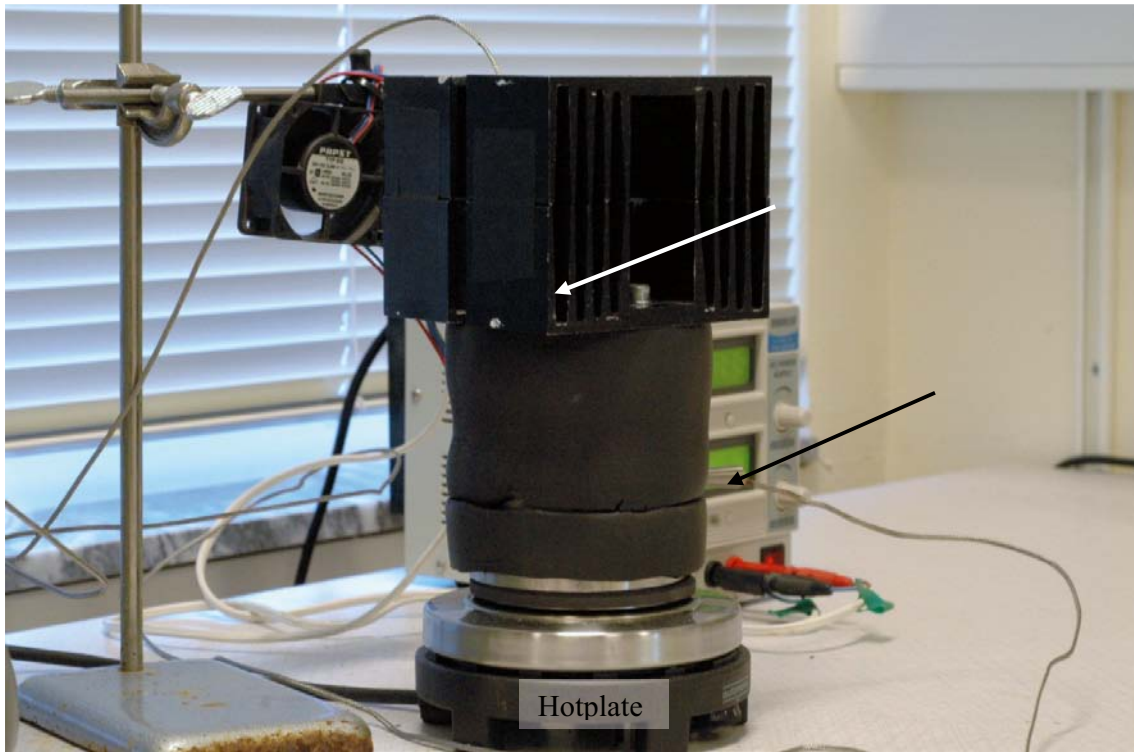
Figure 3-42. *Photo of the set-up. Inserted thermocouples are marked with arrows.*
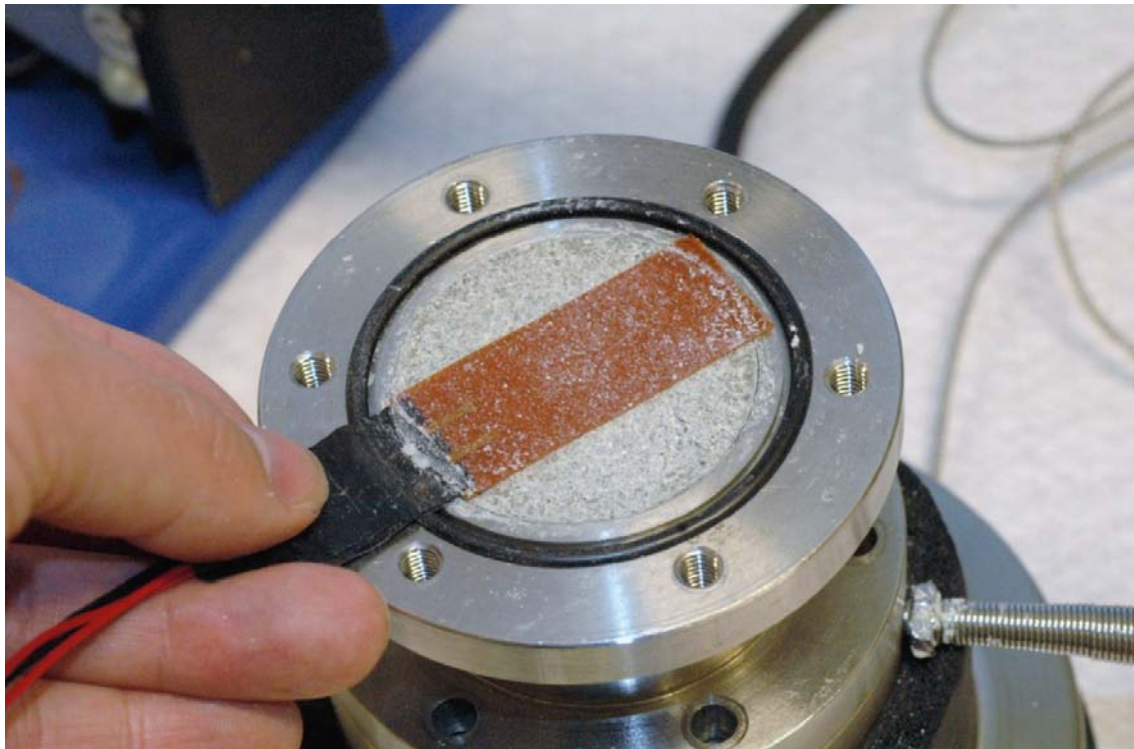

Figure 3-43. *Foil temperature sensor inserted between the sample holder and the end surface of the bentonite.*

Two different initial degrees of saturation were targeted, including 50% and 80%. For each combination of degree of saturation and void ratio the corresponding water content was calculated (see the target values in Table 3-6). MX-80 bentonite was mixed with de-ionized water to the different target water contents.

After compaction and mounting, the temperature gradient was applied and the control was started. The target temperature at the top and bottom was set to 25°C and 35°C for the low gradient and 25°C and 75°C for the high gradient. The testing time was counted from the time when the target temperature was reached. After the testing time the heating was switched off and the specimen was removed from the test device.

The specimens exposed to the high temperature gradient were left to rest and cool for 1 h before removal from the test device. All specimens were divided into 5-6 slices by means of a band saw. The slices were divided into two parts where one part was used for the determination of water content and the other for density measurement.

3.5.3 Test program

The complete test matrix for examining the influence of degree of saturation, void ratio, gradient in temperature and time is shown in Table 3-7 and Table 3-8. The named specimens denote completed tests. In the test series called A the name of each specimen contains information about the target temperature gradient where the letters (a, b) denote 2°C/cm and 10°C/cm, respectively. The name also gives information about degree of saturation (%), void ratio and time (h).

Table 3-6. Target values of w, e, S_r. Calculated values of w corresponding to a combination of S_r and e.

Degree of saturation S_r (%)	50	50	50	80	80
Void ratio e	0.6	0.78	1	0.6	0.78
Calculated w (%)	10.8	14.0	18.0	17.3	22.4

Table 3-7. Test matrix for tests with a temperature gradient of $\Delta T = 2°C/cm$.

Time (h)	$S_r = 50\%$			$S_r = 80\%$	
	e = 0.6	e = 0.78	e = 1	e = 0.6	e = 0.78
6	Aa50_0.6_6	Aa50_0.78_6		Aa80_0.6_6	Aa80_0.78_6
24	Aa50_0.6_24	Aa50_0.78_24		Aa80_0.6_24	Aa80_0.78_24
96	Aa50_0.6_96	Aa50_0.78_96		Aa80_0.6_96	Aa80_0.78_96
240	Aa50_0.6_240	Aa50_0.78_240		Aa80_0.6_240	Aa80_0.78_240

Table 3-8. Test matrix for tests with a temperature gradient of $\Delta T = 10°C/cm$.

Time (h)	$S_r = 50\%$			$S_r = 80\%$	
	e = 0.6	e = 0.78	e = 1	e = 0.6	e = 0.78
6	Ab50_0.6_6	Ab50_0.78_6	Ab50_1_6	Ab80_0.6_6	Ab80_0.78_6
24	Ab50_0.6_24	Ab50_0.78_24	Ab50_1_24	Ab80_0.6_24	Ab80_0.78_24
96	Ab50_0.6_96	Ab50_0.78_96	Ab50_1_96	Ab80_0.6_96	Ab80_0.78_96
240	Ab50_0.6_240	Ab50_0.78_240	Ab50_1_240	Ab80_0.6_240	Ab80_0.78_240
480	Ab50_0.6_480	Ab50_0.78_480	Ab50_1_480		

3.5.4 Test results

The results are evaluated as the distribution of density, water content and degree of saturation along the specimen height and at different time. In Figure 3-44 the variables w, e, S_r and ρ_d are presented as a function of distance from the upper cold surface for specimens exposed to 2°C/cm starting with $S_r = 50\%$ and e = 0.78 and terminated after 6, 24, 96 and 240 hours. In Figure 3-45 the same results are presented as relative or normalized values, calculated as the measured values divided by the average value of the actual variable of the actual specimen.

The complete test results are shown in similar diagrams in Appendix 4. Since the test results will be used for checking and calibrating a material model and associated parameters, all test results are also given as change from the initial states in Appendix 4.

From the reference specimens, the initial distribution of water content and void ratio were determined as shown in Figure 3-46 and Figure 3-47. Both water content and void ratio were shown to be evenly distributed and almost constant for all combinations of void ratio and degree of saturation. The values shown are normalized values where the normalization for each specimen was made by dividing the measured values by the average of the actual specimen.

The distribution of the normalized water content and void ratio from the specimens terminated after 240 h are shown in Figure 3-48 to Figure 3-51.

Exposure to a gradient of ΔT = 2°C/cm resulted in rather small water content gradients for all cases. However, a distinct trend was seen. The specimens exposed to ΔT = 10°C/cm showed very strong gradients. The final water content gradients increased with increased void ratio and decreased degree of saturation.

Exposure to a gradient of ΔT = 2°C/cm resulted in rather small changes of void ratio from the initial state for all cases. The specimens exposed to ΔT = 10°C/cm showed a clear trend compared to the initial state. The final void ratio gradients increased with increased void ratio.

The average values of water content and void ratio used for the normalization in Figure 3-48 to Figure 3-51 are shown in Table 3-9. The average of the final water contents and void ratios from each specimen are shown in Appendix 4.
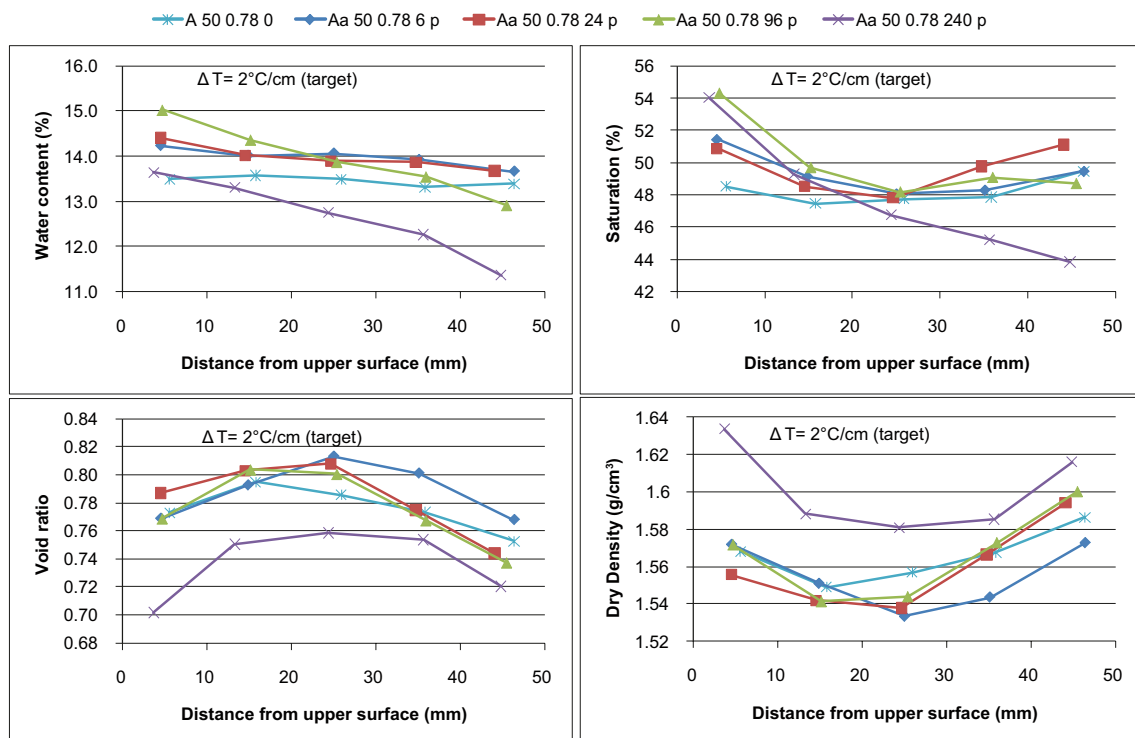

Figure 3-44. *Result shown as water content, degree of saturation, void ratio and dry density as a function of distance from upper surface for the specimens Aa_50_0.78, i.e. having ΔT = 2°C/cm and starting with S_r = 50% and e = 0.78. The initial values and the results after 6, 24, 96 and 240 hours are shown.*
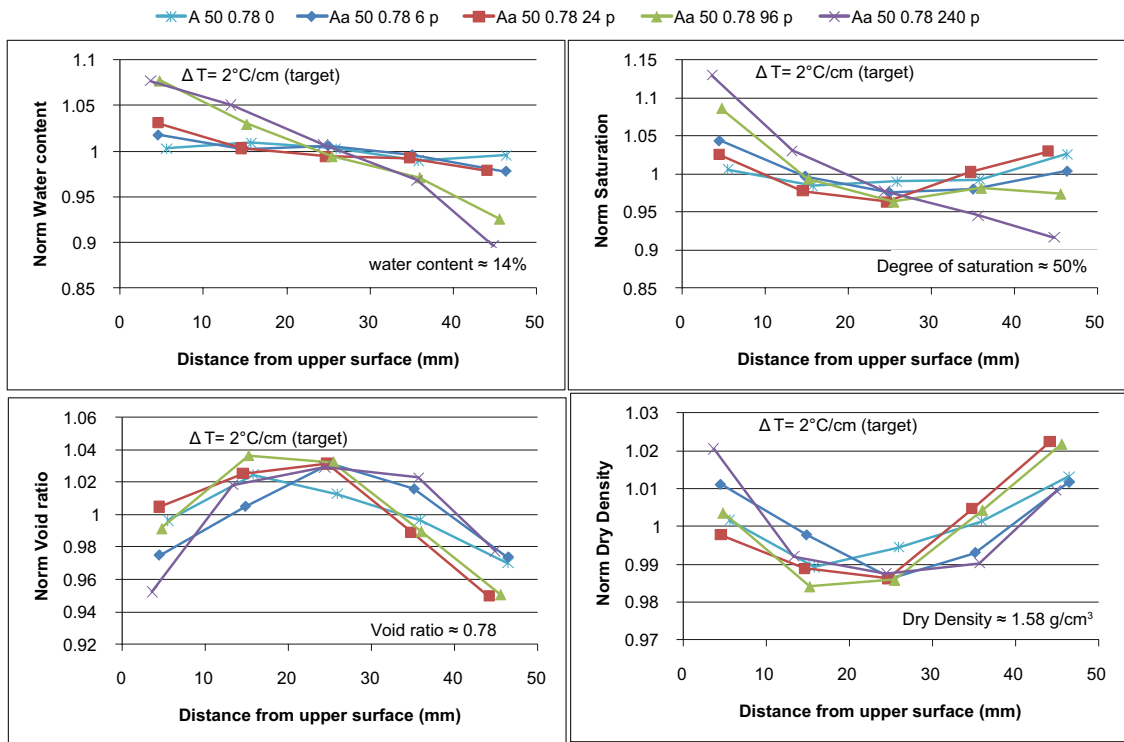
Figure 3-45. *Result from the previous diagram shown as normalized values. The normalization was made by dividing the measured values by the average of the actual specimen.*
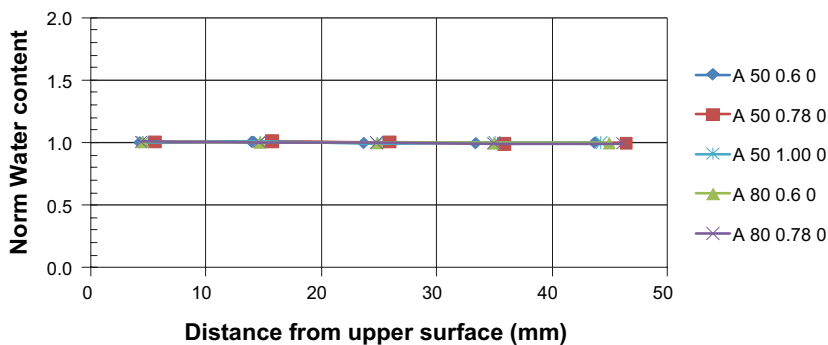

Figure 3-46. *Initial distributions of water content as normalized values. The labels denote the test series, the initial degree of saturation (%), the void ratio and the time which was 0 h.*
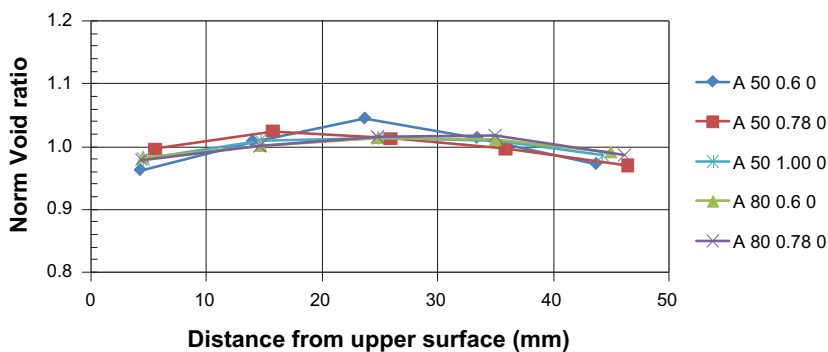

Figure 3-47. *Initial distributions of void ratio as normalized values. The labels denote the test series, the initial degree of saturation (%), the void ratio and the time which was 0 h.*

Figure 3-48. *Normalized water content after 240 hours with a temperature gradient of 2°C/cm. The labels denote type of test, initial degree of saturation (%), void ratio and time (h). The letter p indicates the use of hotplate for the heating.*
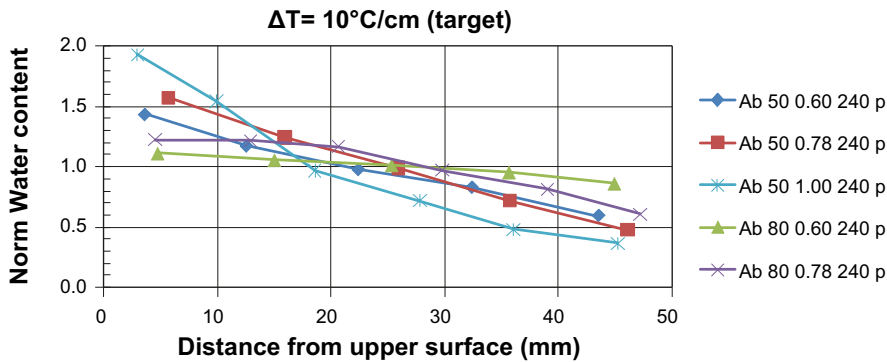
Figure 3-49. *Normalized water content after 240 hours with a temperature gradient of 10°C/cm. The labels denote type of test, initial degree of saturation (%), void ratio and time (h). The letter p indicates the use of hotplate for the heating.*

Figure 3-50. *Normalized void ratio after 240 hours with a temperature gradient of 2°C/cm. The labels denote type of test, initial degree of saturation (%), void ratio and time (h). The letter p indicates the use of hotplate for the heating.*
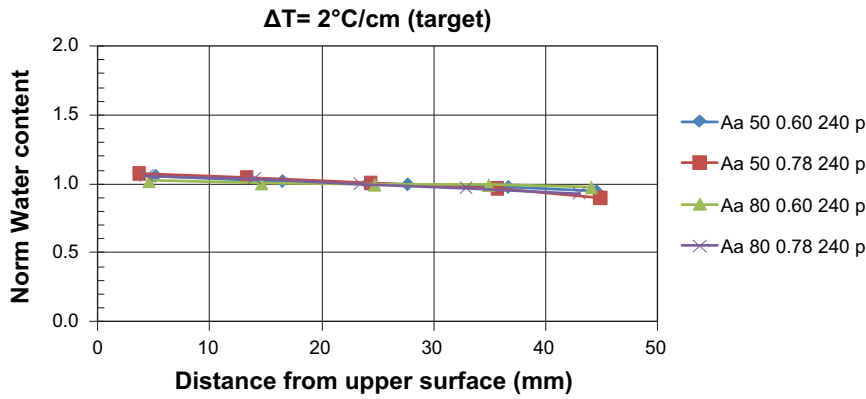
ΔT= 10°C/cm (target)

Figure 3-51. *Normalized void ratio after 240 hours with a temperature gradient of 10°C/cm. The labels denote type of test, initial degree of saturation (%), void ratio and time (h). The letter p indicates the use of hotplate for the heating.*
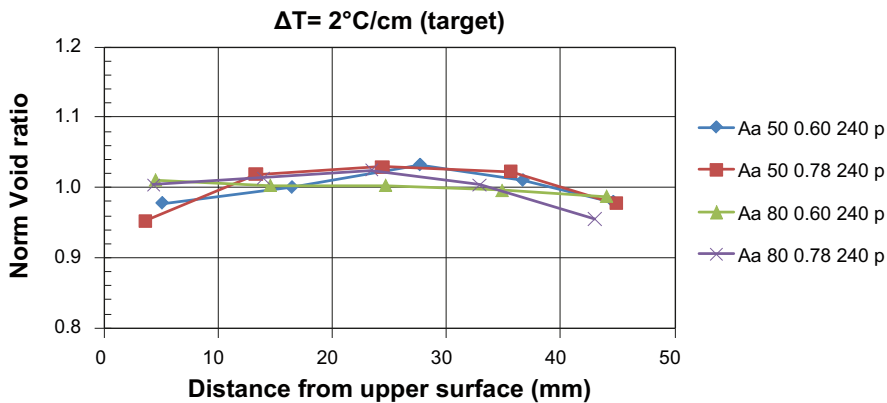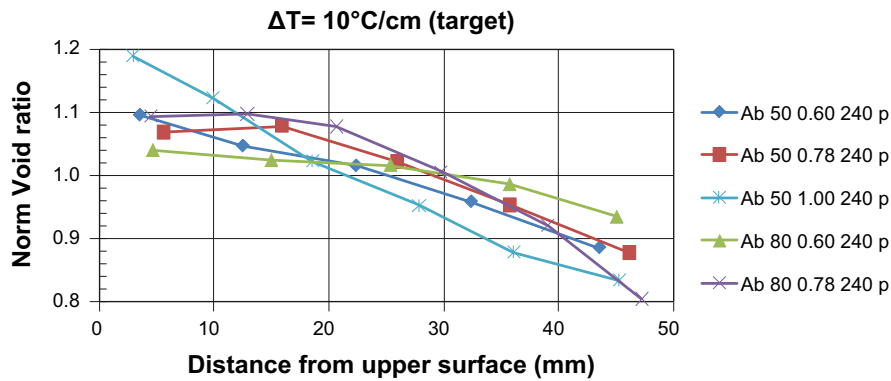
Table 3-9. Average values for the specimens terminated at 240 h. The labels denote type of test (A), gradient in temperature (a–2°C/cm, b–10°C/cm), degree of saturation (%), void ratio and testing time (240 h). The letter p indicates the use of a hotplate for the heating.

Specimen label	Water content (%)	Void ratio
Aa 50 0.60 240 p	10.8	0.63
Aa 50 0.78 240 p	12.7	0.74
Aa 80 0.60 240 p	17.2	0.60
Aa 80 0.78 240 p	24.1	0.80
Ab 50 0.60 240 p	11.2	0.65
Ab 50 0.78 240 p	14.1	0.78
Ab 50 1.00 240 p	19.5	0.95
Ab 80 0.60 240 p	17.0	0.62
Ab 80 0.78 240 p	24.2	0.78

As mentioned earlier the temperature regulation was based on temperatures measured by thermocouples placed some distance from the specimen. In some reference tests the temperature was also measured at the bentonite surfaces with Pt100 sensors. For the low gradient tests with the target 2°C/cm, the actual value varied between 2.0 and 2.2°C/cm with an average of 2.1°C/cm. For the high gradient tests with the target 10°C/cm, the actual value varied between 8.9 and 9.7°C/cm with an average value of 9.2°C/cm. The average temperatures at the bottom and top were 37.2°C and 26.7°C with the low gradient and 78.1°C and 32.3°C with the high gradient, respectively. The results are shown in Appendix 4.

3.5.5 Comments

The test results are focused on the distribution of density, water content and degree of saturation after different testing times and exposed to different temperature gradients. In general the test results will be used for checking and calibrating a material model and associated parameters but the following observations could be made:

- The gradients in water content and void ratio were found to increase with the following conditions:
  - longer testing time
  - higher thermal gradient
  - larger initial void ratio.
- The gradients in water content were constant or increased with decreasing degree of saturation.
- After 96 h only small changes were seen in almost all tests.

In addition some comments could be made regarding the temperature gradients, the constant volume conditions, evaporation during the tests and the method used for the determination of density.

Temperature gradients

In addition to the measurement made on the bentonite surfaces the temperature was also measured at mid-height in four tests, one with the low gradient and three with the high gradient. With the low gradient the temperature at mid-height was 0.5°C lower than the average of the surface temperatures and with the high gradient the measured temperature was 0.5°C and 1.7°C lower than the average of the surface temperatures. The referred measurements were made at mid-height and at the centre of the cross section. One additional measurement with the high gradient was made at mid-height but at 7 mm, approximately the quarter of the diameter, from the cylinder wall and the measured temperature was 1.6°C lower than the average of the surface temperatures. From the measurements at mid-height the temperature of the specimen with the low gradient was approximately $T \approx 31°C$ and with the high gradient $T \approx 56°C$.

The measured values showed that the target gradients were almost achieved and that the gradients were almost linear over the height. In addition, there was an indication that the gradient was one dimensional i.e. the gradient over the cross section was small compared to the gradient over the height.

Constant volume condition

At termination of all tests there was still contact between the specimen and the plates at the bottom and top, respectively. However, in the majority of tests performed with the temperature gradient of 10°C/cm and terminated after 96 hours or more, a slightly smaller diameter was measured at the very end of the specimen towards the warm side compared to the diameter measured at the cool side. The diameter was initially 50 mm and the difference between the warm and cool sides was about 0.3 mm on those specimens. This could have been caused by a small shrinkage of the warm side or by a small expansion of the cool end at dismantling.

From the average void ratio of the reference specimens and the average void ratio determined on each specimen after termination, information about the change in volume can be gained. The difference was less than 0.05 for all specimens but for the majority of the specimens the difference was less than 0.03. The majority of the specimens had a smaller average void ratio after the tests compared to the corresponding reference which indicate decreased volume. However, these values include the scatter involved in the manufacturing or compaction of the specimens.

Evaporation

Evaporation can be evaluated from the cases where the water content of the bentonite was determined just before compaction and mounting of a specimen. A decrease less than 0.4% was measured between start and termination on specimens with water contents between 10.8% and 24%. For example one of the specimens (Ab 50 0.6 480) was compacted from bentonite with a water content of 10.8% and after exposure to a temperature gradient of 10°C/cm for 480 h the average water content after dismantling was 10.4%. The evaporation was considered to be even lower than 0.4% since this value also includes the loss of water during the dismantling and cutting the specimens into slices.

Method used for determination of density

The density was determined according to Section 2.2. The method used for determination of the volume, i.e. submerging the specimen into paraffin oil, involves an inaccuracy when used for specimens with low degree of saturation. Trapped air might escape during the measurement and paraffin oil might be drawn into the specimen during the time of measurement. For the specimen with lowest degree of saturation, i.e $S_r = 18\%$, the change in evaluated density during the first 20 seconds after submerging was 28 kg/m³ from 1,749 kg/m³ to 1,777 kg/m³ with corresponding void ratio 0.65 and 0.63, respectively. The density and corresponding void ratio representing this specimen was considered to be 1,760 kg/m³ and 0.64, evaluated after 15 seconds which was used for all other specimens.

4 Laboratory tests on saturated MX-80

4.1 General

This section was written by L Börgesson and L-E Johannesson 1999 and is part of an unpublished report.

4.2 Triaxial tests

4.2.1 Introduction

The model for simulating the mechanical behaviour of water saturated bentonite that has been suggested by Börgesson et al. (1995) includes a non-linear failure surface and a cap in the q-p plane that separates elastic from plastic behaviour (q = Mises' deviatoric stress; p = average stress). The cap intersects the p-axis at the pre-consolidation stress, which corresponds to the maximum stress that the material has been exposed to. The bentonite in a repository is planned to be compacted with very high pressure at a water content below water saturation and previous triaxial tests on MX-80 have been made on samples produced in that way. After compaction, those samples were saturated in an oedometer and then mounted in a triaxial cell, which means that the stress history expressed as effective stresses are indeterminate. However, in order to determine the shape of the cap, tests on samples that have a known stress history are required. Two such samples have been prepared and tested.

4.2.2 Preparation of samples

A large MX-80 sample with an initial height of about 30 mm and with a diameter of 152 mm was prepared in a Rowe oedometer (see Figure 4-1). The initial water content of the material was about 10%. A pressure of 500 kPa was applied on the top of the MX-80 bentonite by pressurising the water in the diaphragm of the oedometer. At this stage the sample was allowed to take up distilled water through the two porous discs at the top and the bottom. The deformation of the sample was continuously recorded. The results from the measurements are shown in Figure 4-2. The figure shows that at first the height of the sample was reduced due to the load applied on the sample, but after a few days it began to increase in height due to swelling during the water uptake process. After about two weeks the sample was saturated at the external axial effective pressure 500 kPa. A new load step (500–1100 kPa)
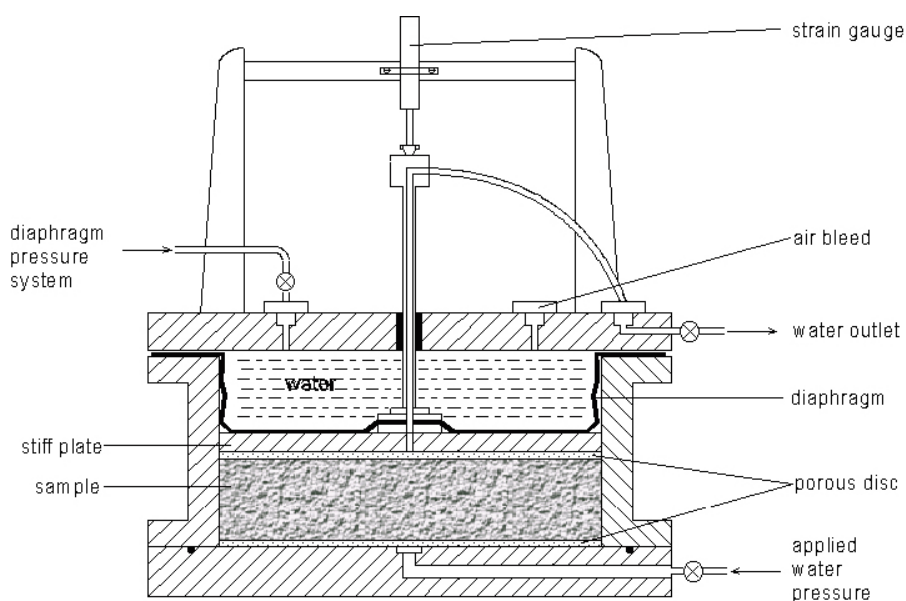

Figure 4-1. *Rowe oedometer with MX-80 sample having a diameter of 152 mm and an initial height of 30 mm.*
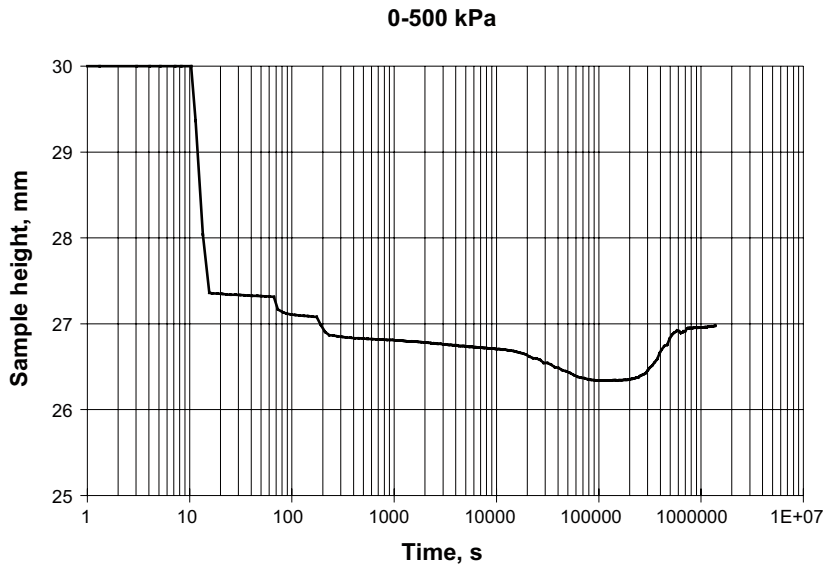
0-500 kPa

Figure 4-2. Measured deformation in the Rowe oedometer at the first load step (0–500 kPa).

was then applied to the sample, which resulted in a compression. The measured deformation of the sample during this load step is shown in Figure 4-3. After about 4 months the sample was taken out from the oedometer. The sample had a height of about 25 mm after the last load step. Several smaller samples with an approximate diameter of 35 mm were then cut from the big sample. The density and water content were measured on five of them. The results from these measurements are shown in Table 4-1.

Two new samples (T38 and T39) with heights of about 75 mm, were made by stacking three smaller samples on top of each other. They were mounted in two triaxial cells where they were further consolidated in order to know the exact preconsolidation pressure. The consolidation was made in the following three steps:

- A cell pressure of 1,100 kPa was applied to the samples with closed pore pressure valves.
- After about 5,500 hours (230 days) the cell pressure was increased to 1,500 kPa and a backpressure of 200 kPa was applied.
- After about another 1,000 hours (40 days) the pore pressure valves were closed and the pore pressure in the samples measured until equilibrium was reasonably well reached.

Measured pore and cell pressures during the consolidation phase are shown in Figure 4-4.
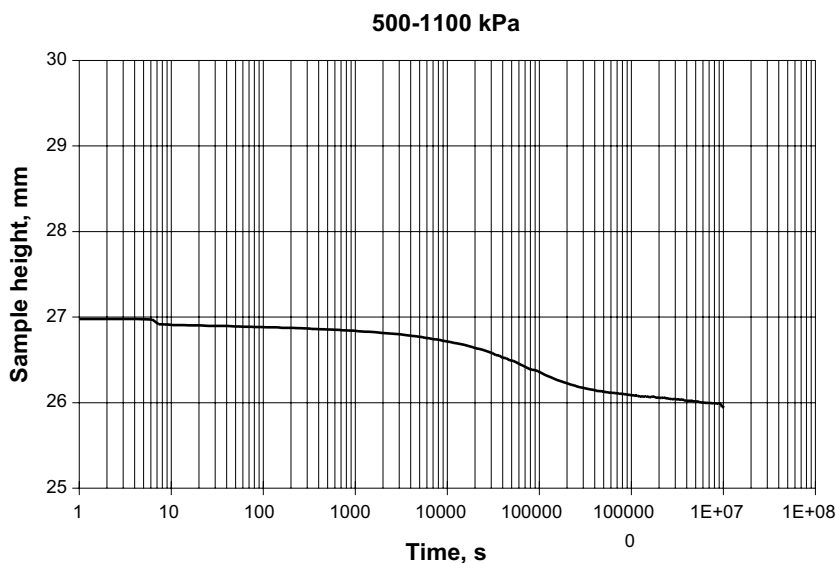
500-1100 kPa

Figure 4-3. Measured deformation in the Rowe oedometer at the second load step (500–1,100 kPa).

Table 4-1. Water content (*w*), bulk density (*ρ*), degree of saturation (*S*_r) void ratio (*e*) and density at saturation (*ρ*_m) measured on samples cut from the clay that was consolidated in the oedometer.

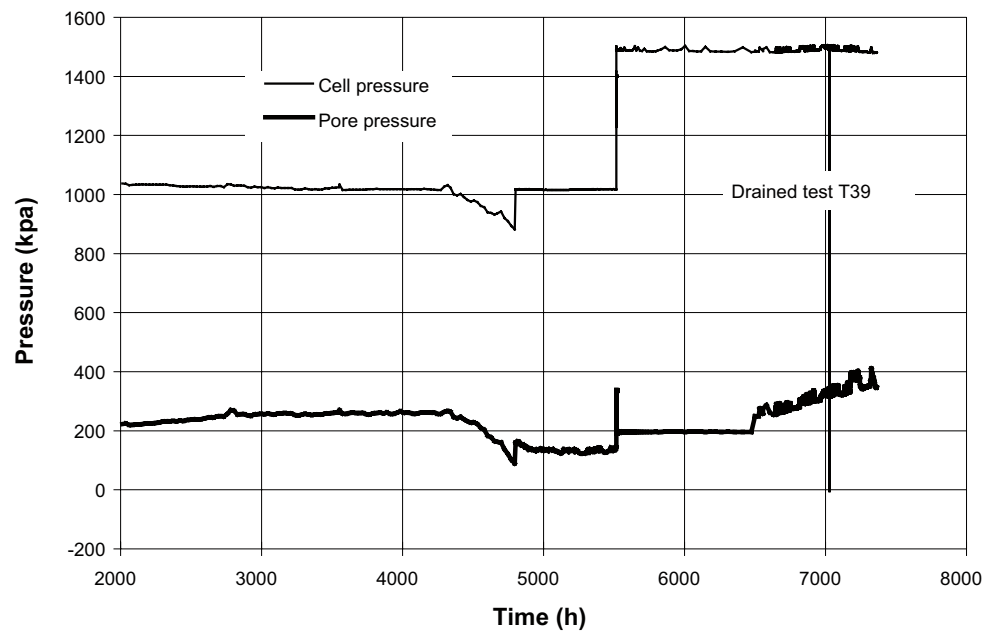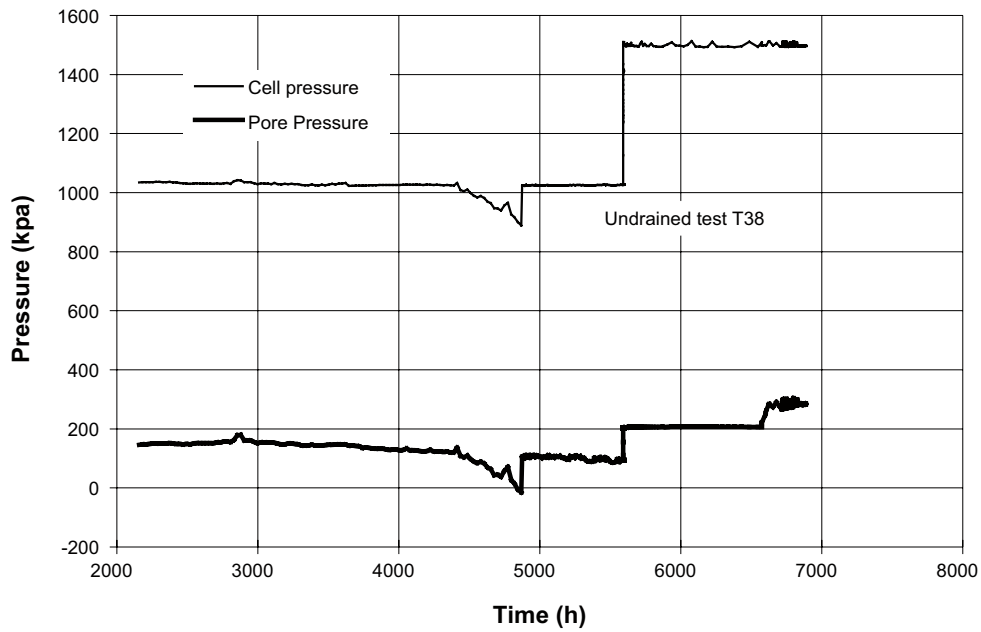|	w (%)	ρ (g/cm³)	S_r (%)	e	ρ_m (g/cm³)
Sample A2	44	1.790	98.5	1.230	1.798
Sample B2	44	1.792	98.6	1.227	1.799
Sample C2	43	1.788	97.6	1.221	1.801
Sample D2	43	1.794	98.7	1.223	1.801
Sample E2	43	1.800	99.1	1.211	1.805
Mean	43	1.794	98.5	1.219	1.802

***Figure 4-4**. Measured cell pressure and pore pressure during consolidation of the two samples in the triaxial cells.*

4.2.3 Test results

After preparation, saturation and consolidation, the shearing phase of the triaxial tests was started. One test was conducted as an undrained triaxial test (T38) and the other one (T39) was allowed to change in volume during the shearing (drained test). The undrained test was made with a constant deformation rate of 0.001 mm/min, while the deformation rate of the drained test was about 0.0001 mm/min. During both tests the vertical strain (ε), the cell pressure (σ_3), the vertical stress (σ_1) and the pore pressure (u) were continuously measured. The volume change of the drained test was also measured by reading the height of a water meniscus, which was in contact with the sample. The deviator stress (q) and the effective average stress (p') defined according to Equations 4-1 and 4-2 were calculated with the following equations:

$$q = \sigma_1 - \sigma_3 \qquad\qquad (4\text{-}1)$$

$$p' = \frac{\sigma_1 + 2\sigma_3 - 3u}{3} \qquad\qquad (4\text{-}2)$$

The results from the tests are plotted in Figure 4-5 and Figure 4-6. After shearing, the water content and density were measured at three locations in each sample. The averages of the measurements are shown in Table 4-2, which also shows the deviator stress and the effective average stress at failure.

4.2.4 Discussion and conclusions

The results will be used for checking the material model and to yield information about some of the parameters in the model. Since the samples are normally consolidated, the shape of the cap can be determined from the undrained test and the plastic strain during expansion of the cap can be determined from the drained test. The tests can be simulated with FEM calculations and the models checked by comparing measured and calculated results.

A comparison of the results with results from earlier triaxial tests made directly on samples compacted with natural water content and saturated at constant volume in oedometers show that there is no significant difference in behaviour. However, those samples were compacted with much higher pressure than the swelling pressure. This shows that the position of the cap in the q-p plane (see Börgesson et al. 1995) is determined by the history of the void ratio rather than by the history of the effective stress.

The deviator stress at failure as a function of the effective stress for the two tests is plotted in Figure 4-7 together with other results. The figure shows that the shear strength also agrees very well with the strength measured in previous tests.

Figure 4-8 shows the measured swelling pressure plotted as a function of void ratio for a number of swelling pressure tests (Börgesson et al. 1995) together with the effective average stress at the end of the described triaxial tests. The new tests yield a little higher pressure, a phenomenon which has been observed during the loading phase of normally consolidated samples in oedometer tests and is caused by irrecoverable plastic strains.
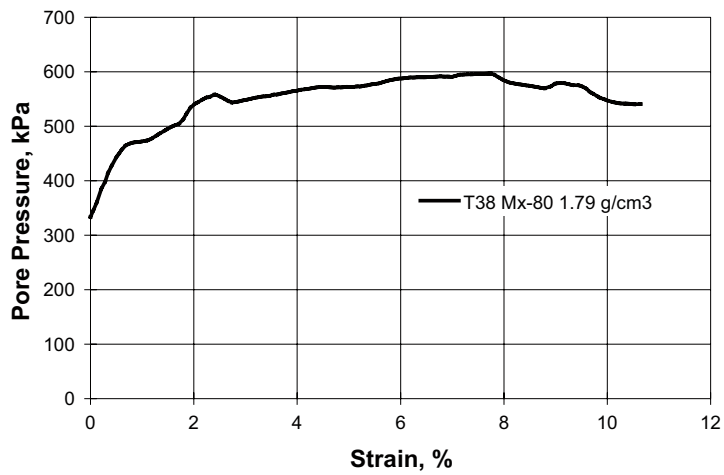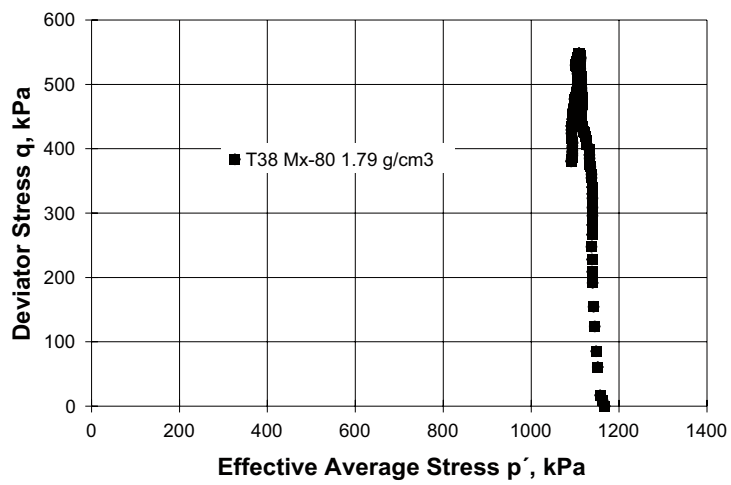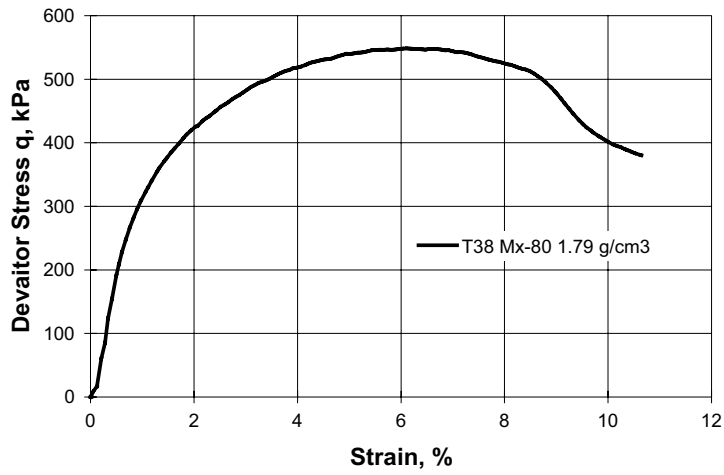
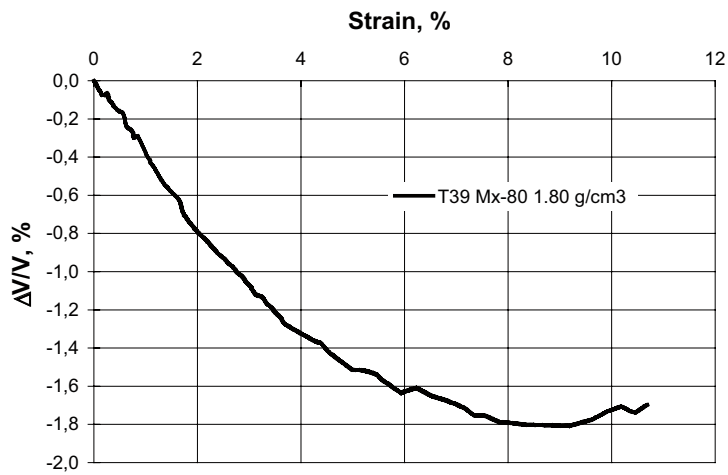**Figure 4-5**. *Results from the undrained triaxial test T38.*
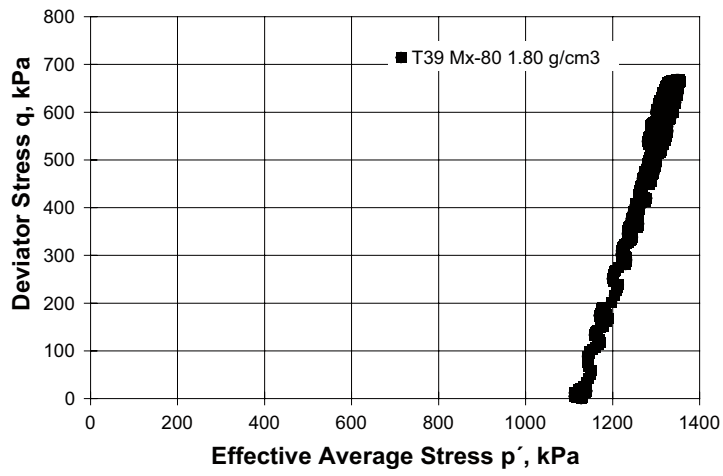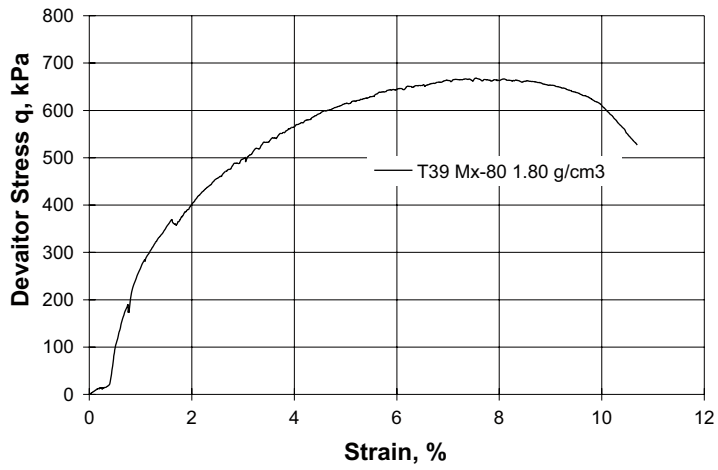
Figure 4-6. *Results from the drained triaxial test T39.*

Table 4-2. Water content (*w*), bulk density (*ρ*), degree of saturation (*S_r*), void ratio (*e*) and density at saturation (*ρ_m*) measured after the tests. The deviator stress (*q_f*) and effective average stress (*p'_f*) at failure are also shown.

Test No.	*w* (%)	*ρ* (g/cm³)	*S_r* (%)	*e*	*ρ_m* (g/cm³)	*q_f* (kPa)	*p'_f* (kPa)
T38	44	1.790	98.4	1.228	1.799	549	1.109
T39	43	1.797	98.5	1.212	1.805	667	1.346

Figure 4-7. *Measured deviator stress at failure plotted as a function of the effective average stress for the two triaxial tests (unfilled triangles) together with earlier test results.*

Figure 4-8. *Relation between measured average effective stress and void ratio in earlier tests and the two new tests (unfilled squares).*

References

SKB's (Svensk Kärnbränslehantering AB) publications can be found at www.skb.se/publications.

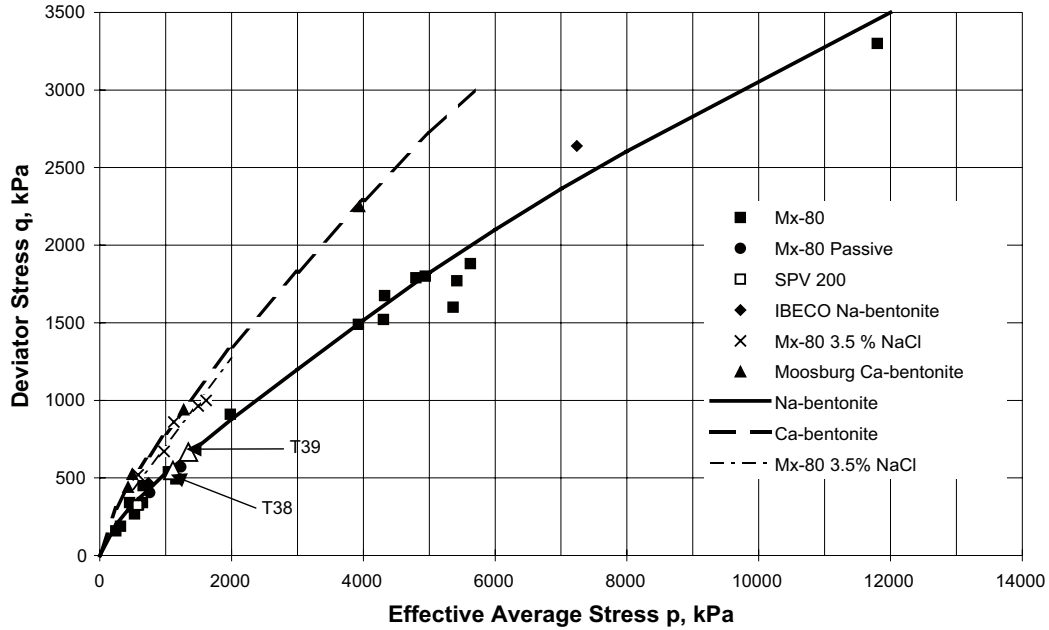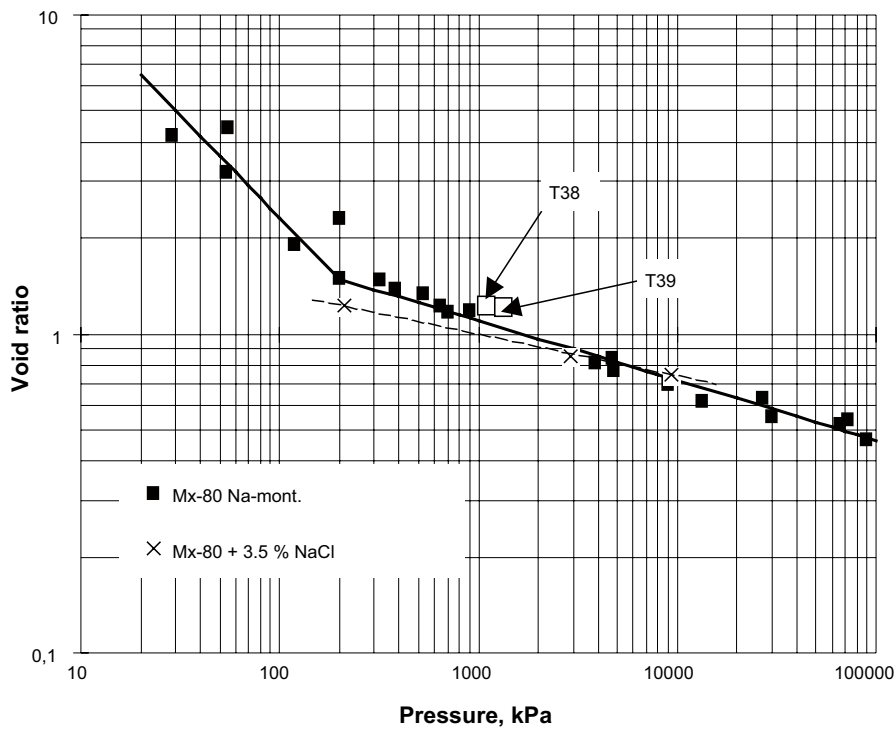**Börgesson L, 2001.** Äspö Hard Rock Laboratory. Compilation of laboratory data for buffer and backfill materials in the Prototype Repository. SKB IPR-01-34, Svensk Kärnbränslehantering AB.

Börgesson L, Hökmark H, Karnland O, 1988. Rheological properties of sodium smectite clay. SKB TR 88-30, Svensk Kärnbränslehantering AB.

Börgesson L, Johannesson L-E, Sandén T, Hernelind J, 1995. Modelling of the physical behaviour of water saturated clay barriers. Laboratory tests, material models and finite element application. SKB TR 95-20, Svensk Kärnbränslehantering AB.

Clarke E C W, Glew D N, 1985. Evaluation of the thermodynamic functions for aqueous sodium chloride from equilibrium and calorimetric measurements below 154°C. Journal of Physical and Chemical Reference Data, 14, pp 489–610.

Dueck A, 2004. Hydro-mechanical properties of a water unsaturated sodium bentonite: laboratory study and theoretical interpretation. Ph.D. thesis. Lund Institute of Technology, Sweden.

Dueck A, 2007. Results from suction controlled laboratory tests on unsaturated bentonite – verification of a model. In: Schanz T (ed). Experimental unsaturated soil mechanics. Berlin: Springer. (Springer proceedings in physics 112), pp 329–335.

Dueck A, 2008. Laboratory results from hydro-mechanical tests on a water unsaturated bentonite. Engineering Geology, 97, pp 15–24.

Dueck A, Börgesson L, 2007. Model suggested for an important part of the hydro-mechanical behaviour of a water unsaturated bentonite. Engineering Geology, 92, pp 160–169.

Fredlund D G, Rahardjo H, 1993. Soil mechanics for unsaturated soils. New York: Wiley.

Greenspan L, 1977. Humidity fixed points of binary saturated aqueous solutions. Journal of Research of the National Bureau of Standards, A. Physics and Chemistry, 81A, pp 89–96.

Kahr G, Kraehenbuehl F, Stoeckli H F, Müller-Vonmoos M, 1990. Study of the water-bentonite system by vapour adsorption, immersion calorimetry and X-ray techniques: II. Heats of immersion, swelling pressures and thermodynamic properties. Clay Minerals, 25, pp 499–506.

Karnland O, Olsson S, Nilsson U, 2006. Mineralogy and sealing properties for various bentonites and smectite-rich clay materials. SKB TR-06-30, Svensk Kärnbränslehantering AB.

Villar M V, Martín P L, Lloret A, 2005. Determination of water retention curves of two bentonites at high temperature. In: Tarantino A, Romero E, Cui Y J (eds). Advanced experimental unsaturated soil mechanics. EXPERUS 2005. Prodeedings of an International Symposium on Advanced Experimental Unsaturated Soil Mechanics, Trento, Italy, 27–29 June 2005. Leiden: Balkema, pp 77–82.

Wadsö L, Svennberg K, Dueck A, 2004. An experimentally simple method for measuring sorption isotherms. Drying Technology, 22, pp 2427–2440.

Retention curves

Results from all retention curves determined with the method with jars in this study are presented in tabular form in Table A1-1.

Values of the criterion Ω

The criterion Ω is used for the decision to terminate a series of measurements, Equation 3-1. The final values of Ω for all series measured with the jars are shown in Figure A1-1. The results are further commented on in Section 3.2.4.

Equation suggested for the retention curves

Test results from measurements of retention curves with free swelling samples starting from different initial water contents were shown in Figure 3-3. A continuous formulation of the specific retention curve is useful for modelling purpose. A mathematical relation according to Equation A1-1 was previously formulated by Kahr et al. (1990). The equation was used with different constants (a, b) to coincide with the measured values representing the different initial water contents; 0% (5.5, 0.14), 10% (6.3, 0.16), 17.5% (7.25, 0.2), 27% (7.5, 0.2) and 64% (6.3, 0.14).

$$w = (a - \ln[-(10^{-6} \cdot \rho_w \cdot R \cdot T/\omega_w) \cdot \ln(RH/100)])/b \ (\%) \tag{A1-1}$$

In Figure A1-2 the curves with the suggested constants are plotted in the range where it is applicable, i.e. where the coincidence with the measurements is good.

Table A1-1. Results from jars. Measured final water contents (%) at different temperatures and RH when starting from given initial water content w$_{initial}$. The labels for the test series are shown to the right.

Temperature 10°C	mol. sieve	LiCl	MgCl$_2$	NaBr	NaCl	KCl	2 molal NaCl	K$_2$SO$_4$	label
RH (%)	0.0	11.3	33.5	62.2	75.7	86.8	93.2	98.2	
w$_{initial}$ (%)									
0	0.5	1.2	3.0	9.4	13.9	18.6	23.0	35.6	8_0_10

Temperature 20°C	mol. sieve	LiCl	MgCl$_2$	NaBr	NaCl	KCl	2 molal NaCl	K$_2$SO$_4$	
RH (%)	0	11.3	33.1	59.1	75.5	85.1	93.2	97.6	
w$_{initial}$ (%)									
0		0.7	2.6	7.3	13.7	17.5	22.5	31.8	1_0_20
9.8		2.6	8.0	11.7	16.4	19.4	23.8	32.7	3_10_20
64.0	0.3	3.0	9.2	16.5	20.9	23.1	28.6	37.1	5_64_53

Temperature 26°C	mol. sieve	LiCl	MgCl$_2$	NaBr	NaCl	KCl	2 molal NaCl	K$_2$SO$_4$	
RH (%)	0.0	11.3	32.7	57.3	75.2	84.2	93.1	97.2	
w$_{initial}$ (%)									
0	0.2	1.1	2.9	7.3	14.0	17.7	23.0	32.4	7_0_26

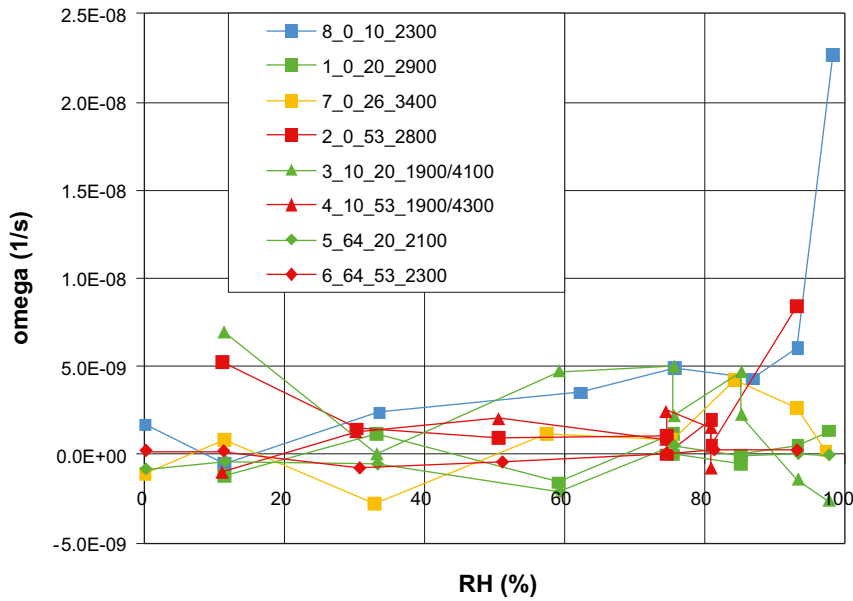| Temperature 53°C	mol. sieve	LiCl	MgCl$_2$	NaBr	NaCl	KCl	2 molal NaCl	K$_2$SO$_4$	
RH (%)	0	11.1	30.2	50.5	74.5	80.9	93.0	95.8	
w$_{initial}$ (%)									
0		0.7	2.1	5.0	13.4	15.8	22.9		2_0_53
9.8		1.3	6.4	9.3	15.8	17.9	26.8		4_10_53
64.0	0.0	1.3	6.9	11.2	19.6	21.4	28.7		6_64_53

Figure A1-1. *The final values of omega Ω (Equation 3-1) for all series with jars. The legend shows: name of the test_initial water content (%)_temperature (°C)_total time (h). In test series 3 and 4 the samples placed at low RH were terminated earlier than the samples placed at high RH.*
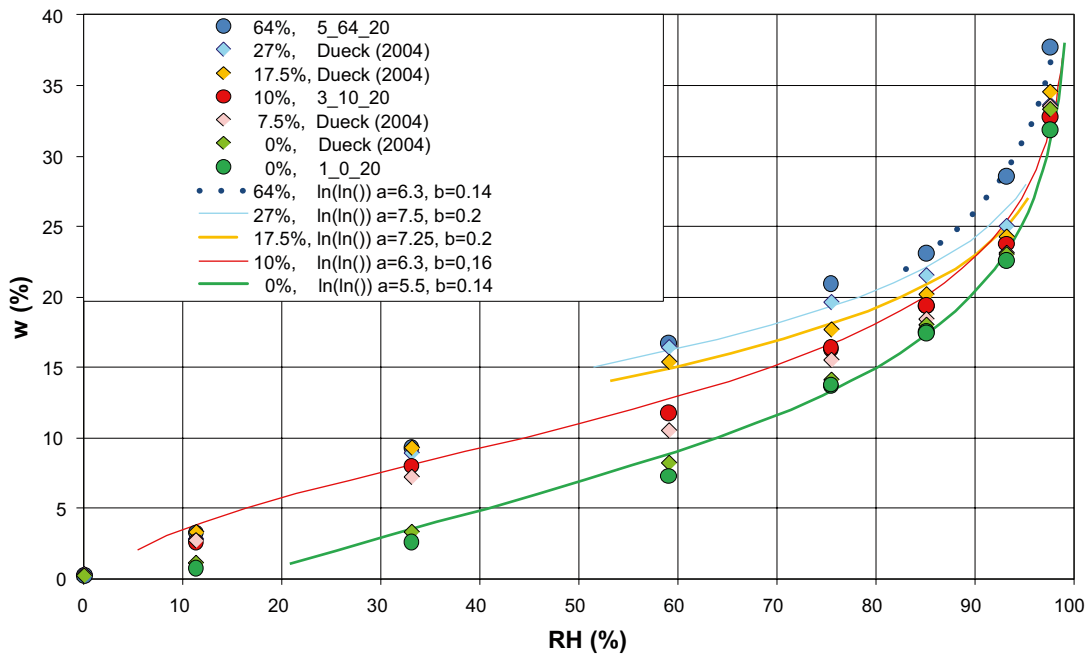

Figure A1-2. *Retention curves from this and previous investigations.*

Model of diffusion in air in a jar

The set up shown in Figure A1-3(left) was used for the determination of retention curves by the method with jars. A simplified model of the transport of water vapour through the air filled gap between the surface of the salt solution and the bentonite surface in the jars was made according to Figure A1-3(right) where the following was assumed:

The diffusion in air takes place in a ring shaped area around the sample (light pink).

The conditions at the level of the upper boundary of the pan with the sample are assumed to be the same as in the cross section of the jar, Figure A1-4.
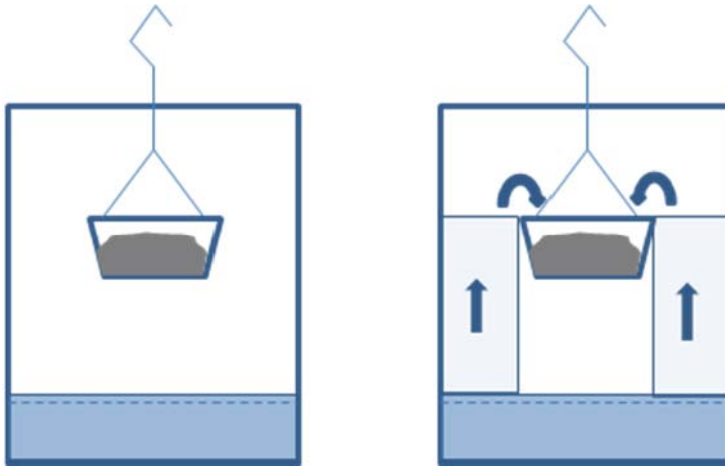
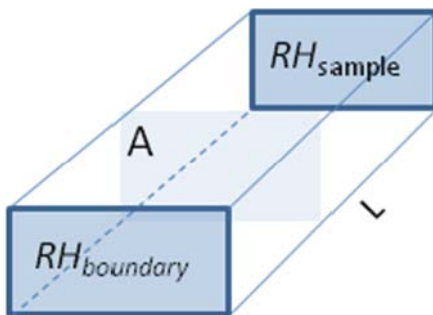**Figure A1-3.** *Test sample in the jar (left) and air diffusion in a ring shaped area around the sample (right).*

Figure A1-4. *Simplified 1D diffusion model with RH$_{boundary}$, RH$_{sample}$, the cross section area A and the length L.*

The vapour diffusion from the surface of the salt solution to the sample was calculated as driven by a gradient in vapour pressure. From Fick's law Equation A1-2 was derived for the mass increments Δm during the time interval Δt.

$$\Delta m = \frac{A \cdot D}{L} \cdot p_s \cdot (RH_{boundary} - RH_{sample}(w)) \cdot \frac{1}{100} \cdot \Delta t \qquad \text{(A1-2)}$$

The calculation was made at temperatures T = 20°C and 53°C with the diffusion constant D = 2.06·10^{-10} (s) and 2.36·10^{-10} (s), respectively. In the calculations the following constants were used: the distance to the water surface L = 0.05 m, the area of the specimen A = 0.001571 m^2 and the saturation pressure of water vapour p$_s$ = 2.3 kPa and 14.2 kPa at 20°C and 53°C, respectively. RH$_{sample}$ (w) (%) was calculated according to the retention curve given by Equation A1-1 for the actual w and the correct initial w. RH$_{boundary}$ (%) was constant and set by the salt solution used. The dry mass of the sample was 10 g.

Results from the modelling at T = 20°C are shown together with measured results in Figures A1-5 and A1-6. Both absoption from w$_{ini}$ = 0% and desorption from w$_{ini}$ = 64% are shown and lines with markers indicate measurements. The colours (medium blue, green, dark blue, light blue) denote the RH generated by the salt solution (97.6%, 93.2%, 75.5%, 59.1%).

In Figures A1-7 and A1-8 results from the model are presented with measurements at RH = 93% at two temperatures. Lines with markers indicate measurements. The colours (brown, blue) denote the temperatures (20°C, 53°C). According these diagrams the required time for the diffusion in air is larger at 20°C than at 53°C.
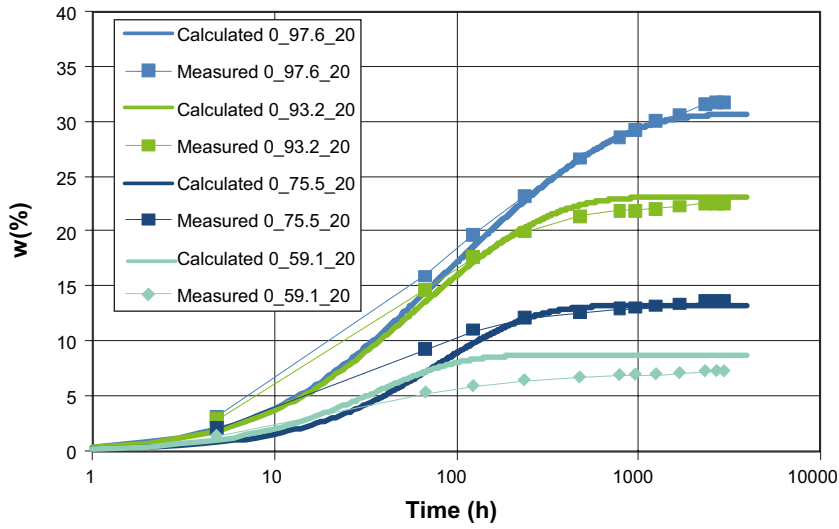
Figure A1-5. *Model results and measurements of absorption from dry conditions (w_i = 0%).*
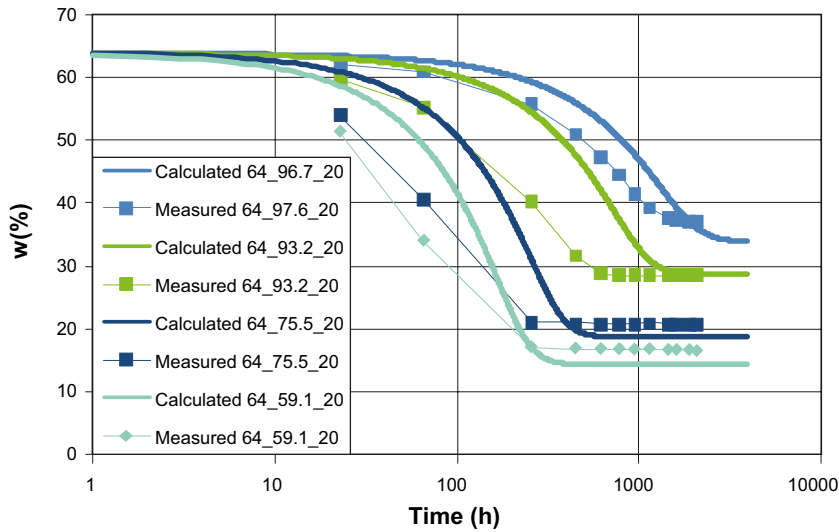

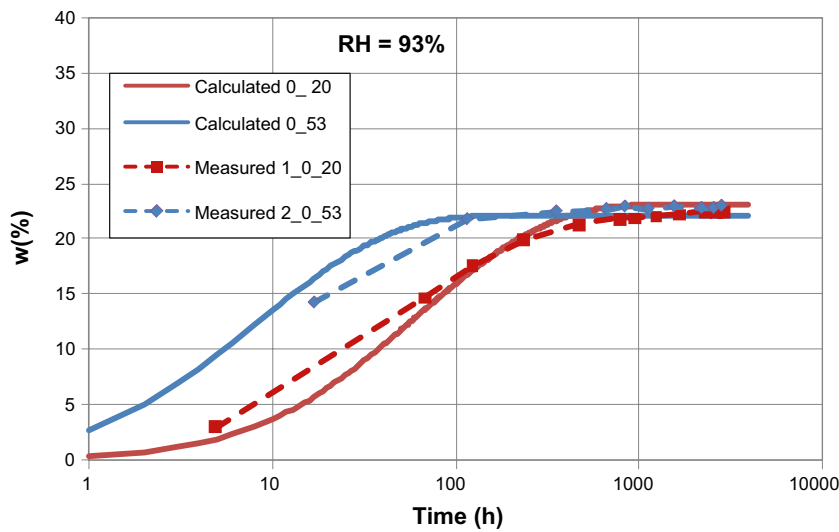**Figure A1-6.** *Model results and measurements of desorption from wet conditions (w_i = 64%).*

Figure A1-7. *Model results and measurements of absorption in RH = 93% from dry conditions (w_i = 0%) at 20°C and 53°C.*
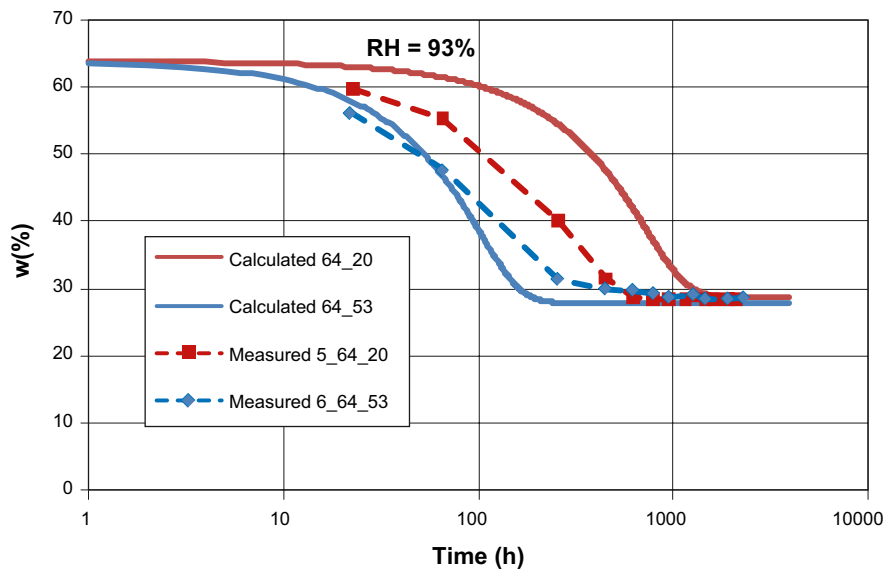
Figure A1-8. *Model results and measurements of absorption in RH = 93% from wet conditions (w_i = 64%) at 20°C and 53°C.*

The simplified analysis of the time delay at absorption and desorption at RH = 98%, 93%, 76% and 59% at the temperature 20°C and at RH = 93% at the temperatures 20°C and 53°C show that the measurements are moderately captured with the model and that the total time used for the measurements exceeds the time delay caused by diffusion and required to achieve the target RH at the boundary of the specimen. This means that, based on this simplified model, enough time was used for the measurements.

Measurements of relative humidity at different temperatures

The relative humidity above bentonite samples at different temperatures was measured in a limited series and one of the test series is presented below to illustrate the trends.

In these test series each temperature was kept during 10 h and the equipment was opened after each change in temperature to avoid any influence of air pressure. Three samples were tested in each series and the water content of the samples was supposed to be constant during the measurements. In all tests the water content after the test was slightly less than the initial value. The specimens were compacted and one of the compacted samples was kept at constant volume conditions while the others were free to swell or shrink. The constant volume sample was compacted directly into the oedometer ring (label: compacted into the ring) where a relative humidity probe was attached through the ring. The other samples were placed in containers (labels: compacted and ring and compacted and calibrator) with possibility to attach RH probes.

The initial and final water contents of the bentonite specimens were 16.4% and 15.9% respectively for all three tests. The measured results are shown versus temperature in Figure A1-9. The sample compacted into the oedometer ring was influenced by radial and axial stresses during the test period which caused the higher relative humidity measured in this case.

The results from one of the measurements (with the label compacted and ring) at temperatures from 20°C to 50°C are shown with retention curves in Figure A1-10 (cf. Figure 3-8). In this diagram comparable measurements made on MX-80 at water contents 9%, 15%, 16% and 19% and at temperatures 30°C, 40°C and 50°C made by Villar et al. (2005) are also shown.

Different influence of temperature is seen in the results from the different techniques. From the sorption balance approximately the same influence of temperature is shown regardless if it is absorption or desorption. In general, the results from the jars show less influence of temperature and at absorption from w_{ini} = 0% the results from the jars show almost no influence of temperature at all. The influence of temperature on the measured RH seems to coincide well with the temperature influence of the desorption part of the retention curves.
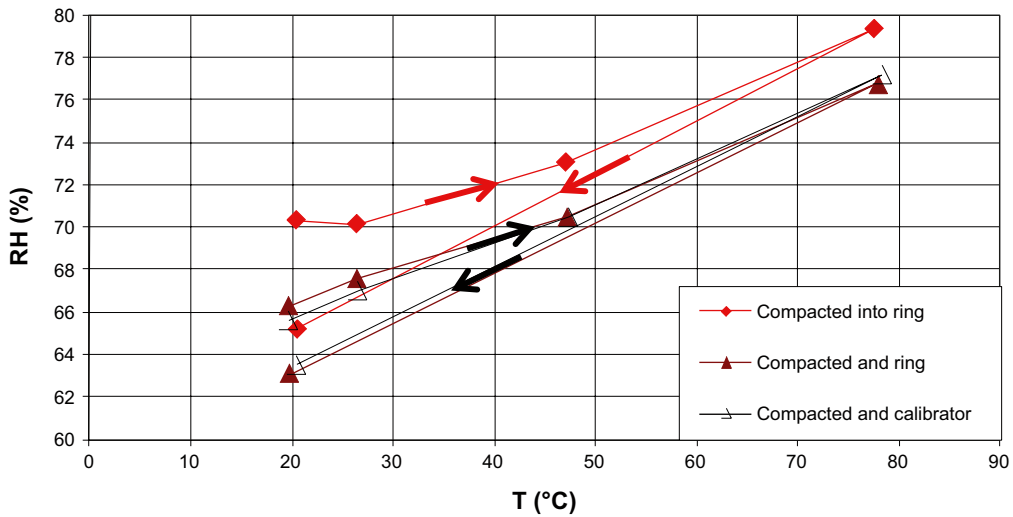
Figure A1-9. *Measured RH above or adjacent to bentonite samples with initial and final water contents $w_{ini} = 16.4\%$ and $w_{final} = 15.9\%$, respectively.*
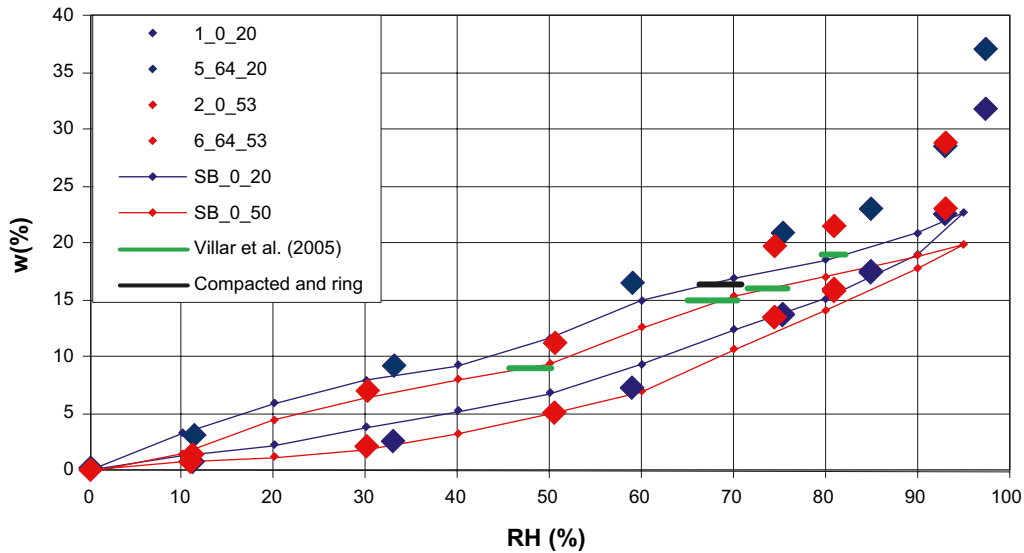
Figure A1-10. *Retention curves at 20°C and 50°C (53°C) determined with the sorption balance and the jar methods. Solid black line represents measured relative humidity from this study at water content $w \approx 16\%$ at temperatures between 20°C and 50°C. Solid green lines represent measured relative humidity by Villar et al. (2005) at water contents 9%, 15%, 16% and 19% at temperatures between 30°C and 50°C.*

Volume change

Compression tests (OCS), tables

The results from each test are presented in two tables, one to the left (red) and one to the right (blue). The name of each test is shown in the upper line, on both sides. The description below is exemplified by marks in the results from the first test.

The data to the left are determined from manually measurements with a calliper or a balance; height H (mm), diameter D (mm), void ratio e, water content w (%) and degree of saturation S_r (%).

The data to the right are values from the continuous registration by sensors and transducers. These values represent the final values from one load step: relative humidity RH (%), axial stress Pax (kPa), radial stress Prad (kPa), average stress Pavr (kPa) and void ratio e (e is here calculated from the continuously measured deformation and the initial void ratio (grey)). The lines 0–4 marked in the test results represent the following states or load steps of the test:

0. Compaction of the test sample and assembly of the equipment.

1. The initial state of the test. The initial void ratio is calculated from the full diameter of the ring (here 50 mm but in all other tests 35 mm).

2. Equilibrium after application of the control of RH ($RH_{applied}$ in green).

3. Application of axial load in steps ($P_{ax, applied}$ (MPa) in yellow). 1-6 load steps.

4. Termination of the test. The final water content and density (with the volume determined by weighing the sample above and submerged into paraffin oil) are evaluated.

Compression tests (OCS), diagrams

The continuous measurements from each test are presented in two diagrams. The name of each test is shown on top of each diagram. Void ratio ranges between 0.5 and 1.05.

The diagram to the left shows axial stress (label F_ax), radial stress (label F_rad) and void ratio (label Def) versus date. The diagram to the right shows relative humidity (label RH) and temperature (label t) versus date.

Swelling/shrinkage tests (SCL), tables

The results from each test are presented in two tables, one to the left (red) and one to the right (blue). The name of each test is shown in the upper line, on both sides. The description below is exemplified by marks in the results from the first test.

The data to the left are determined from manually measurements with a calliper or a balance; height H (mm), diameter D (mm), void ratio e, water content w (%) and degree of saturation S_r (%).

The data to the right are values from the continuous registration by sensors and transducers. These values represent the final values from one load step: relative humidity RH (%), axial stress Pax (kPa), radial stress Prad (kPa), average stress Pavr (kPa), void ratio e (e is here calculated from the continuously measured deformation and the initial void ratio (grey)). The lines 0-3 marked in the test results represent the following states or load steps of the test:

0. Compaction of the test sample and assembly of the equipment.

1. The initial state of the test. Equilibrium after application of the axial load (P (MPa) in green). The initial void ratio is calculated from the full diameter of the ring (here 50 mm but in all other tests 35 mm).

2. Application of RH control ($RH_{applied}$ (%) in yellow). 1–2 steps in RH.

3. Termination of the test. The final water content and density (with the volume determined by weighing the sample above and submerged into paraffin oil) are determined.

Table A2-1. Results from compression tests (comma sign is used as decimal pont).

Test 1 — O1_0705, Date 2005-09-02, File O1_0705_mtr.xls, OCS

m_s (g) 47,86 · ρ_s (g/cm³) 2,78

	P MPa	RH (%)	H mm	D mm	e	w (%)	Sr (%)	
comp	33,10423		14,22	49,43	0,58	9,55	45,43	0
			14,22	50	0,62	9,55	42,72	1
	0,1 and 1	75						2
oedom			15,16	50	0,73	15,77	60,11	3
paraffin					0,74	15,77	59,54	4

Test — O1_0705, Date 2005-09-02, Measurements — sept06

	RH %	Pax kPa	Prad kPa	Pavr kPa	e
	46,52	166,54	0	55,51	0,62
	73,03	158,94			0,74
	72,89	1078,28			0,73

* not reliable Prad values, see also O4_0705

Test 2 — O2_0705, Date 2005-08-26, File O2_0705_mtr.xls, OCS

m_s (g) 23,56 · ρ_s (g/cm³) 2,78

	P MPa	RH %	H mm	D mm	e	w %	Sr %
comp	33,26014		14,16	34,64	0,58	9,55	46,18
			14,16	35	0,61	9,55	43,70
	0,1 and 9 (with 9MPa)	75					
oedom			14,29	35	0,62	16,18	72,28
paraffin					0,70	16,18	64,19

Test — O2_0705, Date 2005-08-26, Measurements — sept06

Test	RH %	Pax kPa	Prad kPa	Pavr kPa	e
	45,46	175,86	0,00	58,62	0,60
oedo	74,48	184,08	3392,26	2322,87	0,72
	74,96	8511,83	5471,34	6484,84	0,62

Test 3 — O3_0705, Date 2005-08-26, File O3_0705_mtr.xls, OCS

m_s (g) 23,53 · ρ_s (g/cm³) 2,78

	P MPa	RH %	H mm	D mm	e	w %	Sr %
comp	33,26		14,00	34,68	0,56	9,55	47,28
			14,00	35,00	0,59	9,55	44,94
	0,1	75					
oedom	0,1	75			0,72	16,21	63,04
paraffin	1	75			0,72	16,21	62,33

Test — O3_0705, Date 2005-08-26, Measurements — sept06

	RH %	Pax kPa	Prad kPa	Pavr kPa	e
	46,80	172,03	0,00	57,34	0,60
	74,73	218,14	3216,56	2217,08	0,74
	75,34	1012,12	3438,25	2629,54	0,71

Test — O1_0905, Date 20/10-05, File O1_0905_mtr.xls, OCS

m_s (g) 47,80 · ρ_s (g/cm³) 2,78

	P MPa	RH (%)	H mm	D mm	e	w (%)	Sr (%)
comp	30,56		14,40	49,40	0,61	9,50	43,62
	0,1		14,40	50,00	0,64	9,50	40,97
	0,1	98					
oedom	1	98	16,29	50,00	0,86	21,85	70,63
paraffin					0,85	21,85	71,21

Test — O1_0905, Date 20/10-05, Measurements — sept06

	RH %	Pax kPa	Prad kPa	Pavr kPa	e
comp					
	48,21	166,65	0,00	55,55	0,64
	90,04	171,78			0,90
oedom	89,92	1093,07	1423,86	1313,60	0,86
paraffin					

* Prad at 0,1 MPa not reliable

Test — O2_0905, Date 2005-10-13, File O2_0905_mtr.xls, OCS

m_s (g) 23,53 · ρ_s (g/cm³) 2,78

	P MPa	RH %	H mm	D mm	e	w %	Sr %
comp	37,42		14,05	34,7	0,57	9,35	45,63
	0,1		14,05	35	0,60	9,35	43,54
	0,1	75					
	1	75					
	9	75					
oedom	1	75	14,05	35	0,60	15,77	73,44
paraffin					0,68	15,77	64,39

Test — O2_0905, Date 2005-10-13, Measurements

	RH %	Pax kPa	Prad kPa	Pavr kPa	e
comp					
	47,46	144,73	0,00	48,24	0,60
	75,48	138,26	3151,43	2147,04	0,71
	75,61	1037,06	3341,88	2573,61	0,70
	74,70	9216,78	5351,34	6639,82	0,59
oedom	74,71	1100,51	3351,81	2601,38	0,60
paraffin					

Test — O4_0905, Date 2005-10-13, File O4_0905_mtr.xls, OCS

m_s (g) 23,52 · ρ_s (g/cm³) 2,78

	P MPa	RH %	H mm	D mm	e	w %	Sr %
comp	33,26		14,02	35,7	0,57	9,35	45,85
			14,02	35	0,59	9,35	43,75
	0,1	85					
	1	85					
	9	85					
oedom	20	85	14,124	35	0,61	18,79	86,20
paraffin					0,62	18,79	84,23

Test — O4_0905, Date 2005-10-13, Measurements

	RH %	Pax kPa	Prad kPa	Pavr kPa	e
comp					0,59
	47,22	181,76	0,00	60,59	0,60
	84,66	185,36	2259,84	1568,35	0,79
	84,47	936,58	2339,88	1872,12	0,78
	84,27	8928,18	5034,44	6332,35	0,70
oedom	83,23	19604,85	10575,09	13585,01	0,61
paraffin					

Test — O2_1005, Date 2005-12-08, File O2_1005_mtr.xls, OCS — sept06

m_s (g) 23,50 · ρ_s (g/cm³) 2,78

	P MPa	RH %	H mm	D mm	e	w %	Sr %
comp	37,42		14,21	34,73	0,59	9,53	44,72
			14,21	35	0,62	9,53	42,92
	0,1	98					
	1	98					
	9	98					
unloaded			15,466	35	0,76	26,86	98,21
paraffin					0,74	26,86	100,68

Test — O2_1005, Date 2005-12-08, Measurements — sept06

	RH %	Pax kPa	Prad kPa	Pavr kPa	e
comp					
	47,37	169,40	0,00	56,47	0,61
	95,68	157,65	1221,38	866,80	1,00
	95,89	1126,95	1438,81	1334,85	0,97
oedom	97,21	9587,45	6125,65	7279,59	0,79
unloaded	97,19	154,12	1097,76	783,21	0,76

Rem. Void ratio(or H) decreases during unloading/dismantling.

Test — O2_1105, Date 2006-01-10, File O2_1105.xls, OCS

m_s (g) 23,53 · ρ_s (g/cm³) 2,78

	P MPa	RH %	H mm	D mm	e	w %	Sr %
comp, assumed	41,58		14,19	34,71	0,59	9,33	44,25
			14,19	35	0,61	9,33	42,33
	1	98					
	9	98					
oedom	1	98	14,418	35	0,64	21,35	92,87
paraffin					0,71	21,35	84,02

Test — O2_1105, Date 2006-01-10, Measurements

	RH %	Pax kPa	Prad kPa	Pavr kPa	e
comp					
	45,29	157,06	0,00	52,35	0,61
	88,11	154,71	1946,38	1349,16	0,82
	88,86	9477,61	5617,12	6903,95	0,62
oedom	87,70	1270,87	2661,22	2197,77	0,64
paraffin					

Test — O4_1105, Date 2006-01-10, File O4_1105.xls, OCS

m_s (g) 23,43 · ρ_s (g/cm³) 2,78

	P MPa	RH %	H mm	D mm	e	w %	Sr %
comp	37,42		14,14	34,72	0,59	9,62	45,45
			14,14	35	0,61	9,62	43,54
	0,1	85					
	1	85					
	9	85					
	20	85					
	9	85					
oedom	1	85	14,365	35	0,64	18,53	80,56
paraffin					0,64	18,53	80,94

Test — O4_1105, Date 2006-01-10, Measurements

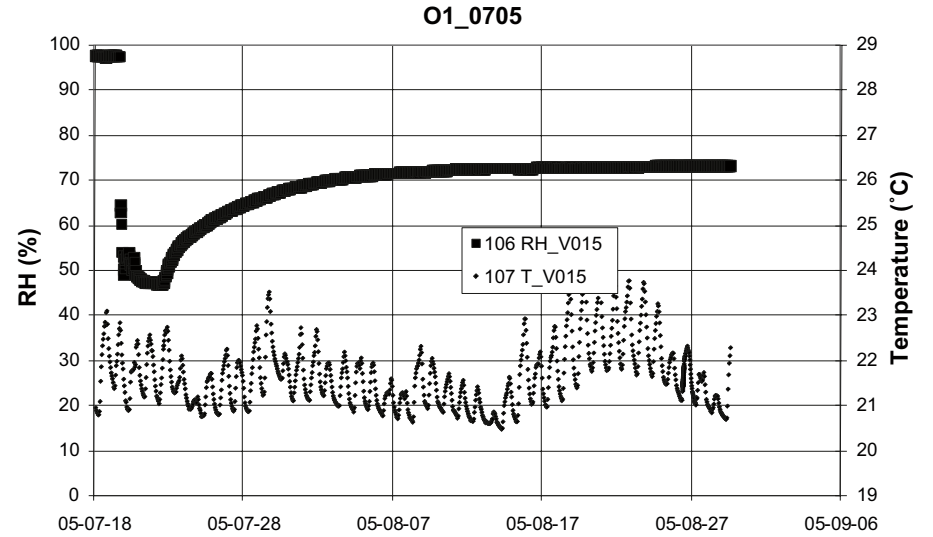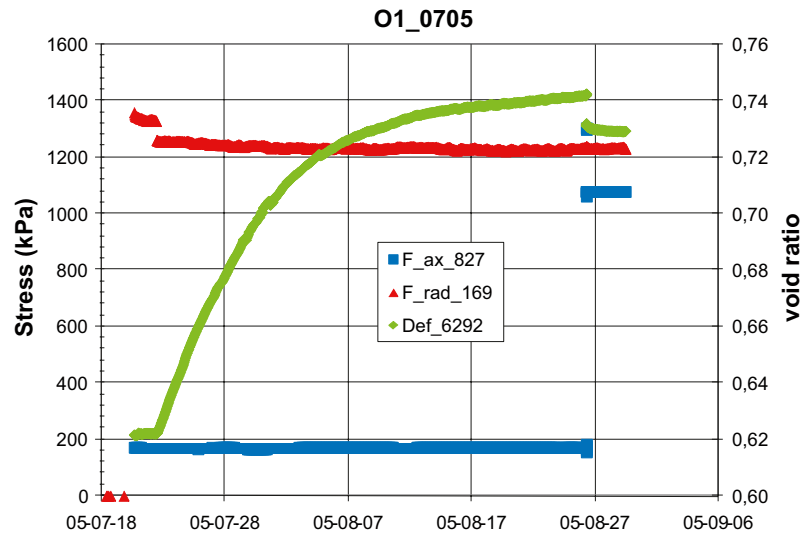|	RH %	Pax kPa	Prad kPa	Pavr kPa	e
comp					
	46,44	175,16	0,00	58,39	0,62
	82,58	177,56	2968,41	2038,13	0,77
	82,37	1003,79	2868,70	2247,06	0,77
	82,94	8813,61	5462,86	6579,78	0,71
	82,67	19770,99	10684,04	13713,02	0,62
	81,65	9117,20	8119,37	8451,98	0,63
	80,91	1000,19	3778,68	2852,52	0,64

sum_ocs_16_f.xls

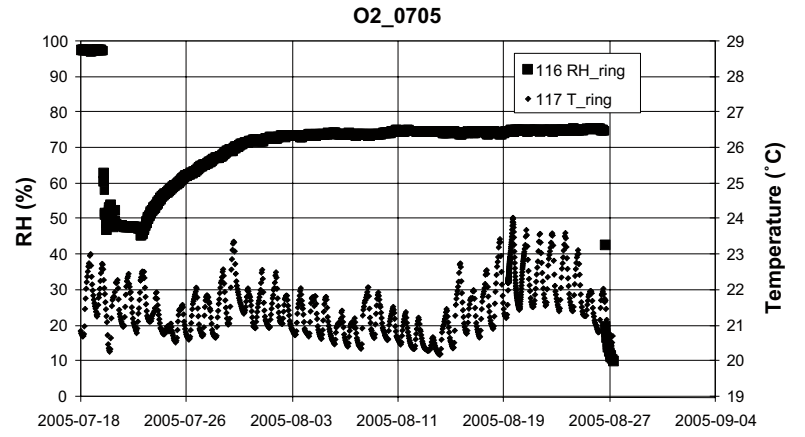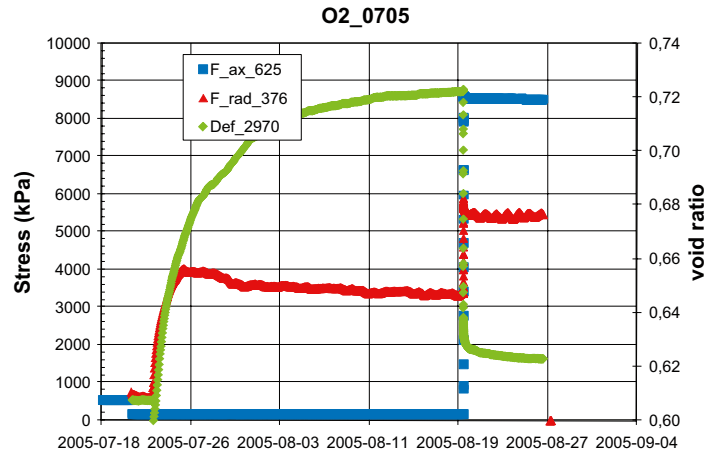**Figure A2-1.** *Results from compression test O1_0705.*

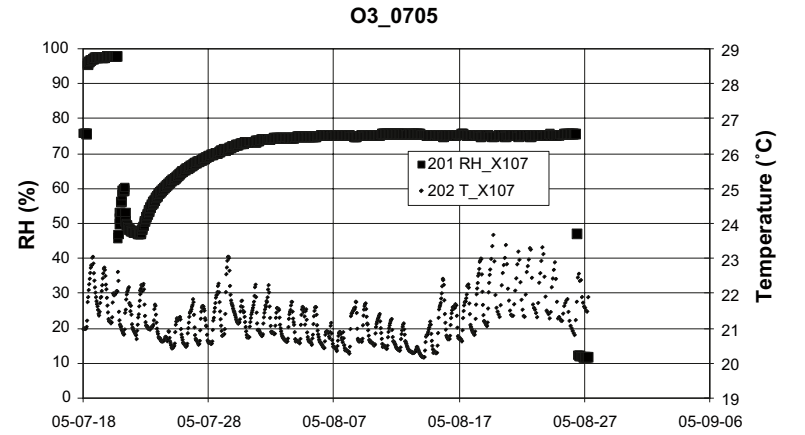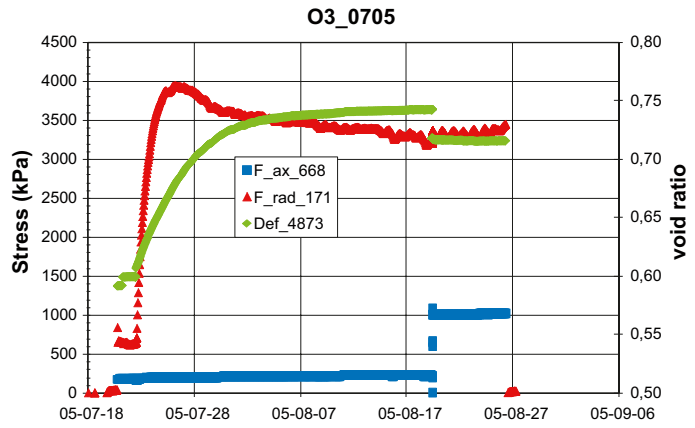**Figure A2-2.** *Results from compression test O2_0705.*

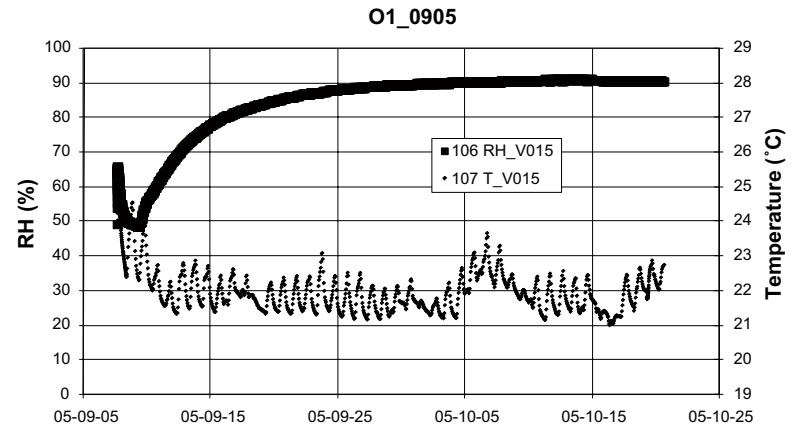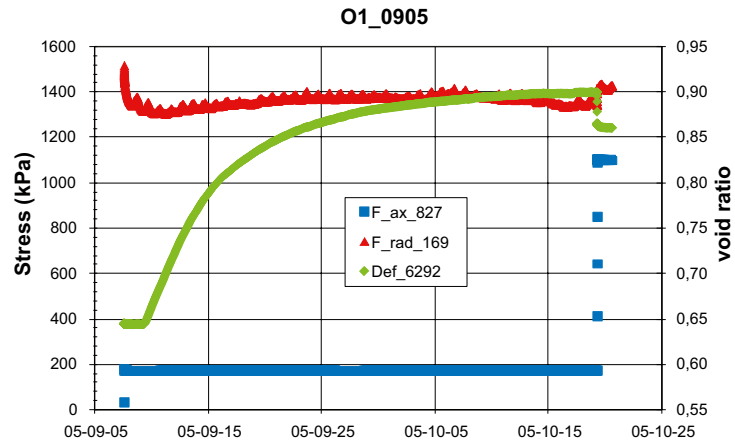**Figure A2-3.** *Results from compression test O3_0705.*

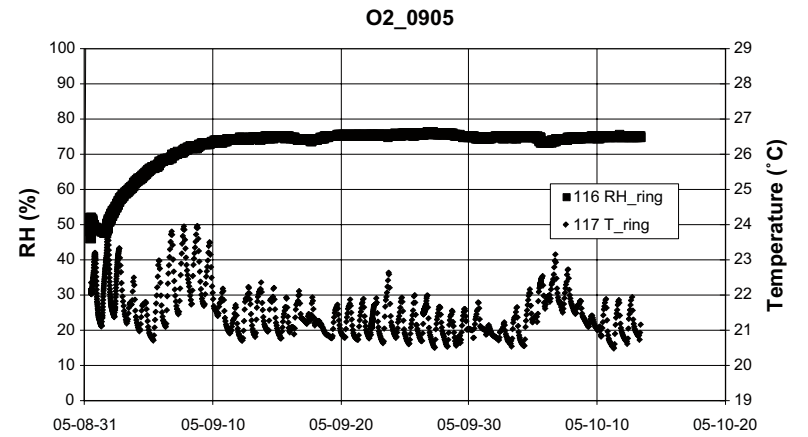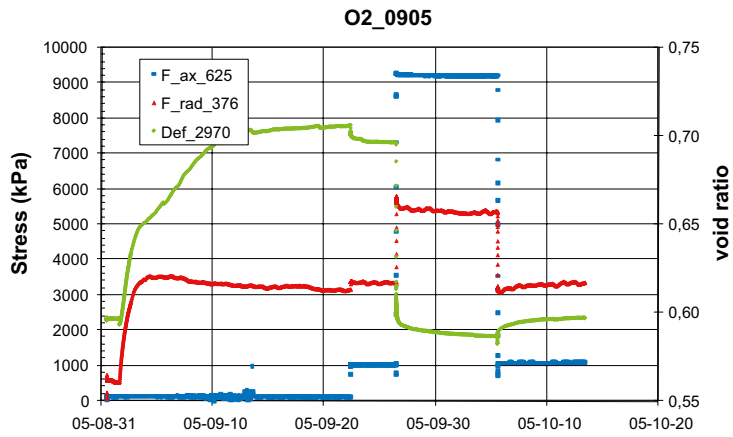**Figure A2-4.** *Results from compression test O1_0905.*

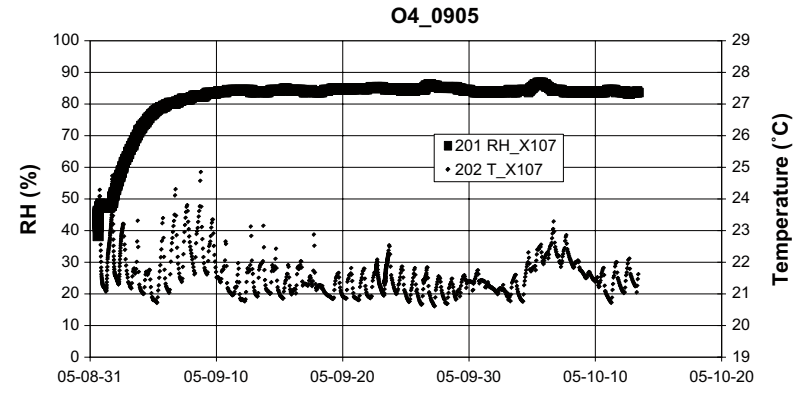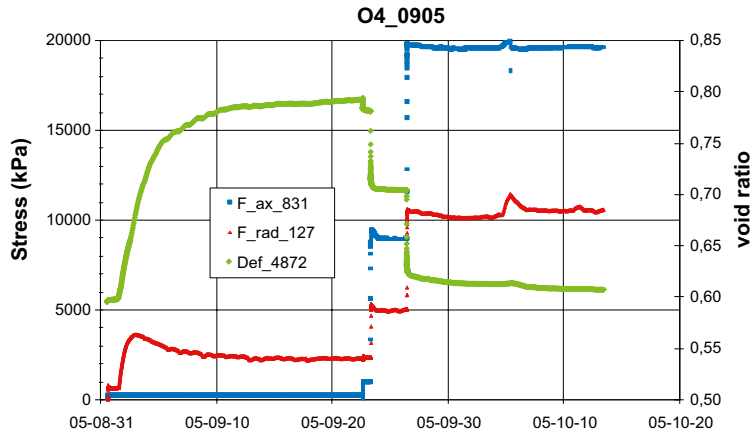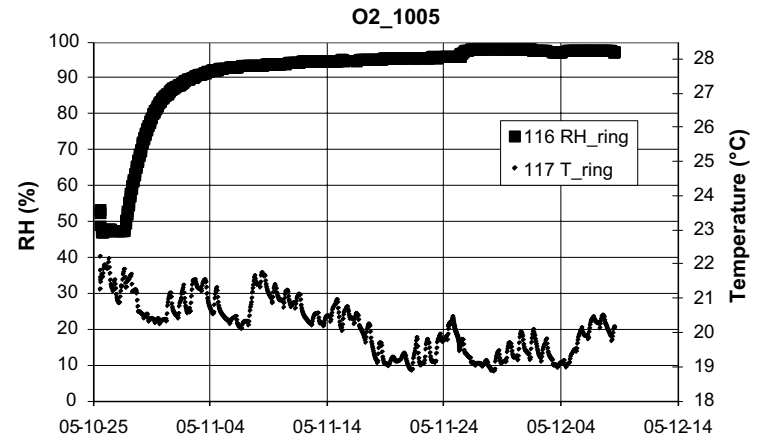**Figure A2-5.** *Results from compression test O2_0905.*

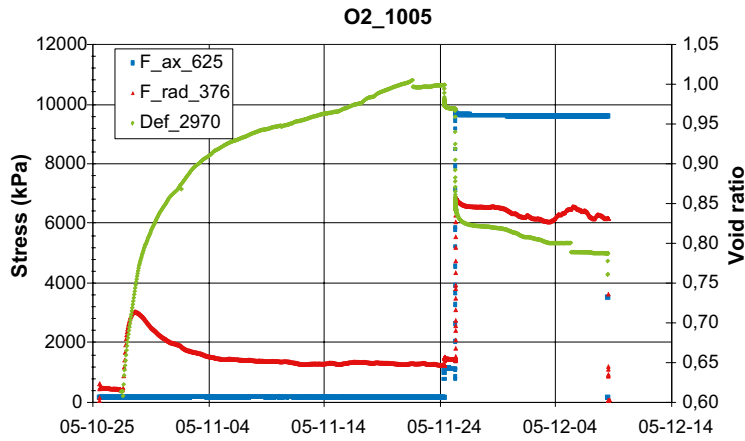**Figure A2-6.** *Results from compression test O4_0905.*

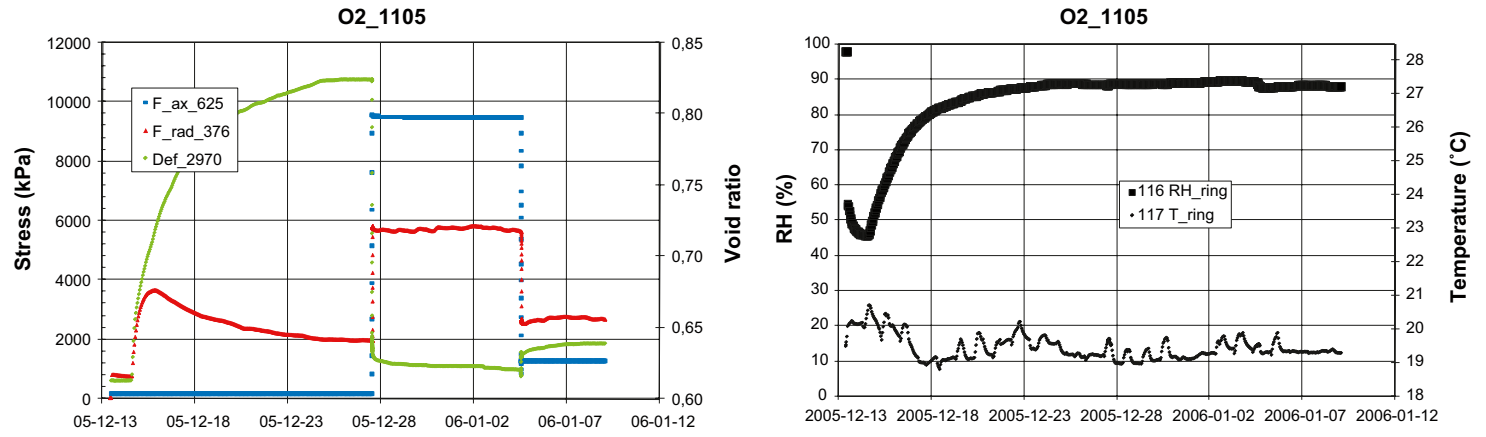**Figure A2-7.** *Results from compression test O2_1005.*

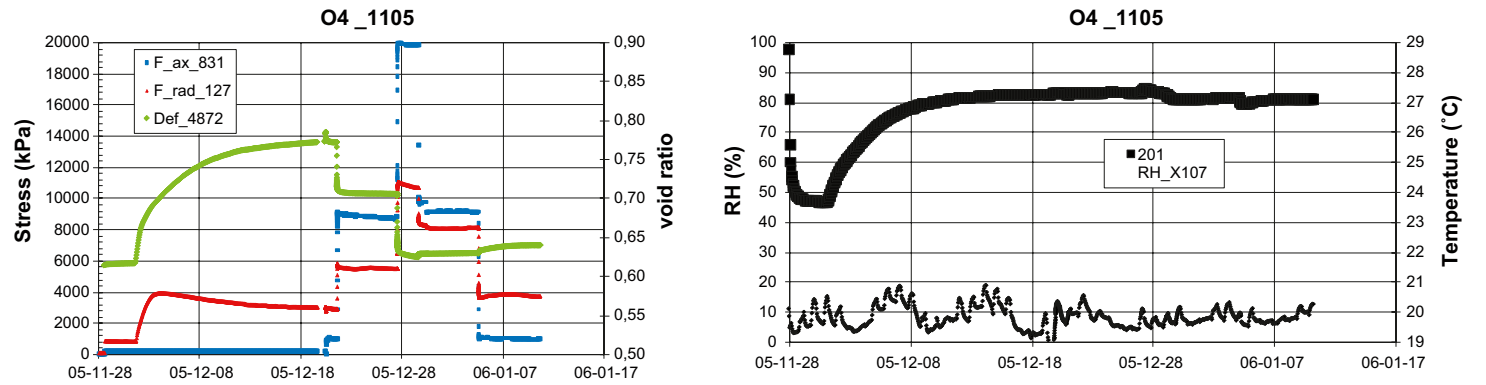**Figure A2-8.** *Results from compression test O2_1105.*

Figure A2-9. *Results from compression test O4_1105.*

Table A2-2. Results from swelling/shrinkage tests (comma sign is used as decimal pont).

Test 1 — O4_0705 Date 2005-08-19 File O4_0705_mtr.xls SCL

m_s (g) 23,53397 ρ_s (g/cm³) 2,78

	P MPa	RH %	H mm	D mm	e	w %	Sr %	
comp	33,26		14,1	34,6425	0,57	9,56	46,62	0
			14,1	35	0,60	9,56	44,10	1
oedom	0,1	75	15,34	35	0,74	16,13	60,33	2
paraffin					0,73	16,13	61,10	3

Test — O4_0705 Date 2005-08-19 Measurements

	RH %	Pax kPa	Prad kPa	Pavr kPa	e
	47,00	167,96	0,00	55,99	0,60
	74,63	168,56	3264,97	2232,84	0,74

Test 2 — O3_0905 Date 2005-09-22 File O3_0905 SCL

m_s (g) 23,52904 ρ_s (g/cm³) 2,78

	P MPa	RH %	H mm	D mm	e	w %	Sr %
comp	33,26		13,97	34,8	0,57	9,35	45,61
	20		13,97	35	0,59	9,35	44,20
oedom	20	85	13,12	35	0,49	15,82	89,47
paraffin					0,59	15,82	73,91

Test — O3_0905 Date 2005-09-22 Measurements (sept06)

	RH %	Pax kPa	Prad kPa	Pavr kPa	e
comp					0,59
	49,09	20819,21	6536,62	11297,48	0,48
oed. Stop	80,76	20610,14	13998,78	16202,57	0,49
oed.unloaded		465,43	3665,29	2598,67	0,56
paraffin					

Test 3 — O1_1005 Date 2005-11-25 File O1_1005_mtr.xls SCL

m_s (g) 47,79447 ρ_s (g/cm³) 2,78

	P MPa	RH (%)	H mm	D mm	e	w (%)	Sr (%)
comp	33,10		14,04	49,4	0,57	9,53	46,88
			14,04	50	0,60	9,53	43,91
oedom	1	75	14,74	50	0,68	14,95	60,82
paraffin					0,69	14,95	60,03

Test — O1_1005 Date 2005-11-25 Measurements (sept06)

	RH %	Pax kPa	Prad kPa	Pavr kPa	e
comp	44,83	1076,22	0,00	358,74	0,60
oedom	70,75	1082,58			0,68
paraffin					

* Prad not reliable, see also O4_0705

Test 4 — O3_1005 Date 2005-11-15 File O3_1005 SCL

m_s (g) 23,45476 ρ_s (g/cm³) 2,78

	P MPa	RH %	H mm	D mm	e	w %	Sr %
comp	37,42		14,03	34,8	0,58	9,53	45,55
	0,1		14,03	35	0,60	9,53	44,16
	0,1	98					
oedom	0,1	75	16,279	35	0,86	19,20	62,32
paraffin			uncertain H		0,78	19,20	68,27

Test — O3_1005 Date 2005-11-15 Measurements (sept06)

	RH %	Pax kPa	Prad kPa	Pavr kPa	e
comp					0,60
	47,23	124,72	0,00	41,57	0,61
	93,42	115,14	1334,17	927,83	0,93
oedom	73,22	108,56	55,42	73,14	0,86
paraffin					uncertain e

Test 5 — O4_1005 Date 2005-11-21 SCL

m_s (g) 23,41107 ρ_s (g/cm³) 2,78

	P MPa	RH %	H mm	D mm	e	w %	Sr %
comp	41,58		14	34,7	0,57	9,35	45,43
			14	35	0,60	9,35	43,36
oedom	9	75	14,147	35	0,62	15,55	70,14
paraffin					0,63	15,55	68,14

Test — O4_1005 Date 2005-11-21 Measurements

	RH %	Pax kPa	Prad kPa	Pavr kPa	e
comp					0,60
	48,13	8952,82	2908,71	4923,41	0,58
oedom	75,59	9386,60	9219,66	9275,30	0,62
paraffin					

Test 6 — O1_1105 Date 2006-01-30 File O1_1105_mtr.xls SCL

m_s (g) 47,75851 ρ_s (g/cm³) 2,78

	P MPa	RH (%)	H mm	D mm	e	w	Sr
comp	35,65		14,22	49,4	0,59	9,59	45,47
			14,22	50	0,63	9,59	42,65
oedom	1	98	15,639	50	0,79	22,42	79,15
paraffin					0,80	22,42	77,59

Test — O1_1105 Date 2006-01-30 Measurements

	RH %	Pax kPa	Prad kPa	Pavr kPa	e
comp					0,59
	46,43	1074,04	0,00	358,01	0,59
oedom	89,12	1082,19	1621,53	1441,75	0,79
paraffin					

Test 7 — O3_1105 Date 2005-12-20 File O3_1105 SCL

m_s (g) 23,42048 ρ_s (g/cm³) 2,78

	P MPa	RH %	H mm	D mm	e	w %	Sr %
comp	33,26		14,1	34,63	0,58	9,63	46,45
	9		14,1	35	0,61	9,63	43,87
oedom	9	98	14,41	35	0,65	20,89	89,95
paraffin					0,67	20,89	86,81

Test — O3_1105 Date 2005-12-20 Measurements

	RH %	Pax kPa	Prad kPa	Pavr kPa	e
comp					0,60
	47,24	8899,28	2542,13	4661,18	0,58
oedom	91,10	9224,98	7765,93	8252,28	0,65
oedom					

Test 8 — O2_1205 Date 2006-02-06 File O2_1205 SCL

m_s (g) 23,4637 ρ_s (g/cm³) 2,78

	P MPa	RH %	H mm	D mm	e	w %	Sr %
comp	37,42		14,12	34,71	0,58	9,47	45,16
			14,12	35	0,61	9,47	43,19
	9	98					
		98					
oedom		75	13,472	35	0,54	17,47	90,65
paraffin					0,58	17,47	83,13

Test — O2_1205 Date 2006-02-06 Measurements

	RH %	Pax kPa	Prad kPa	Pavr kPa	e
comp *	43,90	0,00	0,00	0,00	0,60
	47,46	9411,23	3784,01	5659,75	0,52
	88,18	9924,64	9076,24	9359,04	0,57
oedom	71,68	9586,88	4173,38	5977,88	0,54

Test 9 — O3_1205 Date 2006-02-09 File O3_1205 SCL

m_s (g) 23,43846 ρ_s (g/cm³) 2,78

	P MPa	RH %	H mm	D mm	e	w %	Sr %
comp	33,26		14,1	34,7	0,58	9,51	45,45
	0,1		14,1	35	0,61	9,51	43,40
oedom	0,1	98	16,543	35	0,89	23,79	74,51
paraffin					0,87	23,79	75,79

Test — O3_1205 Date 2006-02-09 Measurements (sept06)

	RH %	Pax kPa	Prad kPa	Pavr kPa	e
comp					0,61
	45,48	145,68	0,00	48,56	0,61
oedom	92,79	121,14	920,16	653,82	0,89
oedom					

Test 10 — O4_1205 Date 2006-02-04 File O4_1205_mtr SCL

m_s (g) 23,45639 ρ_s (g/cm³) 2,78

	P MPa	RH %	H mm	D mm	e	w %	Sr %
comp	41,58		14	34,7	0,57	9,47	46,26
			14	35	0,60	9,47	44,15
oedom	0,1	85	15,662	35	0,79	18,29	64,70
paraffin					0,77	18,29	66,07

Test — O4_1205 Date 2006-02-04 Measurements (sept06)

	RH %	Pax kPa	Prad kPa	Pavr kPa	e
comp					0,60
	48,18	239,37	0,00	79,79	0,60
	81,98	243,57	3019,59	2094,25	0,79

sum_ocs_16_f.xls

Swelling/shrinkage tests (SCL), diagrams

The continuous measurements from each test are presented in two diagrams. The name of each test is shown on top of each diagram. Void ratio ranges between 0.4 and 0.95.

The diagram to the left shows axial stress (F_ax), radial stress (F_rad) and void ratio (Def) vs. date. The diagram to the right shows relative humidity (RH) and temperature (t) vs. date.
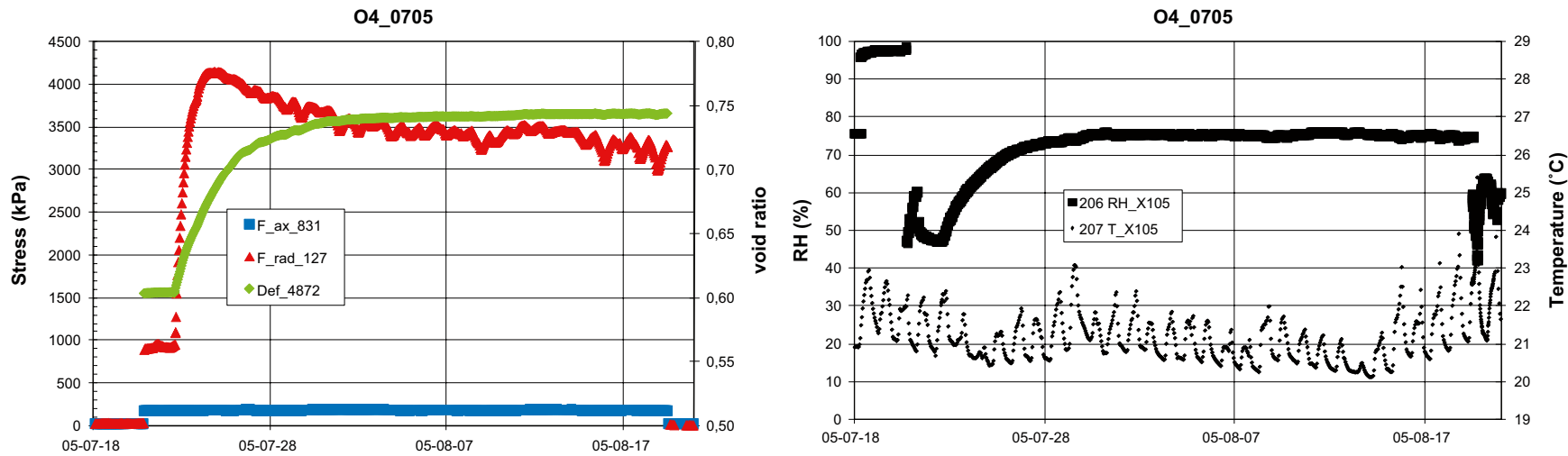

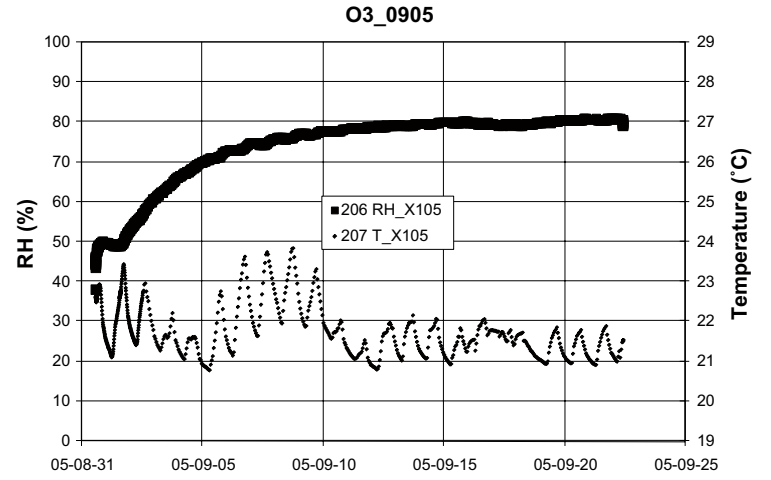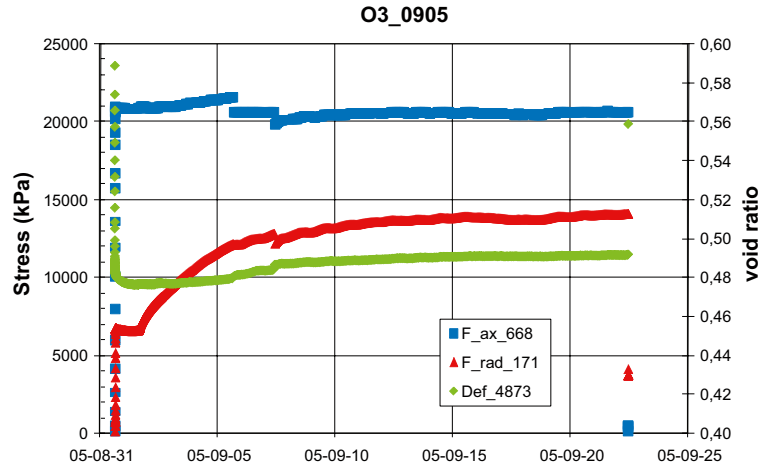**Figure A2-10.** *Results from swelling/shrinkage test O4_0705.*

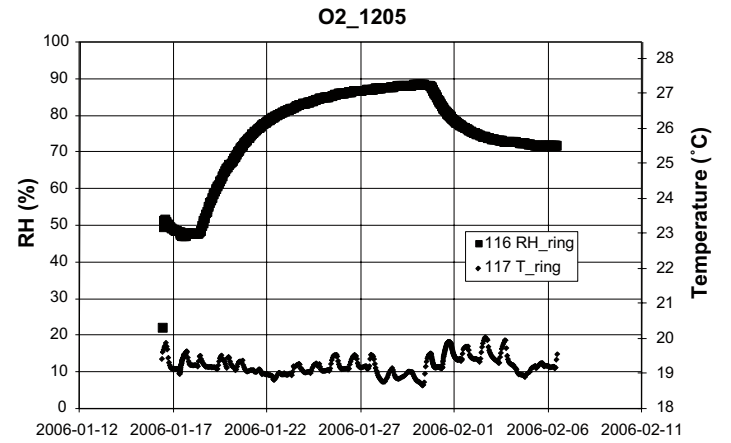**Figure A2-11.** *Results from swelling/shrinkage test O3_0905.*
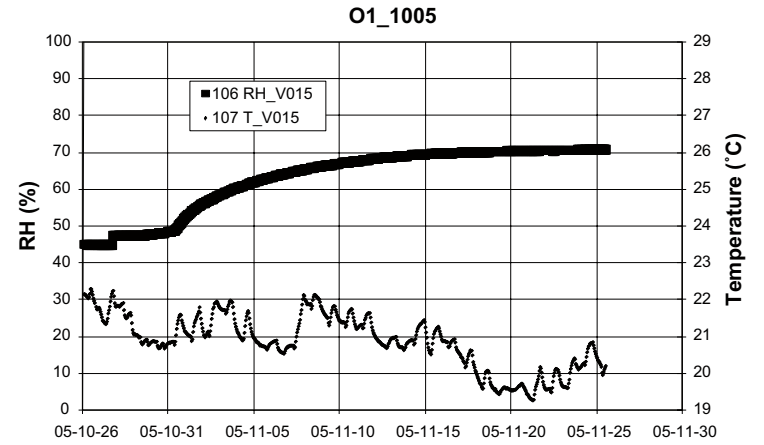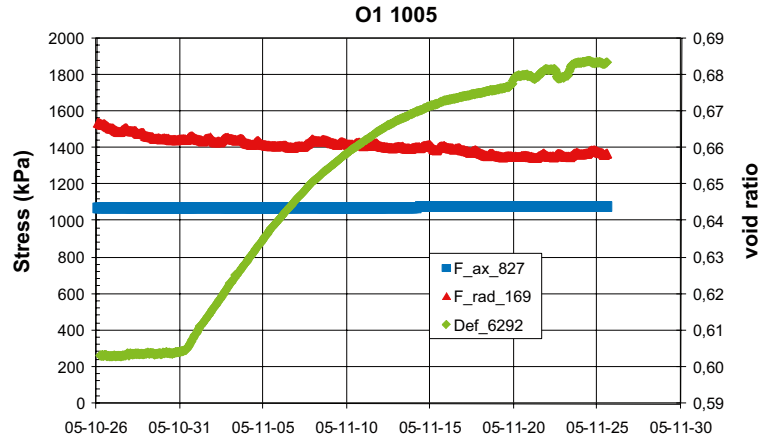
Figure A2-12. *Results from swelling/shrinkage test O1_1005.*
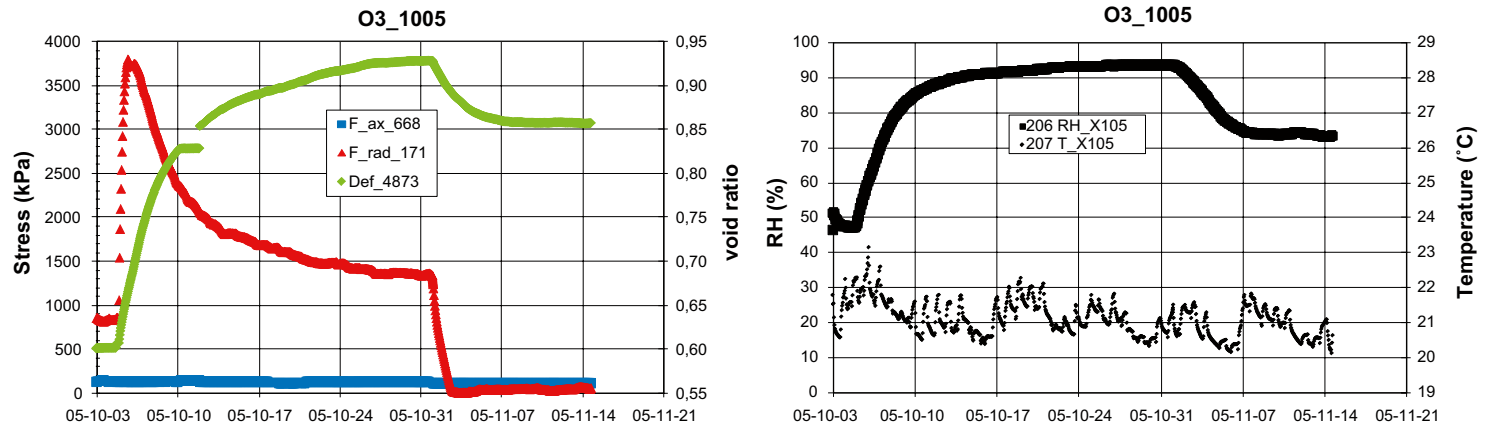
Figure A2-13. *Results from swelling/shrinkage test O3_1005.*
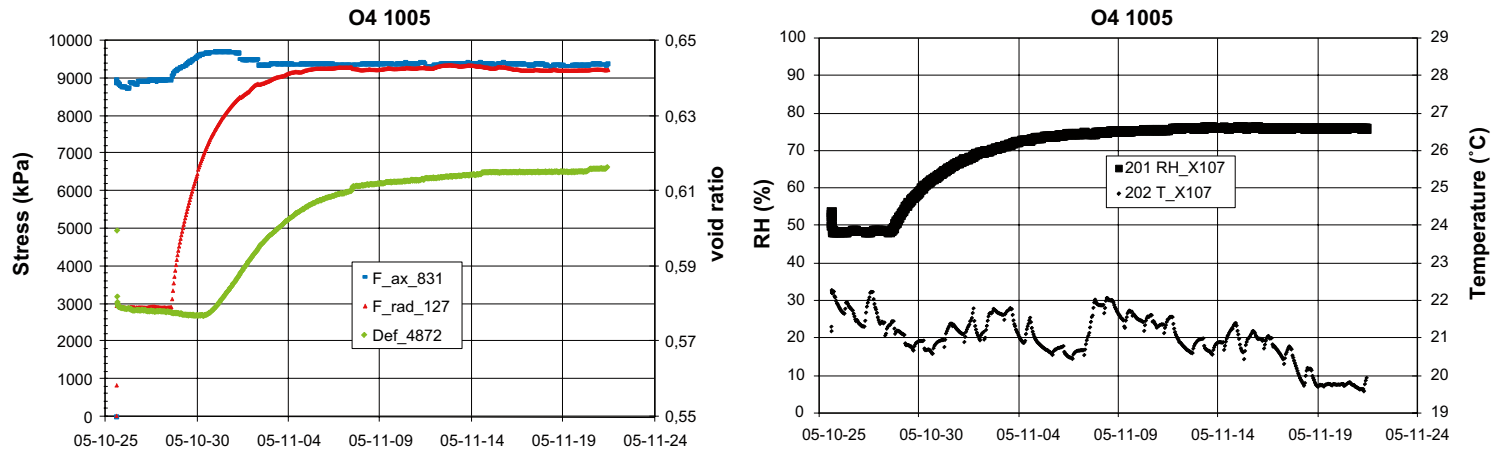
Figure A2-14. *Results from swelling/shrinkage test O4_1005.*
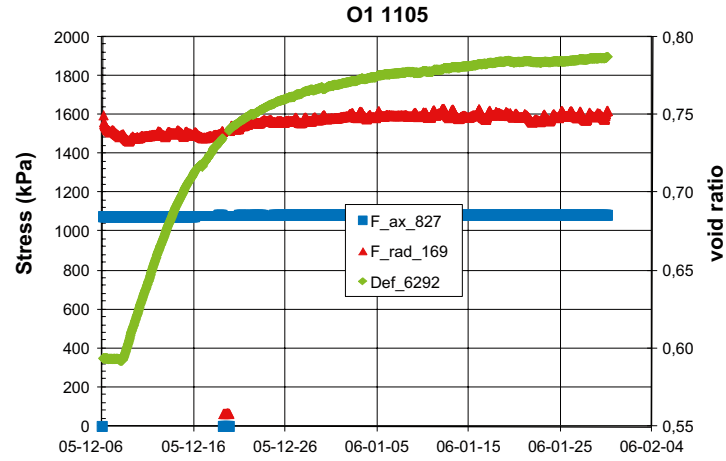
Figure A2-15. *Results from swelling/shrinkage test O1_1105.*
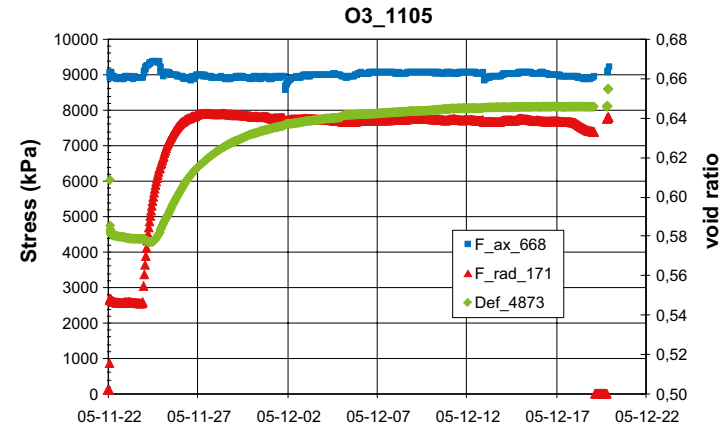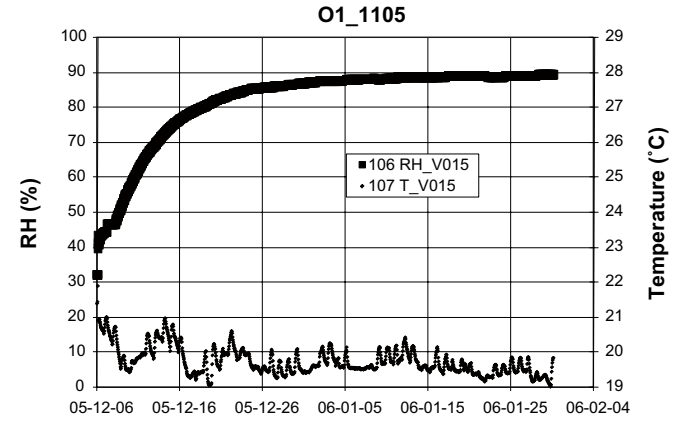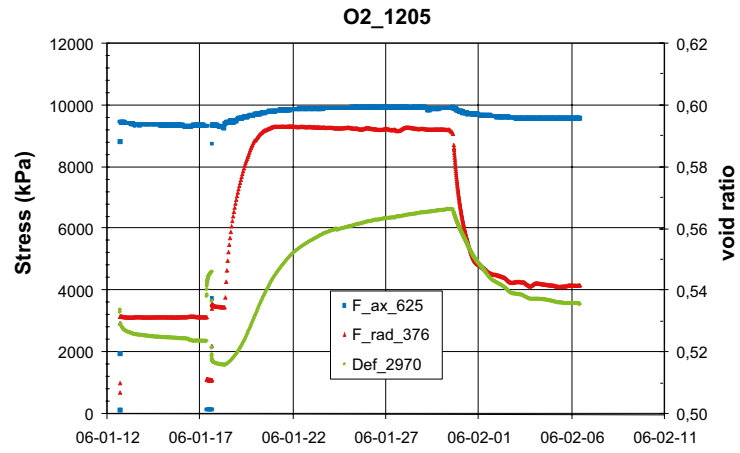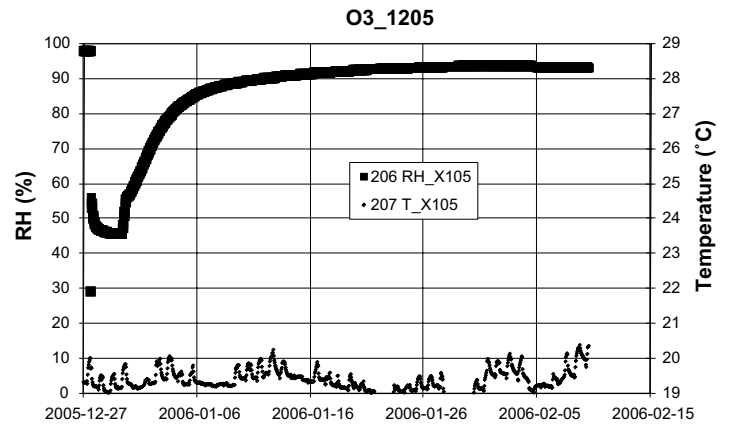

Figure A2-16. *Results from swelling/shrinkage test O3_1105.*
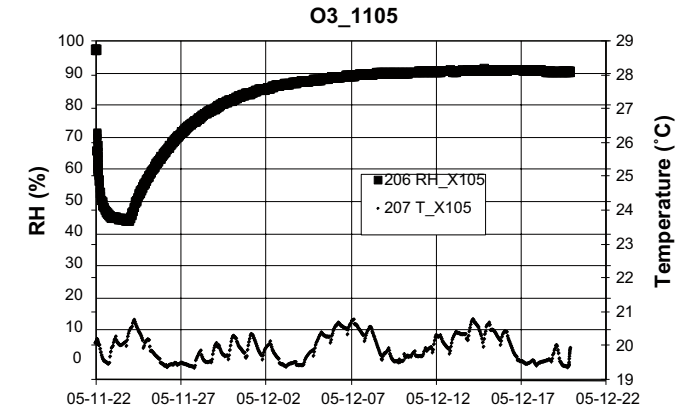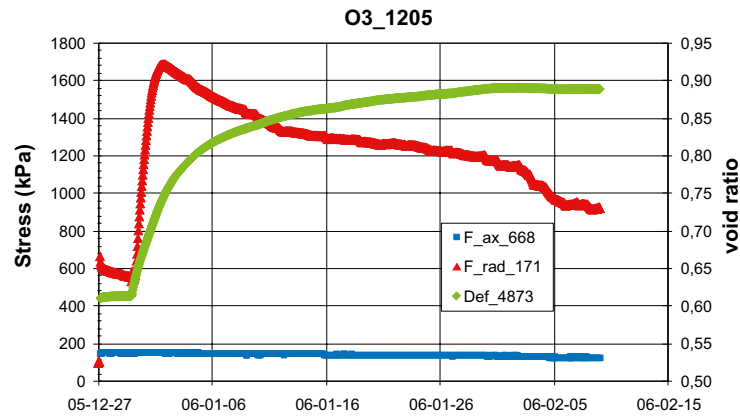
Figure A2-17. *Results from swelling/shrinkage test O2_1205.*

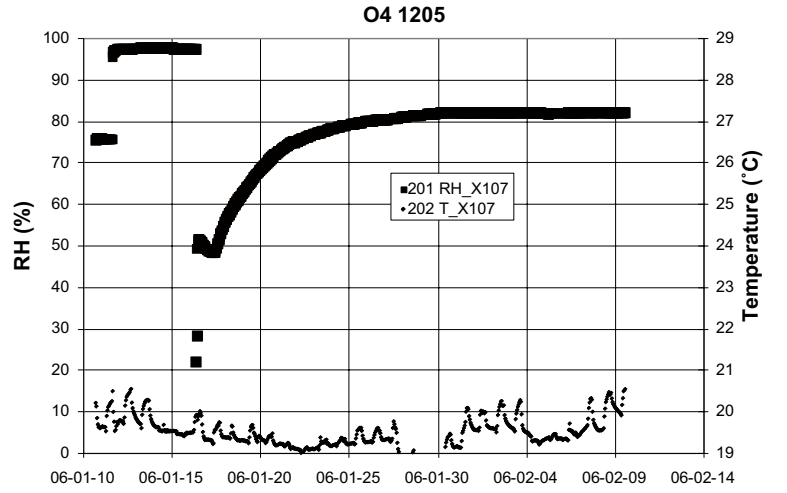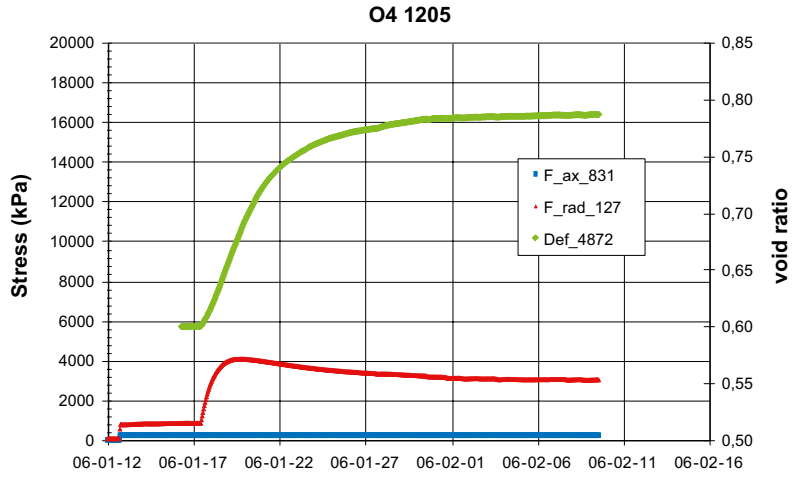**Figure A2-18.** *Results from swelling/shrinkage test O3_1205.*

Figure A2-19. *Results from swelling/shrinkage test O4_1205.*

Calculated moduli

Table A2-3. Calculated moduli from all compression tests and swelling/shrinkage tests.

OCS Test	Axial stress (kPa) Initial	Final	Mean stress (kPa) Initial	Final	Suction (MPa) Initial	Final	Void ratio Initial	Final	Deformation in 1 or 2 directions	**modulus i** -D(1+e)/Dln(p)
Loading										
O1_0705	159	1078	<900	<1200	45.44	45.72	>0,58	0.73	2	
O2_0705	184	8512	2323	6485	42.60	41.67	0.72	0.62	1	0.097
O3_0705	218	1012	2217	2630	42.12	40.94	0.74	0.71	1	0.157
O1_0905	172	1093	<900	1314	15.17	15.37	>0,61	0.86	2	
O2_0905	138	1037	2147	2574	40.68	40.43	0.71	0.70	1	0.054
	1037	9217	2574	6640	40.43	42.17	0.70	0.59	1	0.115
O4_0905	185	937	1568	1872	24.08	24.41	0.79	0.78	1	0.063
	937	8928	1872	6332	24.41	24.74	0.78	0.70	1	0.063
	8928	19605	6332	13585	24.74	26.54	0.70	0.61	1	0.127
O2_1005	158	1127	867	1335	6.38	6.07	1.00	0.97	1	0.069
	1127	9587	1335	7280	6.07	4.09	0.97	0.79	1	0.107
O2_1105	155	9478	1349	6904	18.30	17.08	0.82	0.62	1	0.125
O4_1105	178	1004	2038	2247	27.68	28.05	0.77	0.77	1	0.001
	1004	8814	2247	6580	28.05	27.06	0.77	0.71	1	0.062
	8814	19771	6580	13713	27.06	27.51	0.71	0.62	1	0.110
Unloading										
O2_0905	9217	1101	6640	2601	42.17	42.15	0.59	0.60	1	0.011
O2_1105	9478	1271	6904	2198	17.08	18.97	0.62	0.64	1	0.017
O4_1105	19771	9117	13713	8452	27.51	29.31	0.62	0.63	1	0.011
	9117	1000	8452	2853	29.31	30.63	0.63	0.64	1	0.009
Absorption from initial state of loading/unloading(OCS)										
O1_0705	167	159	56	<900	110.65	45.44	0.58	>0,58	2	
O2_0705	176	184	59	2323	113.99	42.60	0.58	0.72	2	0.150
O3_0705	172	218	57	2217	109.79	42.12	0.56	0.74	2	0.188
O1_0905	167	172	56	<900	105.51	15.17	0.61	>0,61	2	
O2_0905	145	138	48	2147	107.76	40.68	0.57	0.71	2	0.140
O4_0905	182	185	61	1568	108.50	24.08	0.57	0.79	2	0.149
O2_1005	169	158	56	867	108.06	6.38	0.59	1.00	2	0.143
O2_1105	157	155	52	1349	114.56	18.30	0.59	0.82	2	0.129
O4_1105	175	178	58	2038	110.92	27.68	0.59	0.77	2	0.132

SCL Test	Axial stress (kPa) Initial	Final	Mean Stress (kPa) Initial	Final	Suction (MPa) Initial	Final	Void ratio Initial	Final	Deformation 1 or 2 directions	**modulus s** -D(e+1)/Dln(s)
Absorption										
O4_0705	168	169	56	2233	102.20	39.62	0.57	0.74	2	0.183
O3_0905	20819	20610	11297	16203	96.31	28.93	0.48	0.49	1	0.013
O1_1005	1076	1083	359	<1300	108.60	46.84	0.57	0.68	2	0.141
O3_1005	125	115	42	928	101.53	9.21	0.58	0.93	2	0.144
O4_1005	8953	9387	4923	9275	98.98	37.88	0.58	0.62	1	0.040
O1_1105	1074	1082	358	1442	103.85	15.60	0.59	0.79	2	0.106
O3_1105	8899	9225	4661	8252	101.50	12.62	0.58	0.65	1	0.036
O2_1205	9411	9925	5660	9359	100.89	17.03	0.52	0.57	1	0.028
O3_1205	146	121	49	654	106.65	10.13	0.58	0.89	2	0.130
O4_1205	239	244	80	2094	98.86	26.90	0.57	0.79	2	0.167
Desorption										
O3_1005	115	109	928		9.21	42.19	0.93	0.78	2	0.096
O2_1205	9925	9587	9359	5978	17.03	45.08	0.57	0.54	1	0.032

sum_ocs_scl_2010

Remarks:

<900   Red text/number – No exact value, only upper or lower limit given

0.78   Blue number – The void ratio determined after dismantling is lower than the void ratio determined from the measured deformation and the initial void ratio. For the other test the opposite is valid or the two values of void ratio are the same.

Description of a HM-model

General

The HM model includes two equations which relate the variables stress, relative humidity and degree of saturation or water content and void ratio (Dueck 2004). The equations were mainly based on tests with constant volume conditions. The stress was mainly measured as an axial swelling pressure but was regarded as a mean stress and in the following P is used as boundary mean stress. The included relationships are further described by Dueck and Börgesson (2007). Equation A2-1 describes the relation between the mean stress P and the actual relative humidity RH_{act} of the sample and the relative humidity according to the retention curve at the actual water content, RH_{ret}. The retention curve is derived from Equation A1-1 with the constants a and b for the appropriate initial water contents or interpolated between them.

$$P(RH_{act}, w) = -\frac{R \cdot T \cdot \rho_w}{\omega_v} \cdot \ln(\frac{RH_{ret}(w)}{RH_{act}})$$ (A2-1)

Equation A2-2 describes the relation between the mean stress and the degree of saturation S_r at a specified void ratio e. The initial degree of saturation of the unloaded sample $S_{r,ini}$ is included. The swelling pressure at saturation P_{ret}, Equation A2-3, can be calculated from the retention curve which here includes the water content at saturation w_s calculated from the void ratio e, Equation A2-4.

$$P(S_r, e) = \frac{S_r - S_{r,ini}}{1 - S_{r,ini}} \cdot P_{ret}(e)$$ (A2-2)

$$P_{ret}(e) = -\frac{R \cdot T \cdot \rho_w}{\omega_v} \cdot \ln(\frac{RH_{ret}(w_s)}{100})$$ (A2-3)

$$w_s = 100 \cdot \frac{e \cdot \rho_w}{\rho_s}$$ (A2-4)

Comparison with test results

In this investigation the tests included change in volume and since the model was mainly based on results from constant volume tests it was interesting to compare the test results and the calculations from the model.

After the swelling under the small load, i.e. the first part of the tests in the OCS series, a new retention curve was chosen according to the calculated water content at that moment interpolated between the curves valid for 17.5% and 27%. At loading the water content was not allowed to increase and at unloading the water content was not allowed to decrease.

In the calculations the evaluation was made in steps. From the measured variables RH and P at a specific time the water content w, void ratio e and degree of saturation S_r were calculated from Equations A2-1 to A2-4. Since the equations are not explicitly expressed in the unknown variables, void ratio was assumed and iterations made until agreement was achieved between the calculated and measured stress P.

The calculated and measured results are compared for some of the performed tests in Figures A2-20 to A2-25. The mean stress is plotted vs. measured void ratios to the left and degree of saturation vs. void ratio to the right. Measurements are shown as filled symbols and calculations are shown as unfilled symbols. The measured values are shown in Tables A2-1 and A2-2 and as an example the measured results from the test O2_0705 are shown in Table A2-4 (cf. Table A2-1) where the values used for Figure A2-20 are marked.

In Figures A2-20 and A2-21 measured results and results from the model are compared for tests where the applied relative humidity was 75%. In Figures A2-22 and A2-23 the controlled relative humidity was 85% and in Figures A2-24 and A2-25 the controlled relative humidity was 98%. Results from measurement and modelling for all tests concerning volume change when applying one step of relative humidity are shown in next section. The results from measurements and modelling with $RH_{applied} = 85\%$ were also presented as a conference paper by Dueck (2007).

Table A2-4. Description of the values used in the comparison with the model.

Test	O2_0705	Date		2005-08-26	File	O2_0705_mtr.xls		OCS
					ms (g)	23,55771	ρ_s (g/cm3)	2,78
	P	RH	H	D	e		w	Sr
	MPa		mm	mm			%	%
comp	33,26014		14,16	34,6425	0,57501		9,55	46,1822
			14,16	35	0,607685		9,55	43,699
	0,1 and 9	75						
oedom	(with 9MPa)		14,29	35	0,622445		16,18363	72,2803
paraffin					0,700901		16,18363	64,18947

Test sept06	O2_0705	Date	2005-08-26		
Test	RH	Pax	Prad	Pavr	e
	%	kPa	kPa	kPa	
	45,46152	175,8599	0	58,61997	0,597643
	74,48123	184,0842	3392,2555	2322,865	0,72222
oedo	74,96162	8511,833	5471,3423	6484,839	0,622915
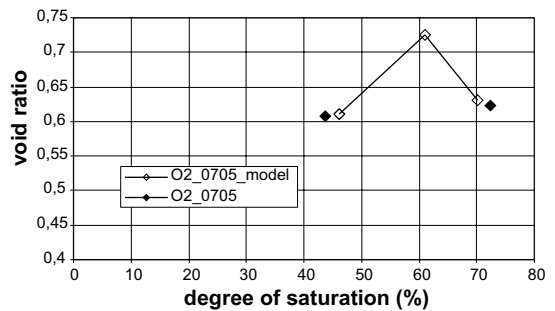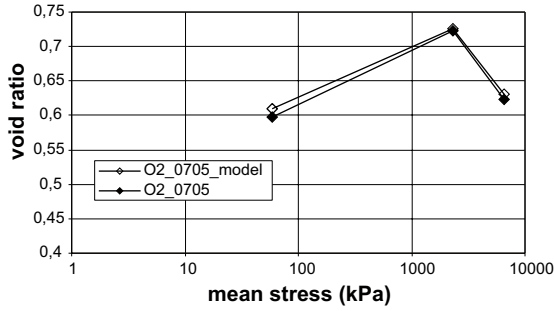
Figure A2-20. *Mean stress vs. void ratio (left figure) and degree of saturation vs. void ratio (right figure). Measured values (filled symbols) and calculated from the model (unfilled symbols). Results from RH = 75% and test type OCS.*
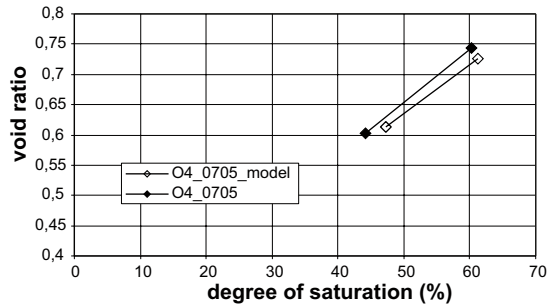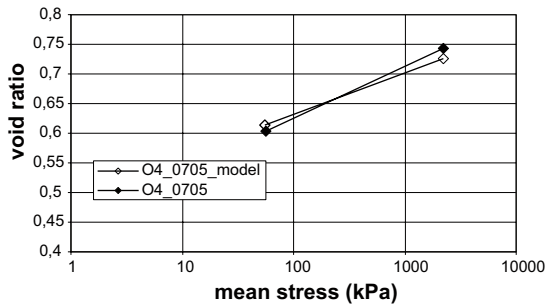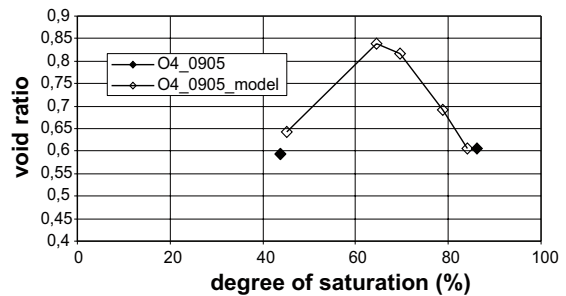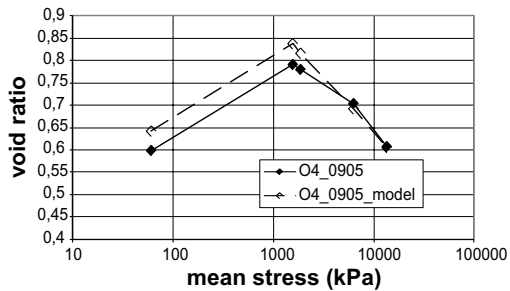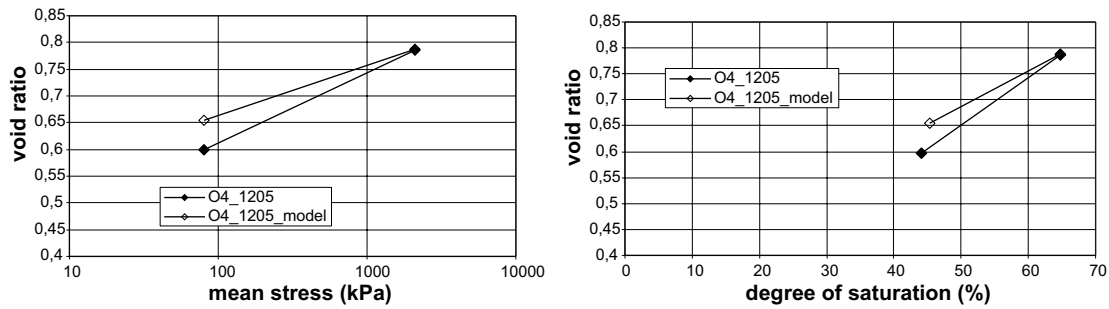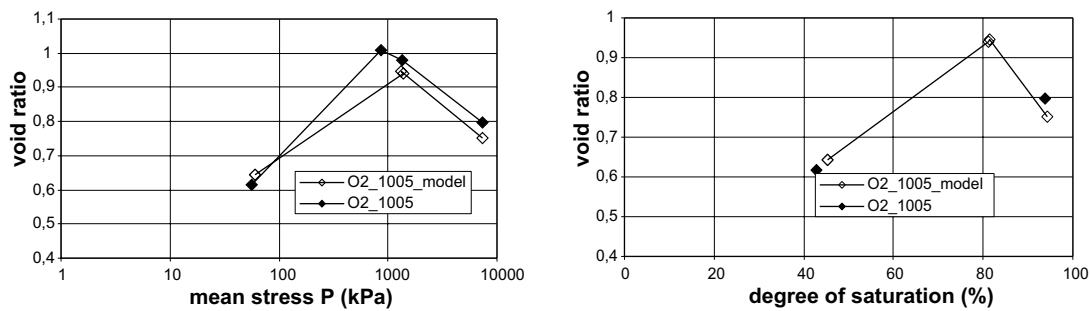

Figure A2-21. *Mean stress vs. void ratio (left figure) and degree of saturation vs. void ratio (right figure). Measured values (filled symbols) and calculated from the model (unfilled symbols). Results from RH = 75% and test type SCL.*
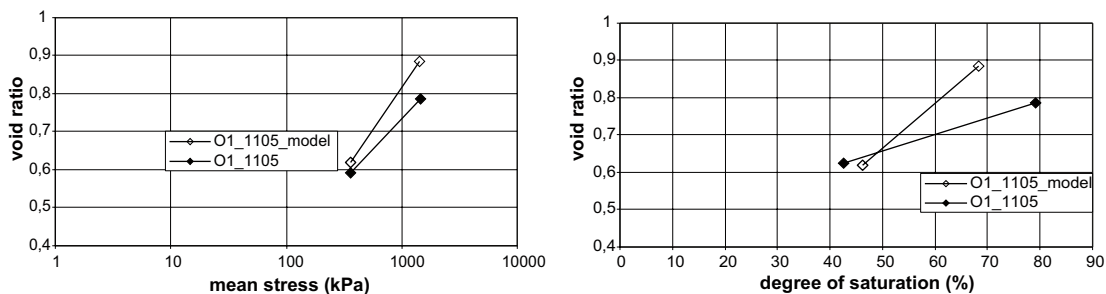

Figure A2-22. *Mean stress vs. void ratio (left figure) and degree of saturation vs. void ratio (right figure). Measured values (filled symbols) and calculated from the model (unfilled symbols). Results from RH = 85% and test type OCS.*

Figure A2-23. *Mean stress vs. void ratio (left figure) and degree of saturation vs. void ratio (right figure). Measured values (filled symbols) and calculated from the model (unfilled symbols). Results from RH = 85% and test type SCL.*

Figure A2-24. *Mean stress vs. void ratio (left figure) and degree of saturation vs. void ratio (right figure). Measured values (filled symbols) and calculated from the model (unfilled symbols). Results from RH = 98% and test type OCS.*

Figure A2-25. *Mean stress vs. void ratio (left figure) and degree of saturation vs. void ratio (right figure). Measured values (filled symbols) and calculated from the model (unfilled symbols). Results from RH = 98% and test type SCL.*

Comments

Good agreement was shown between the measured and calculated results in the used range of relative humidity. In the calculations the maximum swelling pressure are calculated from the Equation A2-3 which includes $RH_{ret}(w_s)$ for the water content at saturation w_s. In some of the tests RH_{ret} was larger than 97% and in this range the relation used has low accuracy. Less good correspondence was also seen between the measurements and the calculations cf. Figure A2-25.

The model used, presented by Dueck and Börgesson (2007), was mainly based on results from constant volume tests but the present results show good agreement between measured and calculated void ratio also after volume change.

Results from the HM-model

Each specimen is presented as void ratio versus means stress and degree of saturation in Figures A2-26 to A2-40. The measured values are represented by filled symbols and the calculated from the model are represented by unfilled symbols. Some of the diagrams are also shown as Figures A2-20 to A2-25. At removal of load, e.g. the final part of test O2_0905 in Figure A2-27, the maximum mean stress was included in the calculation in addition to the measured RH and P.
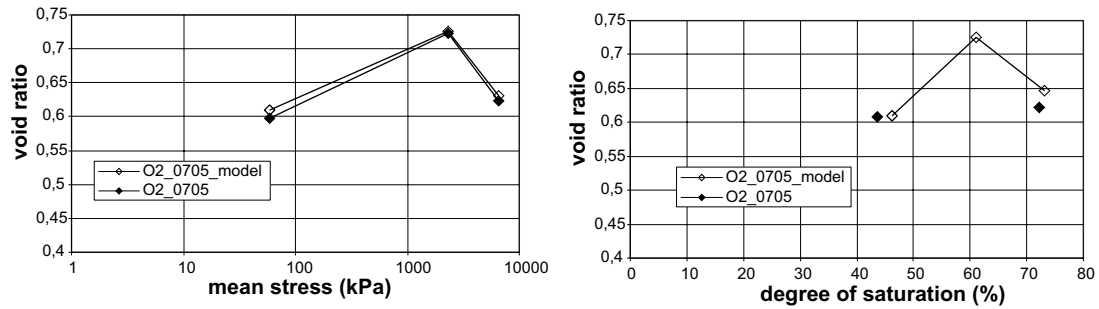

Figure A2-26. *Results from RH = 75% and test type 1 or OCL (O2_0705).*
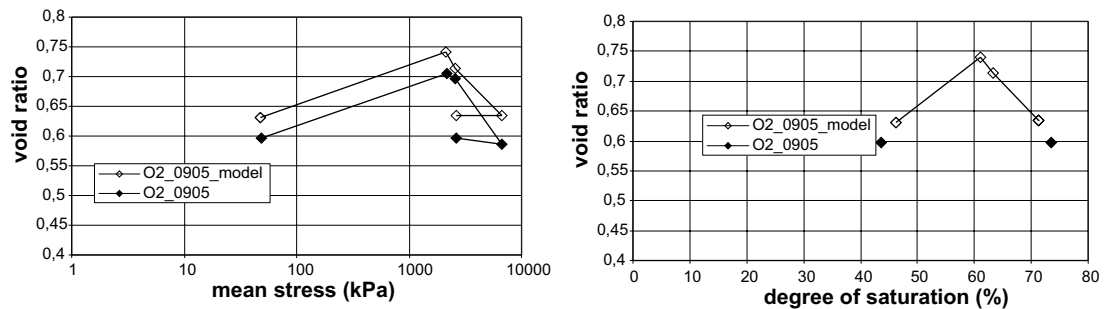
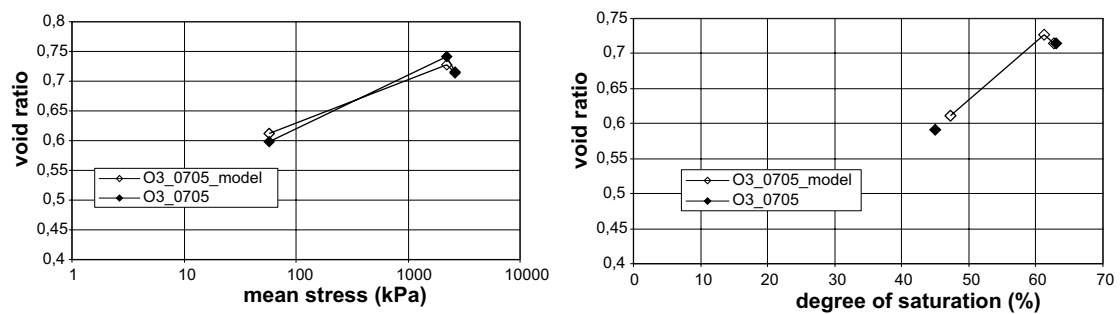*Figure A2-27.* *Results from RH = 75% and test type 1 or OCL (O2_0905).*

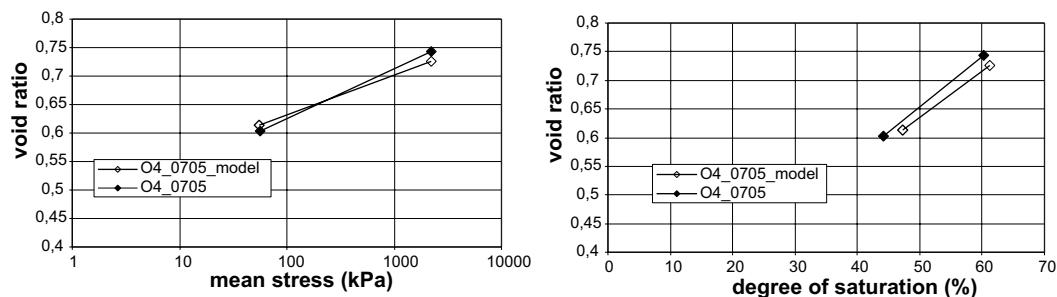*Figure A2-28.* *Results from RH = 75% and test type 1 or OCL (O3_0705).*

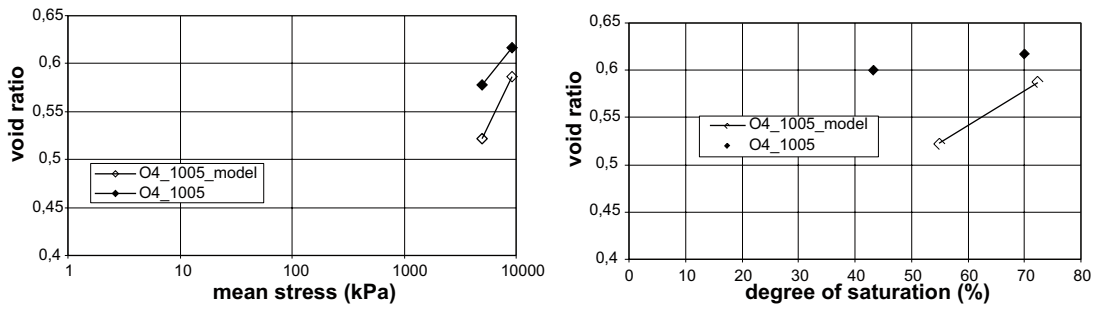*Figure A2-29.* *Results from RH = 75% and test type 2 or SCL (O4_0705).*

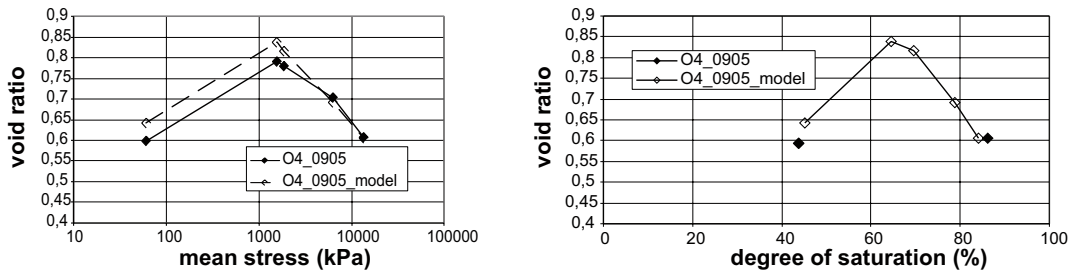**Figure A2-30.** *Results from RH = 75% and test type 2 or SCL (O4_1005).*

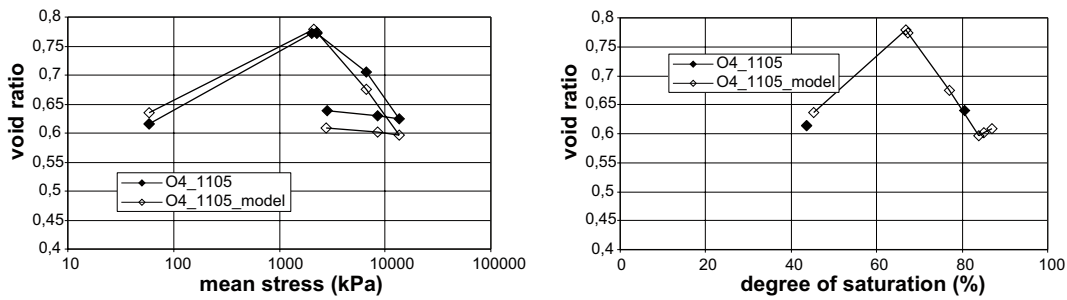**Figure A2-31.** *Results from RH = 85% and test type 1 or OCL (O4_0905).*

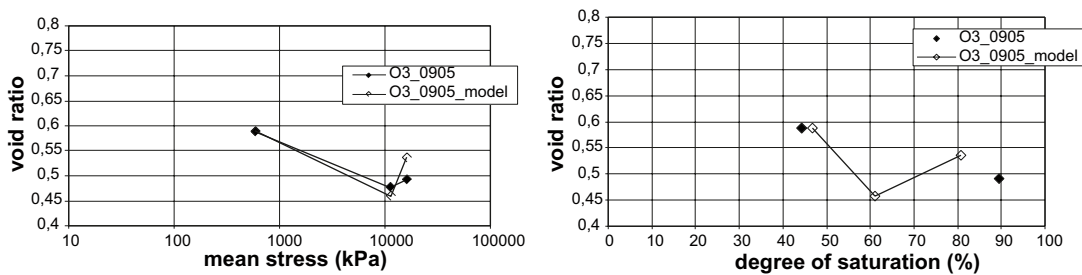**Figure A2-32.** *Results from RH = 85% and test type 1 or OCL (O4_1105).*

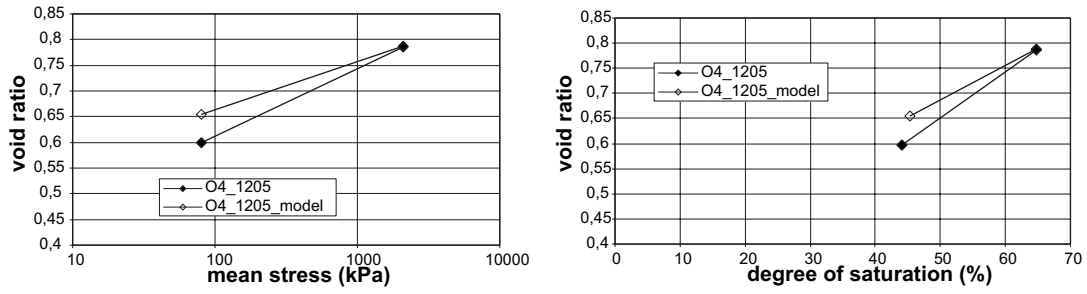**Figure A2-33.** *Results from RH = 85% and test type 2 or SCL (O3_0905).*

Figure A2-34. *Results from RH = 85% and test type 2 or SCL (O4_1205).*

Figure A2-35. *Results from RH = 98% and test type 1 or OCL (O1_0905).*
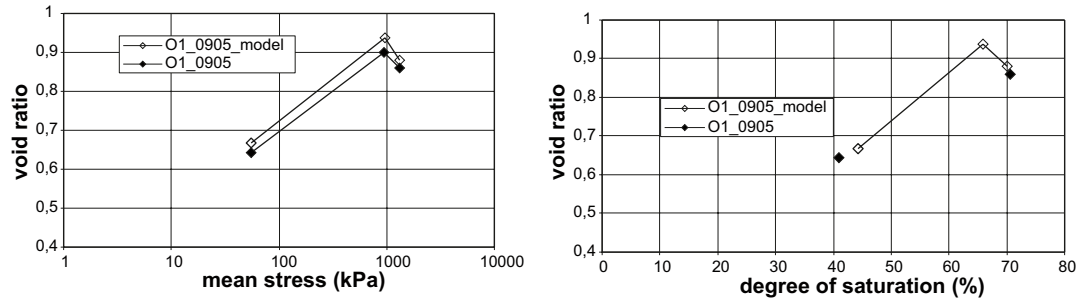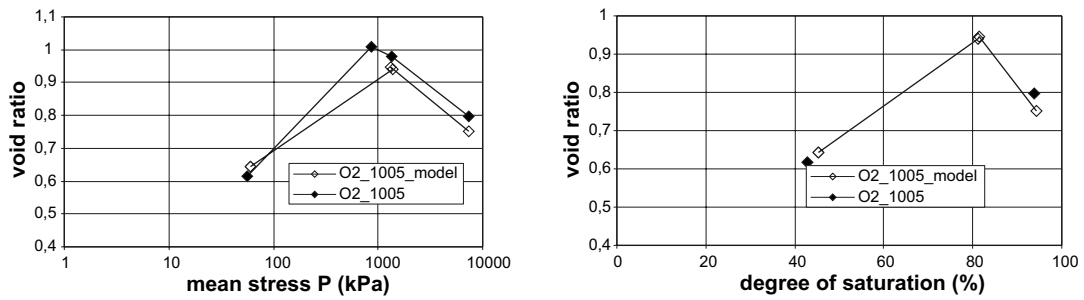

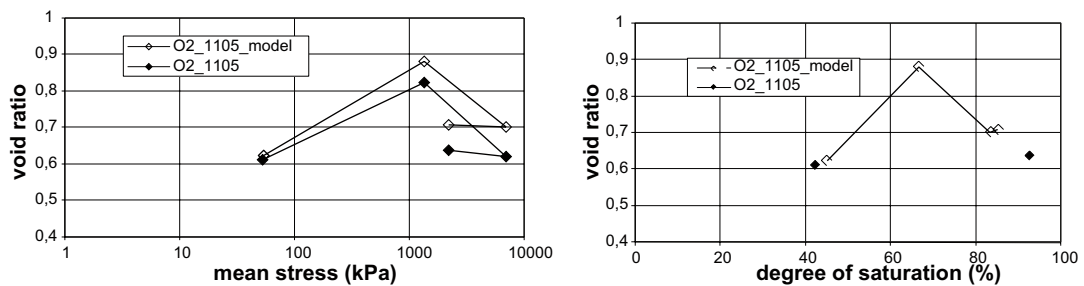**Figure A2-36.** *Results from RH = 98% and test type 1 or OCL (O2_1005).*

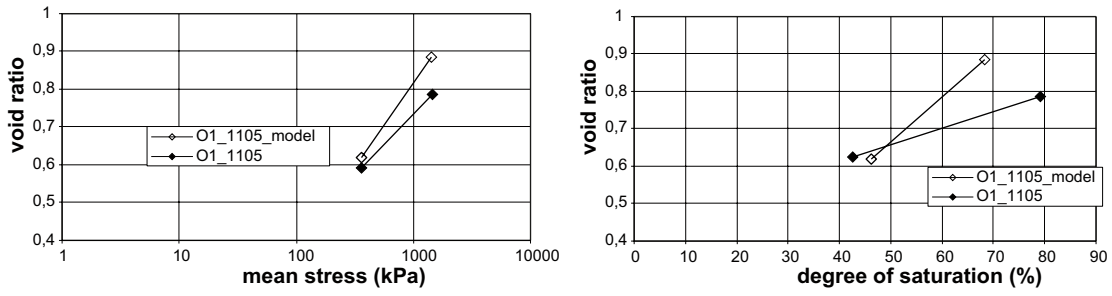**Figure A2-37.** *Results from RH = 98% and test type 1 or OCL (O2_1105).*

Figure A2-38. *Results from RH = 98% and test type 2 or SCL (O1_1105).*
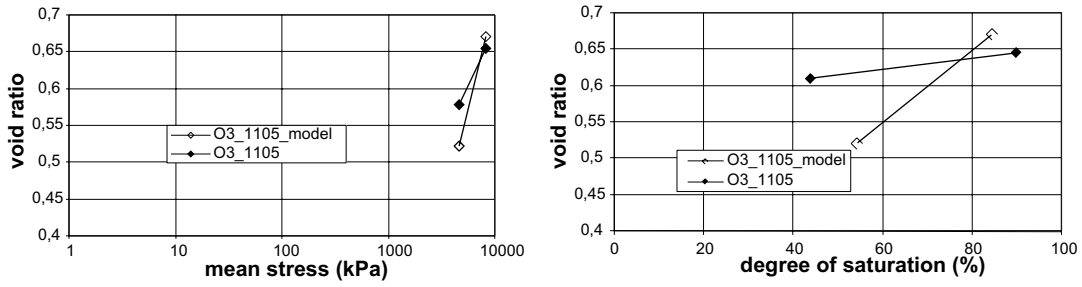

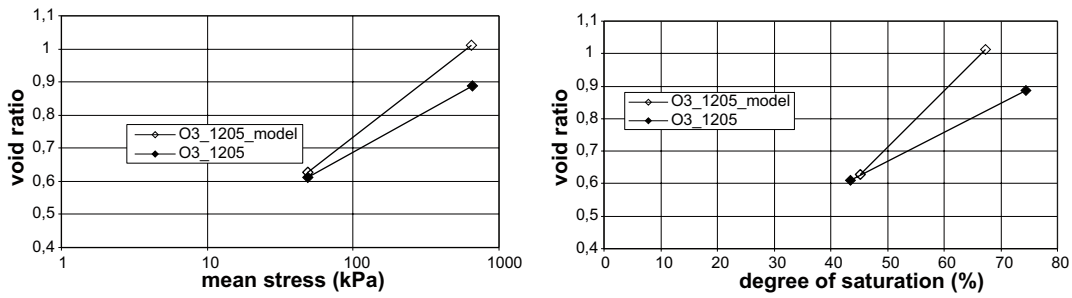**Figure A2-39.** *Results from RH = 98% and test type 2 or SCL (O3_1105).*

Figure A2-40. *Results from RH = 98% and test type 2 or SCL (O3_1205).*

Moisture transport

Results from all tests, tables

The results from all moisture transport tests are presented in Tables A3-1 to A3-6. The results are presented as water content, void ratio, relative humidity and swelling pressure versus time and versus distance from upper surface. The more detailed description below is illustrated with coloured circles and arrows in Table A3-1.

- The results are presented versus distance from upper surface of the specimens (encircled in red) and versus time (encircled in blue).

- The water content w and void ratio e were determined on slices of each specimen after finished test. Each slice represented a certain distance from the upper surface of the specimen. Since the tests were finished after different time periods the determined w and e are presented at different distances and at different times (purple arrows).

- The relative humidity are evaluated at different times and presented as values measured by the upper, middle and lower sensors (green arrow). The relative humidity set by the salt solution is shown in the first column (yellow arrow).

- The swelling pressure are evaluated from each finished test and presented with the appropriate time (black arrow).

Table A3-1. Results from moisture transport test TR3.

Transport test

Test No **TR_3**   Date   **2005-11-23**
Variables w, e and RH vs time(h) and distance(mm): Tables

distance (mm)	2.5	10	20	30	37.5
	A	B	C	D	E

Variable: water content (%)

	time					
TR_3_comp	0	9.4	9.4	9.4	9.4	9.4
TR_3_C	71	13.8	11.0	9.8	9.5	9.6
TR_3_B	313	15.2	13.3	11.7	10.7	10.6
TR_3_B2	362	14.3	12.9	11.4	10.7	10.6
TR_3_A	607	14.4	13.4	12.3	11.6	11.3

Variable: void ratio e

	time	A	B	C	D	E
TR_3_comp	0		0.62	0.65	0.70	
TR_3_C	71		0.65	0.64	0.66	
TR_3_B	313	0.70	0.64	0.62	0.62	0.63
TR_3_B2	362		0.65	0.64	0.65	
TR_3_A	607	0.65	0.64	0.63	0.66	

distance from upper	0	10	20	30	(mm)

Variable: RH (%)

Cyl No	time with circulation		RHup (%)	RHmid (%)	RHdown(%)	P (kPa)
	0	85	49.5	49.4	49.5	
TR_3_C	71	85	57.6	52.2	50.1	2558
TR_3_B	313	85	66.2	60.9	56.9	4570
TR_3_B2	362	85	67.3	62.1	58.1	6036
TR_3_A	607	85	68.4	65.3	62.2	7657

Table A3-2. Results from moisture transport test TR4.

Transport test

Test No **TR_4** Date **2005-11-25**
Variables w, e and RH vs time(h) and distance(mm): Tables

distance (mm)		2.5	10	20	30	37.5
		A	B	C	D	E

Variable: water content (%)

	time					
average	0 av	16.3	16.3	16.3	16.3	16.3
TR_4_C	171	17.2	16.9	16.6	16.4	16.3
TR_4_B	319	17.0	17.0	16.8	16.7	16.6
TR_4_A	463	16.7	16.6	16.5	16.7	16.5

Variable: void ratio e

	time	A	B	C	D	E
average	0 av	0.60	0.60	0.60	0.60	0.60
TR_4_C	171	0.61	0.60	0.60	0.61	0.61
TR_4_B	319	0.60	0.60	0.60	0.61	0.61
TR_4_A	463	0.59	0.59	0.60	0.61	0.62

distance from upper	0	10	20	30	(mm)

Variable: RH (%)

Cyl No	time with circulation		RHup (%)	RHmid (%)	RHdown(%)	P (kPa)
	0 av	85	75.2	74.0	74.8	
TR_4_C	171	85	75.4	74.9	74.8	673
TR_4_B	319	85	75.4	75.3	75.2	2640
TR_4_A	463	85	74.0	74.3	74.3	2317

Table A3-3. Results from moisture transport test TR5.

Transport test

Test No **TR_5** Date **2006-01-30**
Variables w, e and RH vs time(h) and distance(mm): Tables

distance (mm)		2.5	10	20	30	37.5
		A	B	C	D	E

Variable: water content (%)

	time					
average	0 av 0	16.5	16.5	16.5	16.5	16.5
TR_5_B	153	16.9	16.8	16.6	16.6	16.2
TR_5_C	463	16.8	16.7	16.5	16.5	16.5

Variable: void ratio e

	time	A	B	C	D	E
average	0 av 0	0.61				
TR_5_B	153	0.60	0.61	0.62	0.63	0.63
TR_5_C	463	0.60	0.60	0.60	0.62	0.63

distance from upper	0	10	20	30	(mm)

Variable: RH (%)

Cyl No	time with circulation		RHup (%)	RHmid (%)	RHdown(%)	P (kPa)
	0 av 0	85				
TR_5_B	153	85	75.2	74.8	74.8	2734
TR_5_C	463	85	74.0	74.3	74.3	2972
	153	85	75.2	74.8	74.8	
	463	85	74.0	74.3	74.3	TR_4.xls

Table A3-4. Results from moisture transport test TR6.

Transport test						
Test No **TR_6** Date **2006-01-31**						
Variables w, e and RH vs time(h) and distance(mm): Tables						

distance (mm)	2.5	10	20	30	37.5
	A	B	C	D	E

Variable: water content (%)

	time	A	B	C	D	E
average	0 av	16.3	16.3	16.3	16.3	16.3
TR_6_C	160	18.9	17.9	16.9	16.6	16.7
TR_6_A	509	18.2	17.8	17.3	17.1	16.9

Variable: void ratio e

	time	A	B	C	D	E
average	0 av	0.62	0.62	0.62	0.62	0.62
TR_6_C	160	0.66	0.65	0.65	0.66	0.67
TR_6_A	509	0.63	0.63	0.63	0.64	0.65

distance from upper	0	10	20	30	(mm)

Variable: RH (%)

Cyl No	time with circulation		RHup (%)	RHmid (%)	RHdown(%)	P (kPa)
	0	98	71.5	72.2	72.5	
TR_6_C	160	98	80.6	80.2	79.3	6295
TR_6_A	509	98	80.8	80.9	80.0	5680

Table A3-5. Results from moisture transport test TR7.

Transport test						
Test No **TR_7** Date **2006-01-31**						
Variables w, e and RH vs time(h) and distance(mm): Tables						

distance (mm)	2.5	10	20	30	37.5
	A	B	C	D	E

Variable: water content (%)

	time	A	B	C	D	E
average	0_av	9.5	9.5	9.5	9.5	9.5
TR_7_C	48	14.6	11.3	9.7	9.6	9.5
TR_7_B	147	15.0	12.3	10.2	9.5	9.6
TR_7_A	632	15.8	14.2	13.0	11.9	11.8

Variable: void ratio e

	time	A	B	C	D	E
average	0 av	0.53	0.53	0.53	0.53	0.53
TR_7_C	48		0.58	0.56	0.59	
TR_7_B	147	0.63	0.59	0.57	0.58	
TR_7_A	632	0.61	0.59	0.58	0.60	0.61

distance from upper	0	10	20	30	(mm)

Variable: RH (%)

Cyl No	time with circulation		RHup (%)	RHmid (%)	RHdown(%)	P (kPa)
	0_av	98	48.0	48.7	48.8	
TR_7_C	48	98	54.1	50.1	48.8	6778
TR_7_B	147	98	62.8	55.6	51.7	9879
TR_7_A	632	98	73.0	68.7	64.6	13900

Table A3-6. Results from moisture transport test TR1/2.

```
┌─────────────────────────────────────────────────────────────────────────┐
│ Transport test                                                            │
│ Test No    TR_1/2    Date      2005-11-25                                 │
│ Variables w, e and RH vs time(h) and distance(mm): Tables                 │
│                                                                           │
│                                                                           │
│            distance F1 (mm)        6.4      17       28                   │
│            distance F2 (mm)         6      16.8     29.2                  │
│                                                                           │
│ Variable: water content (%)                                              │
│            time*                                                          │
│                   0             9.4      9.4      9.4                      │
│ F1         574                 23.5     20.1     17.9                      │
│ F2         613                 24.5     20.8     18.4                      │
│                                                                           │
│                                                                           │
│                                                                           │
│ Variable: void ratio e                                                    │
│            time *                                                         │
│                   0             0.64     0.64     0.64    **               │
│ F1              574             0.70     0.68     0.68                     │
│ F2              613             0.72     0.68     0.67                     │
│                                                                           │
│                                                                           │
│                                                                           │
│ distance from wet                                                         │
│            F1              0    16.5    (mm)                              │
│            F2              0    16.4    (mm)                              │
│ Variable: RH (%)                                                          │
│            time*                                                          │
│ Cyl No                          RH (%)                    P (kPa)         │
│                   0    100      42        ***                             │
│ F1         574    100      88.3                           8700            │
│ F2         613    100      91.4                           9400            │
│                                                                           │
│            * corrected time for not continous water transport             │
│            ** initially e = 0.64 and Sr = 41%    *** average              │
└─────────────────────────────────────────────────────────────────────────┘
```

(file: TR_sum_final.xls)

Moisture redistribution

Test results as absolute and normalized values, diagrams

The results from all tests are presented as distribution of density, water content and degree of saturation along the specimen height at different time in Figures A4-1 to A4-9. Each Figure contains all results from one type of specimen, e.g. Aa 50 0.60 or Ab 50 0.60, where Aa or Ab denote the temperature gradient 2°C/cm or 10°C/cm, respectively and the figures represent the initial degree of saturation and the initial void ratio.

In each Figure the variables w, e, S_r and ρ_d are presented as a function of distance from the upper cold surface of the specimens. In the lower part of each Figure the results are presented as relative or normalized values, calculated as the measured values, presented in the upper part of the table, divided by the average value of the actual variable of the actual specimen.

At the top of each Figure the legend is shown which denotes temperature gradient (Aa or Ab)_initial degree of saturation (%)_initial void ratio_ time in hours, e.g. Aa 50 0.60 6. The marks ✳, ◆, ■, ▲, ✕ and ● denote the elapsed times 0 h, 6 h, 24 h, 96 h, 240 h and 480 h. The temperature gradients Aa and Ab denote 2°C/cm and 10°C/cm, respectively and the final letter p indicates that the heating was obtained by a hotplate.
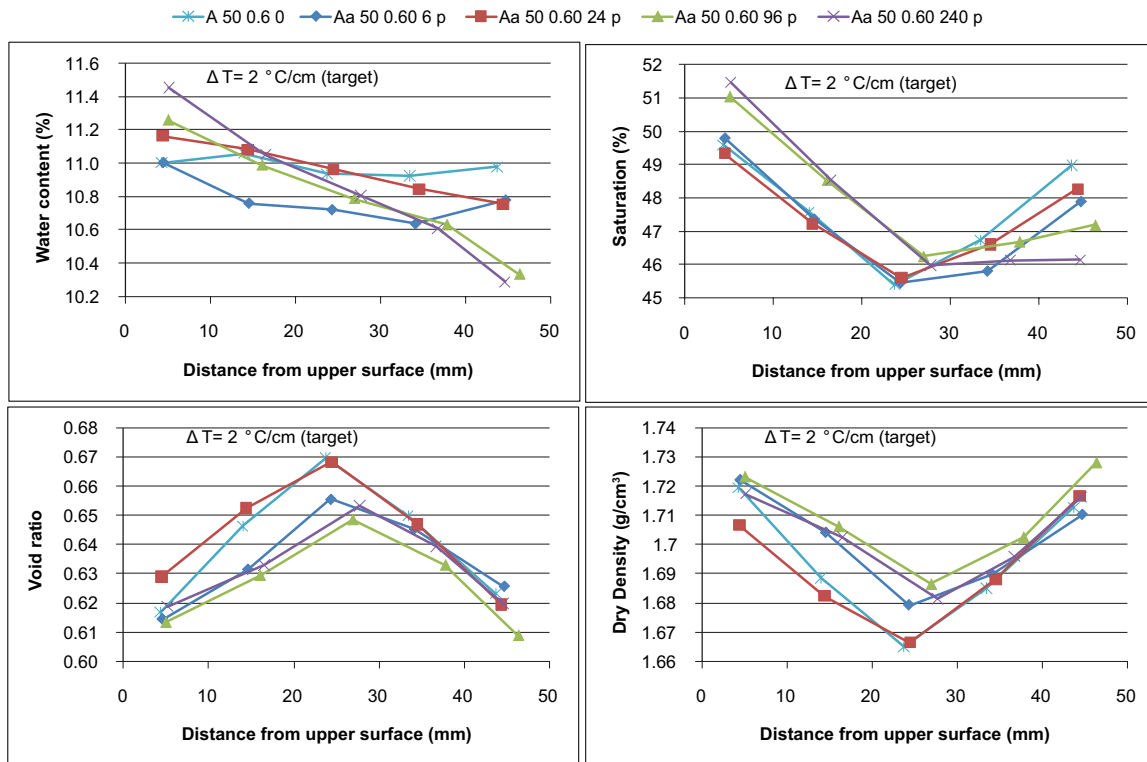
Normalized values
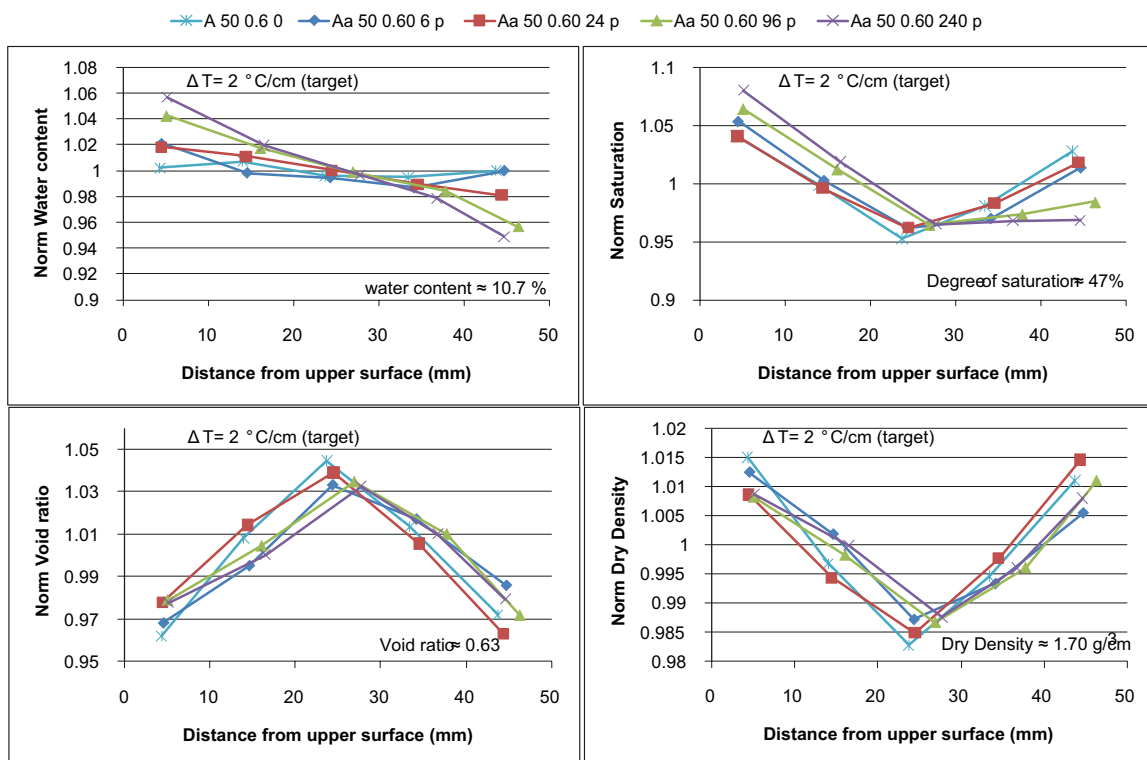
Figure A4-1. *Results from specimen type Aa 50 0.60.*
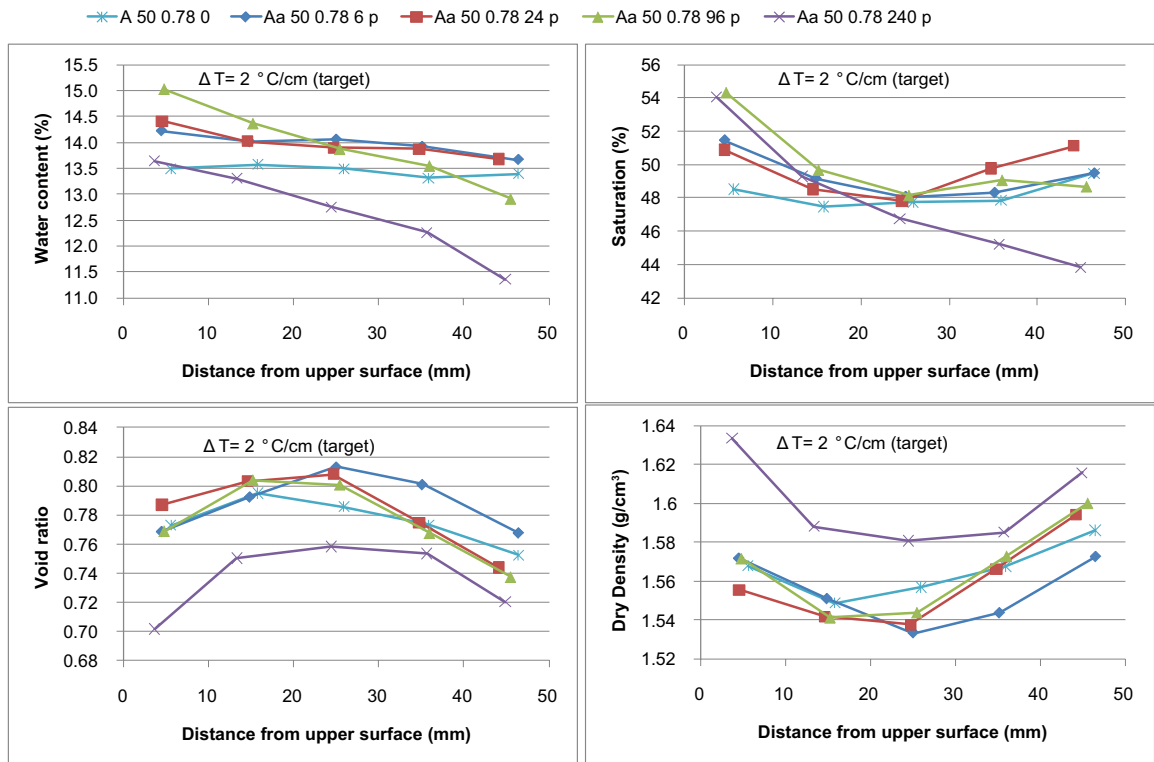
Normalized values
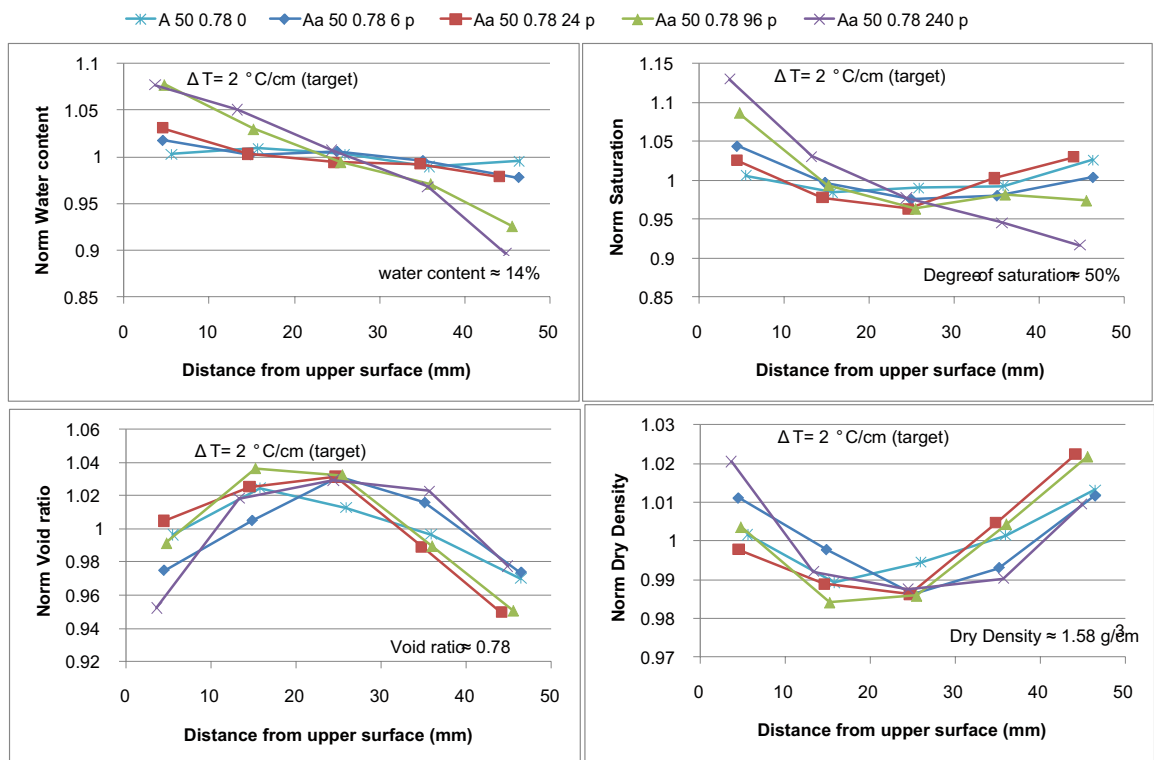
Figure A4-2. *Results from specimen type Aa 50 0.78.*
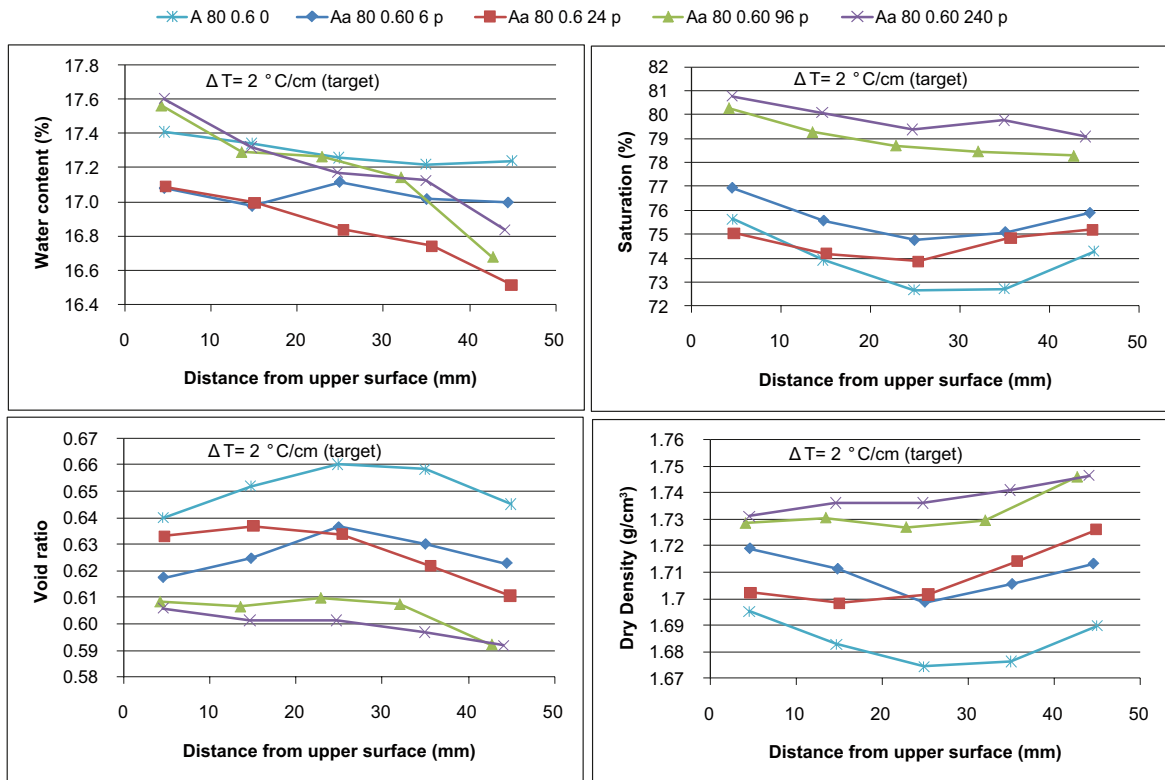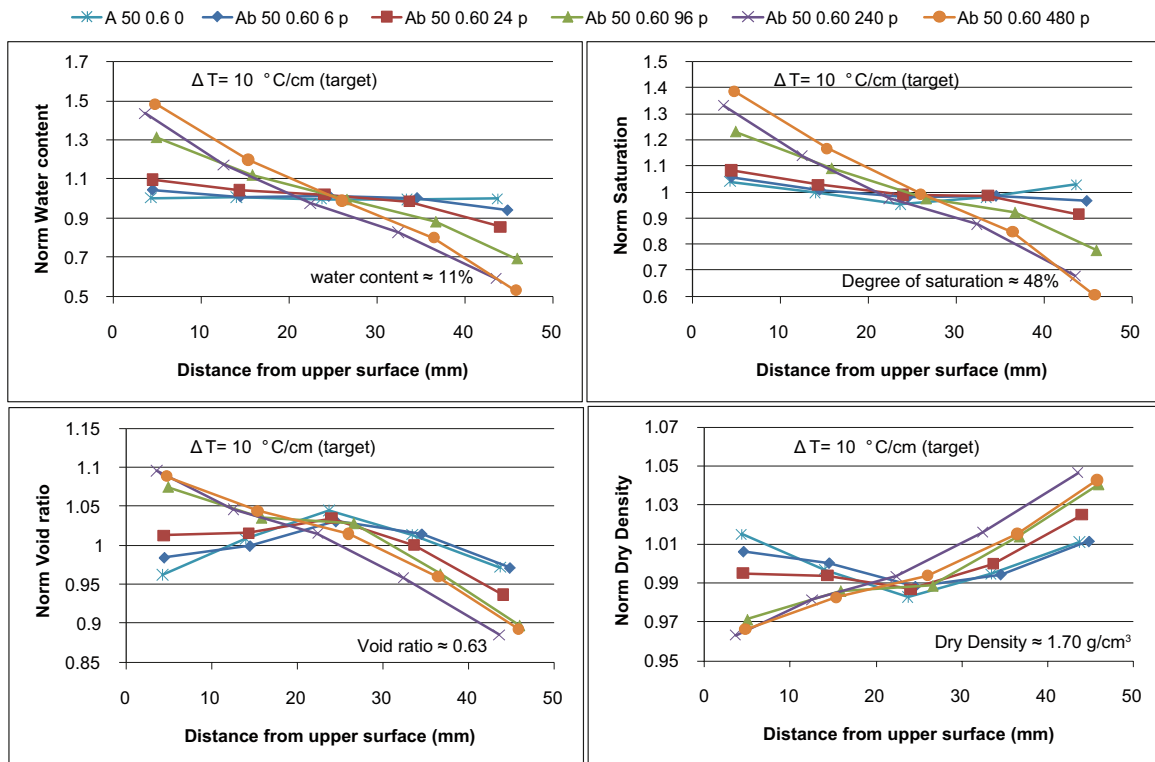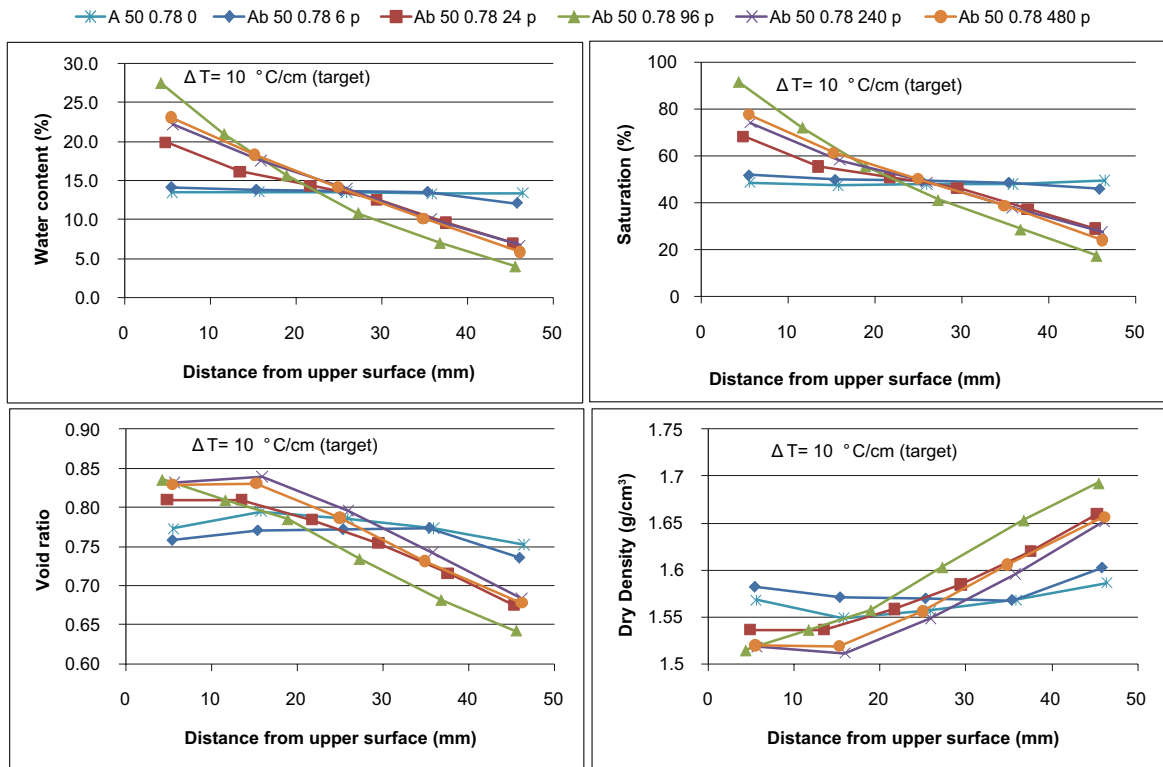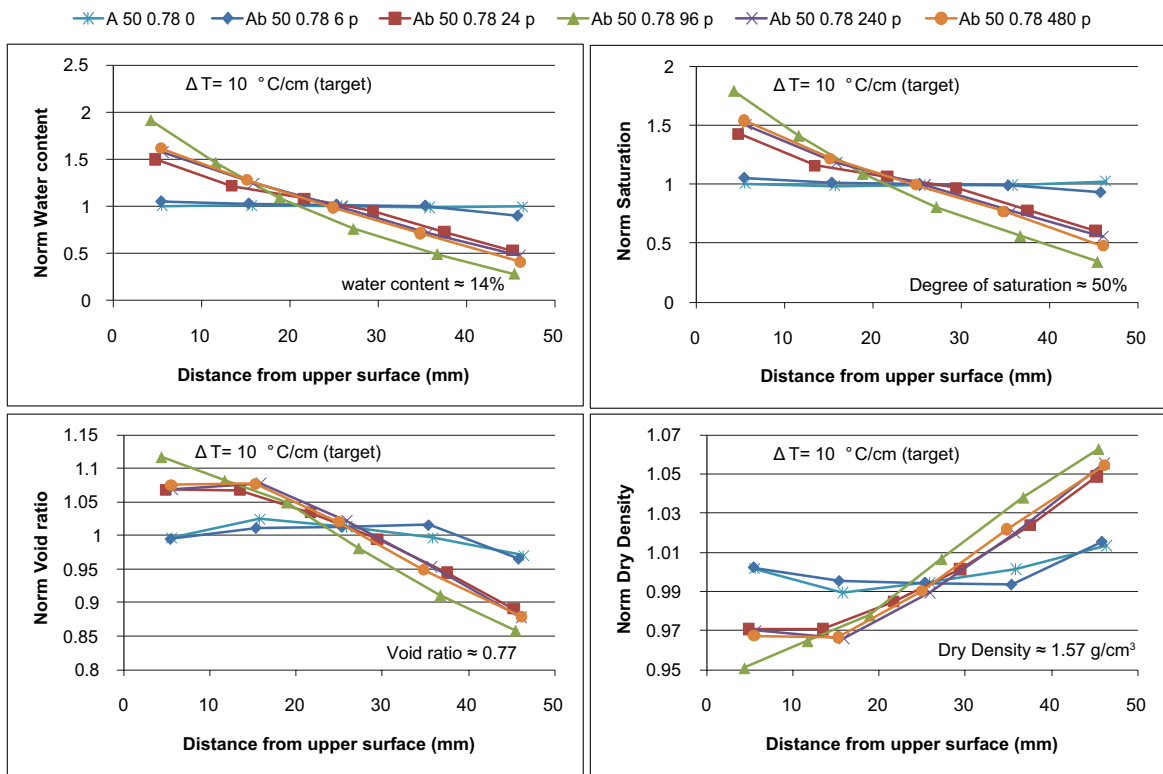
Normalized values
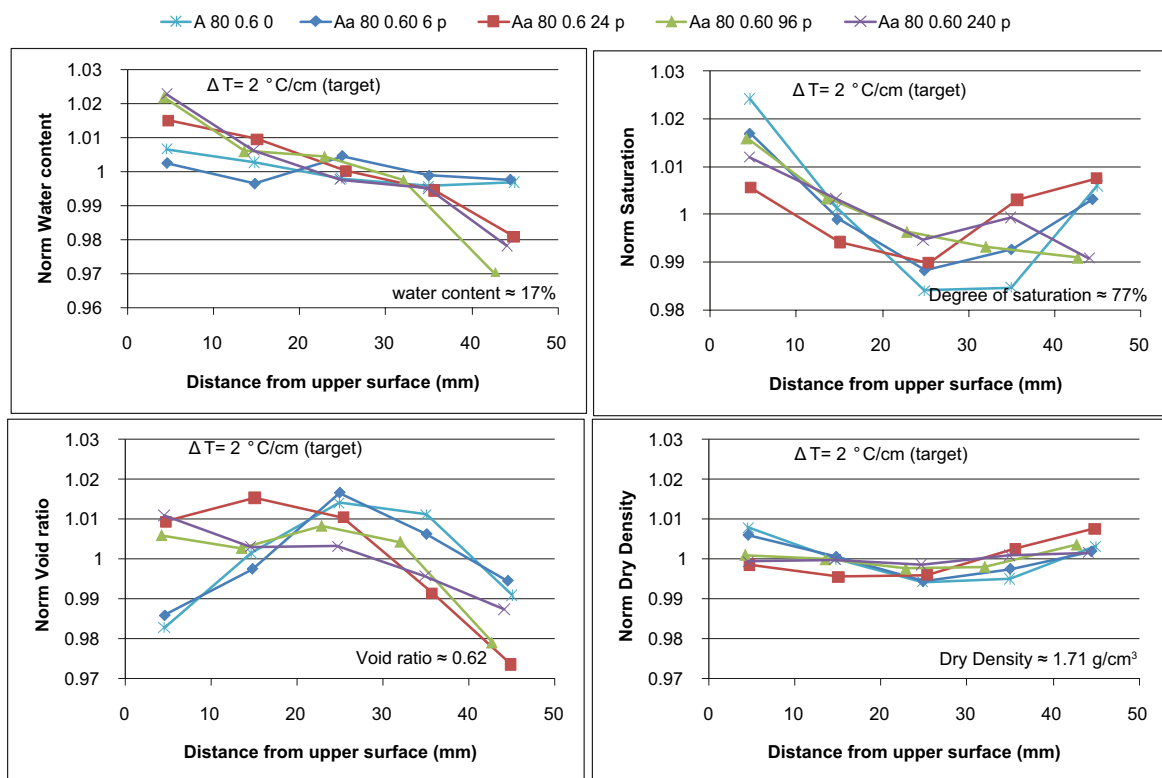
Figure A4-3. *Results from specimen type Aa 80 0.60.*
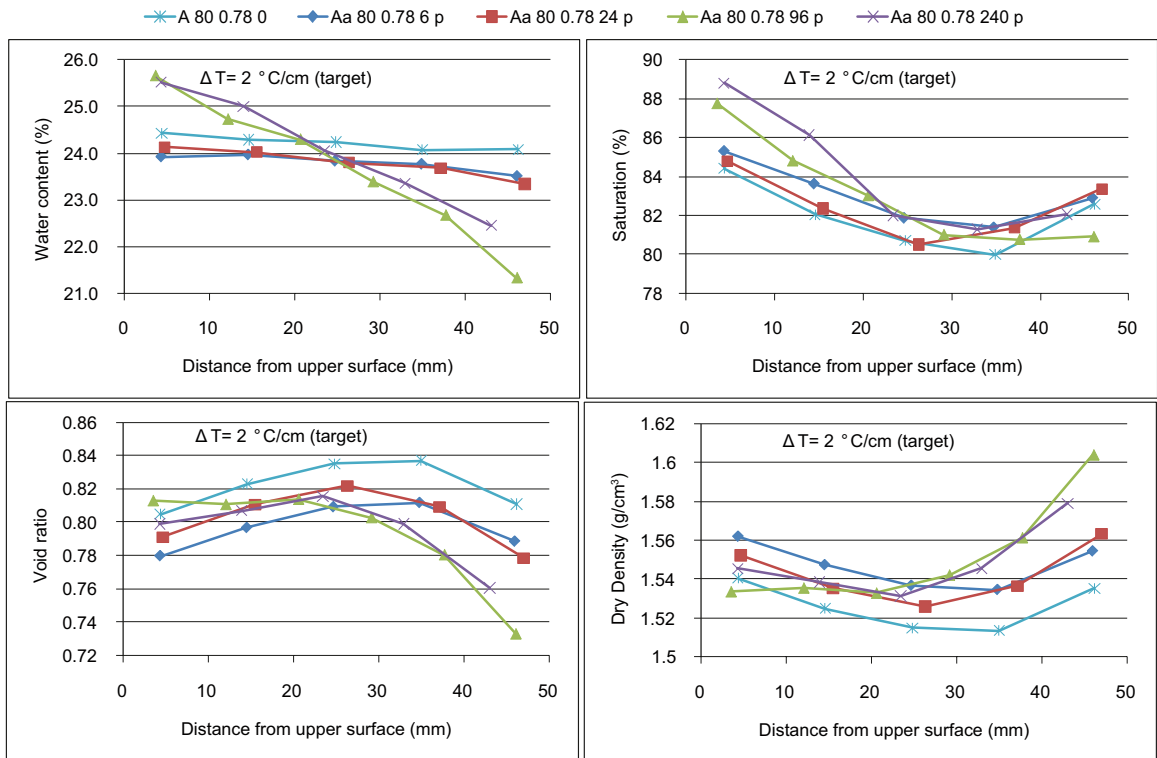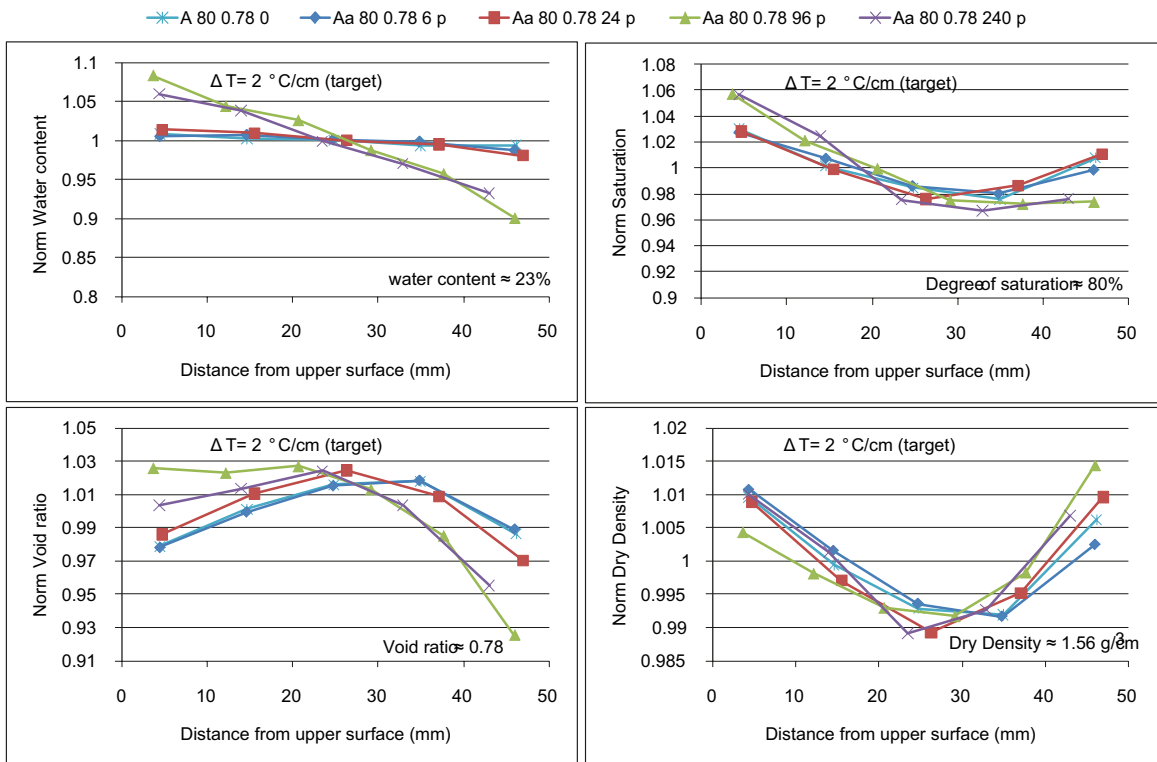
Figure A4-4. *Results from specimen type Aa 80 0.78.*
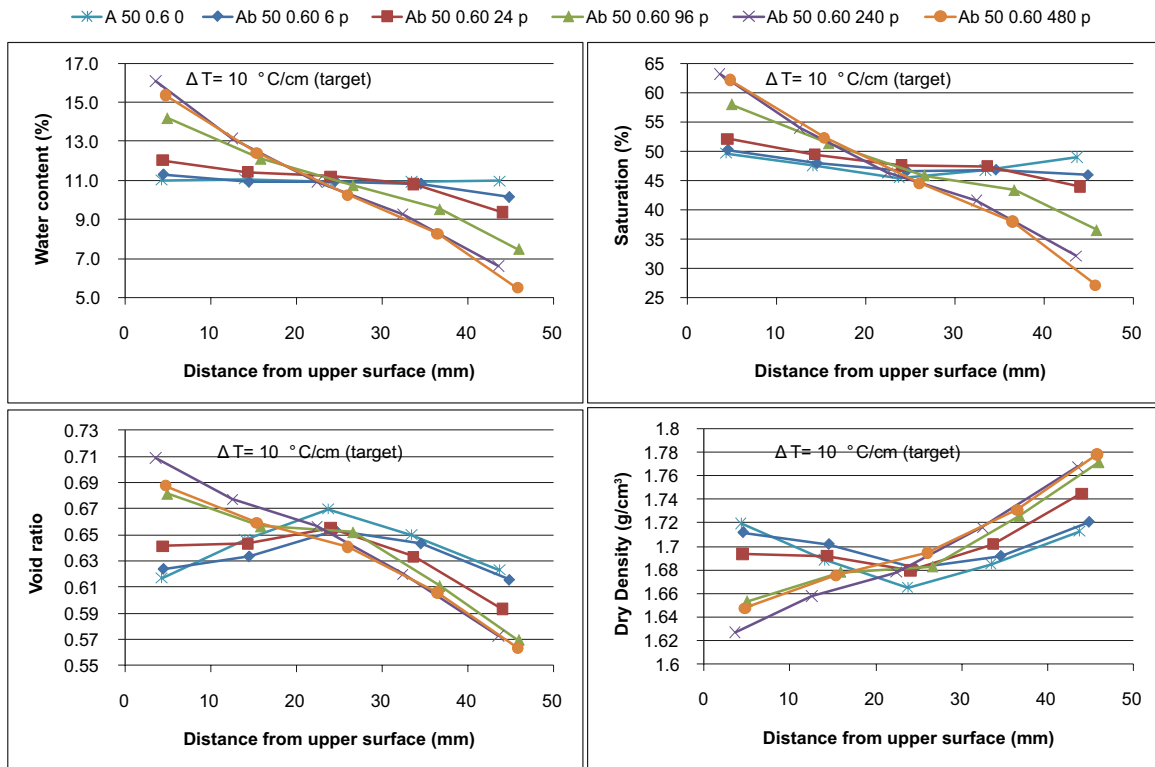
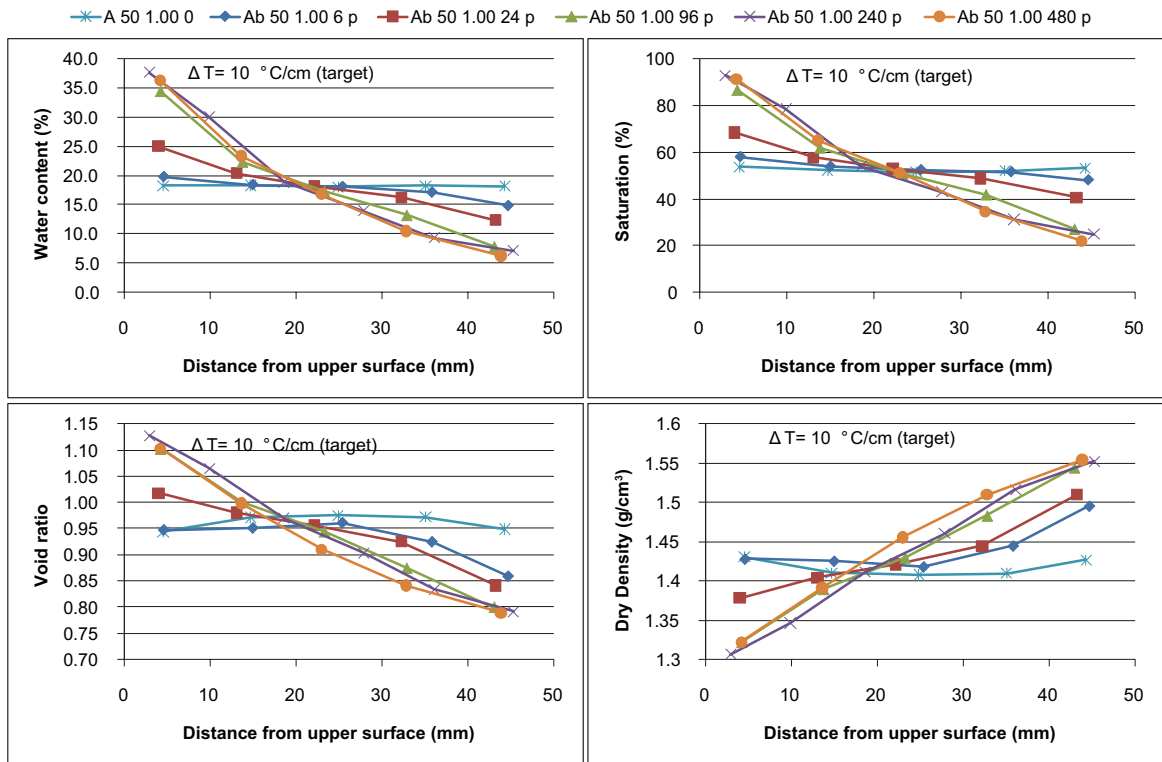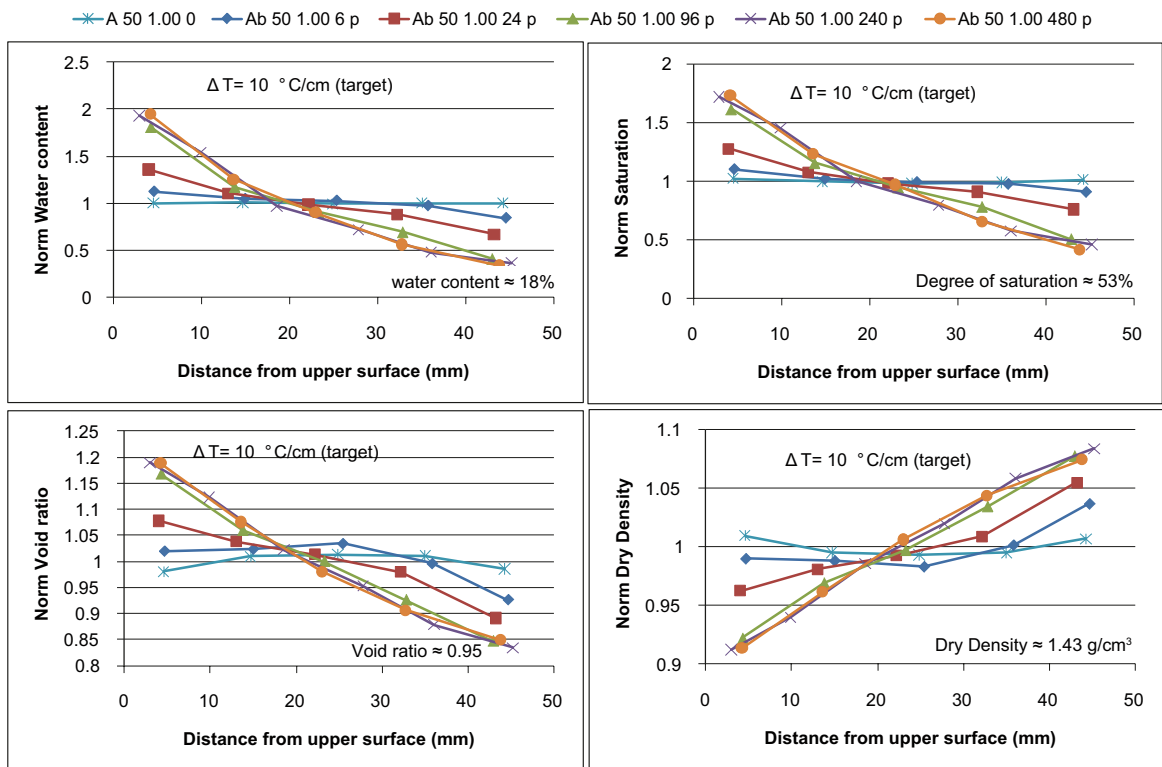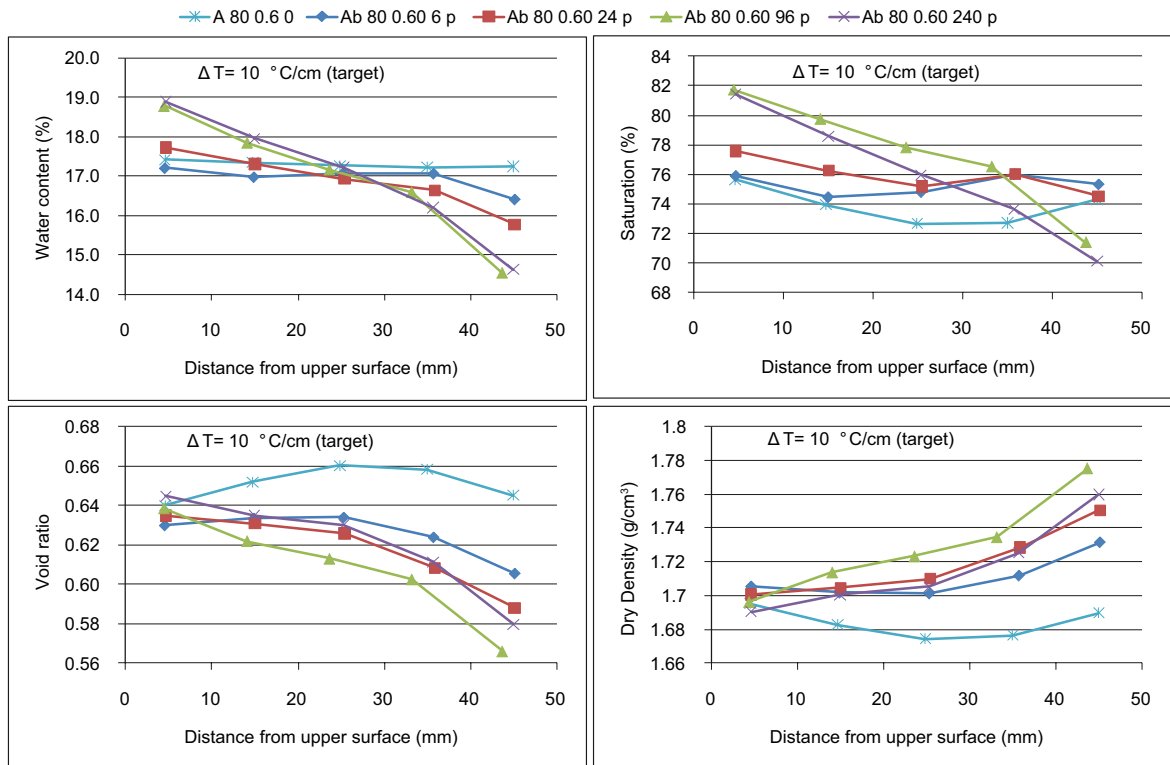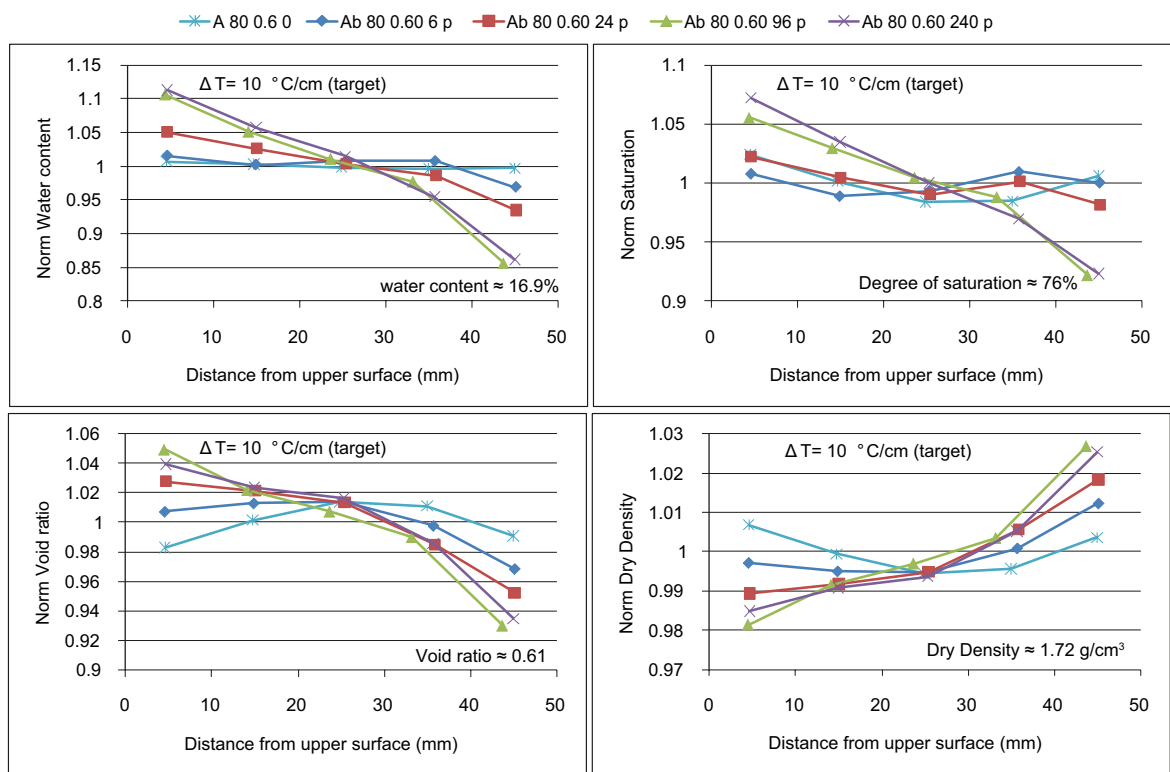**Figure A4-5.** *Results from specimen type Ab 50 0.60.*

Normalized values

Figure A4-6. *Results from specimen type Ab 50 0.78.*

Figure A4-7. *Results from specimen type Ab 50 1.00.*
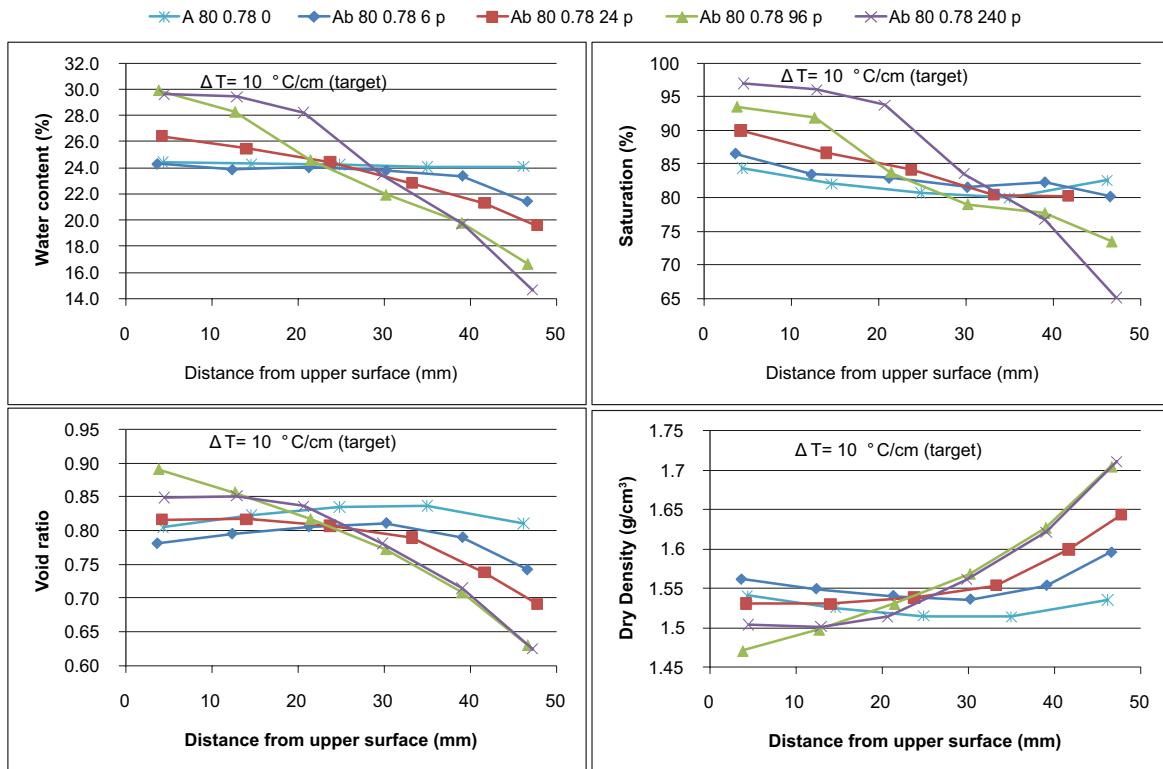
Normalized values

Figure A4-8. *Results from specimen type Ab 80 0.60.*
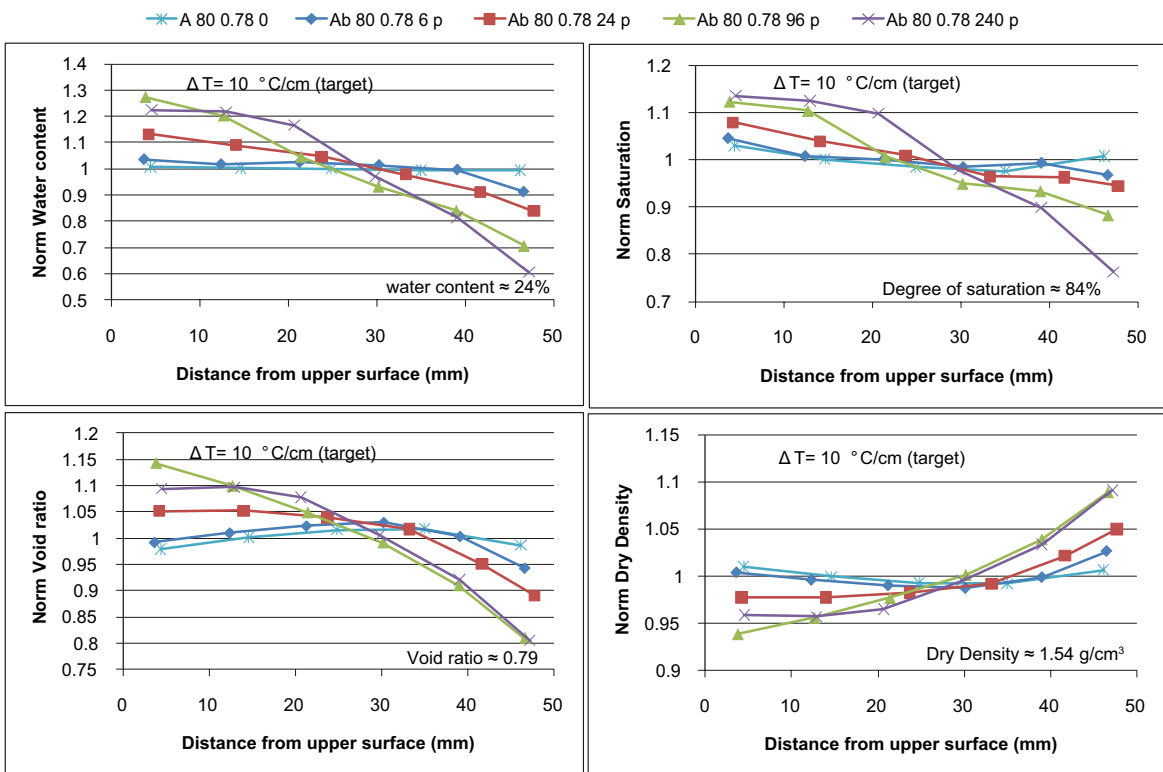
Normalized values

Figure A4-9. *Results from specimen type Ab 80 0.78.*

Test results as change from initial state, diagrams

The results from all tests are presented as distribution of absolute value and change of density and water content along the specimen height at different time in Figures A4-10 to A4-18. Each figure contains all results from one type of specimen, e.g. Aa 50 0.60 or Ab 50 0.60, where Aa or Ab denote the temperature gradient 2°C/cm or 10°C/cm, respectively and the figures represent the initial degree of saturation and the initial void ratio.

In each Figure the variables w and ρ_d are presented as a function of distance from the upper cold surface of the specimens. Values are interpolated or extrapolated to be marked equidistant on the x-axis.

At the top of each Figure the legend is shown which denotes temperature gradient (Aa or Ab)_initial degree of saturation (%)_initial void ratio_ time in hours, e.g. Aa 50 0.60 6. The marks ✳, ◆, ■, ▲, ✕ and ● denote the elapsed times 0 h, 6 h, 24 h, 96 h, 240 h and 480 h. The temperature gradients Aa and Ab denote 2°C/cm and 10°C/cm, respectively and the final letter p indicates that the heating was obtained by a hotplate.
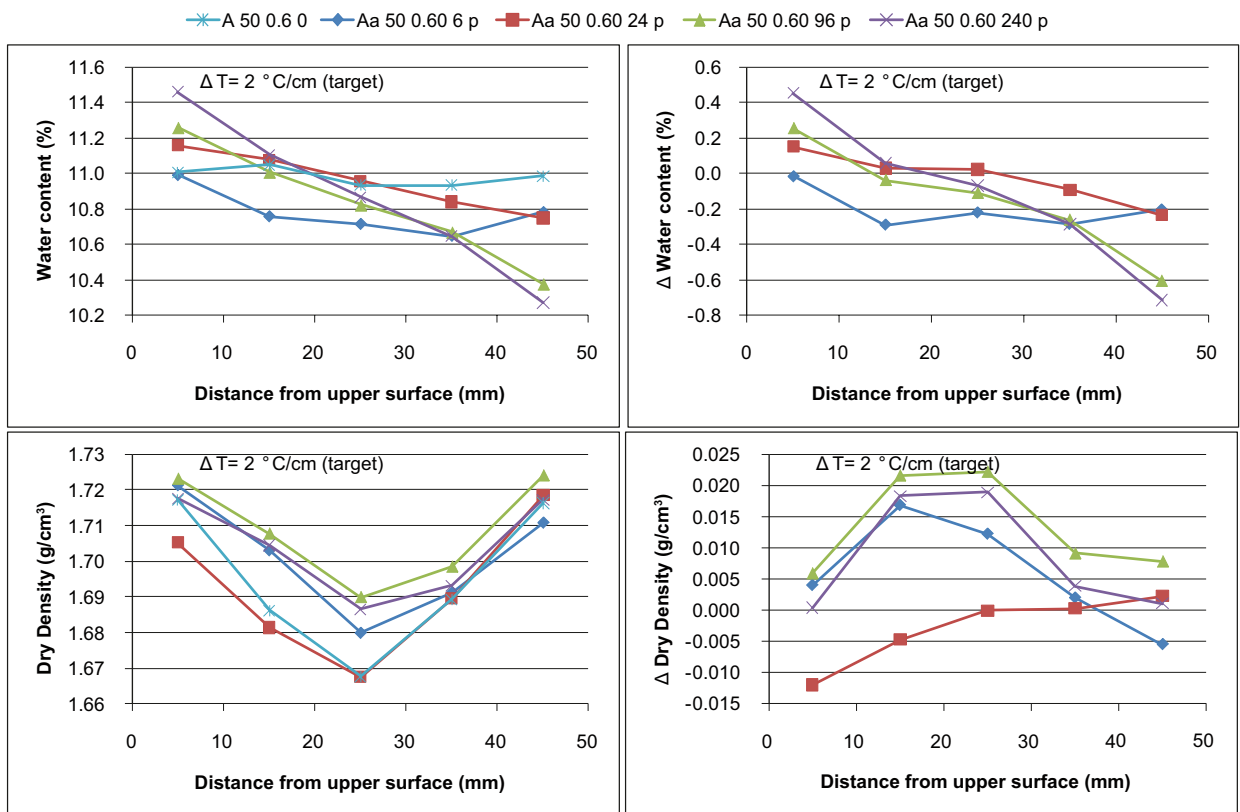

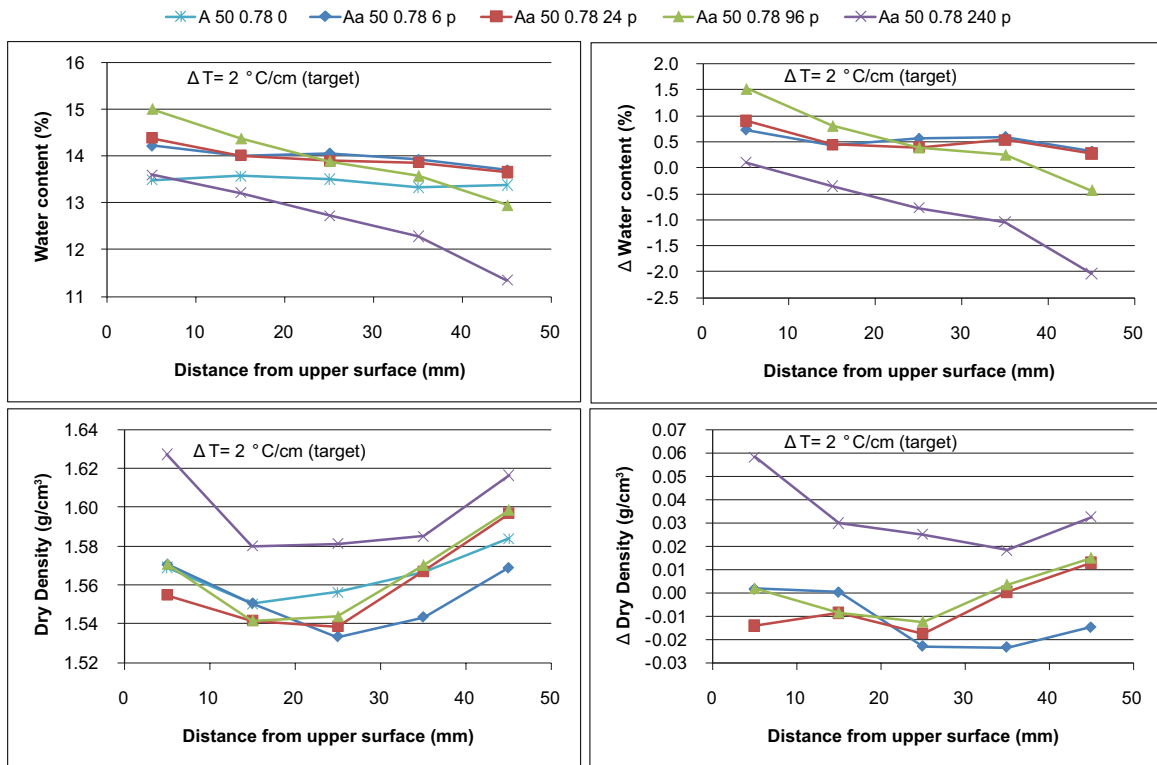**Figure A4-10.** *Results from specimen type Aa 50 0.60.*
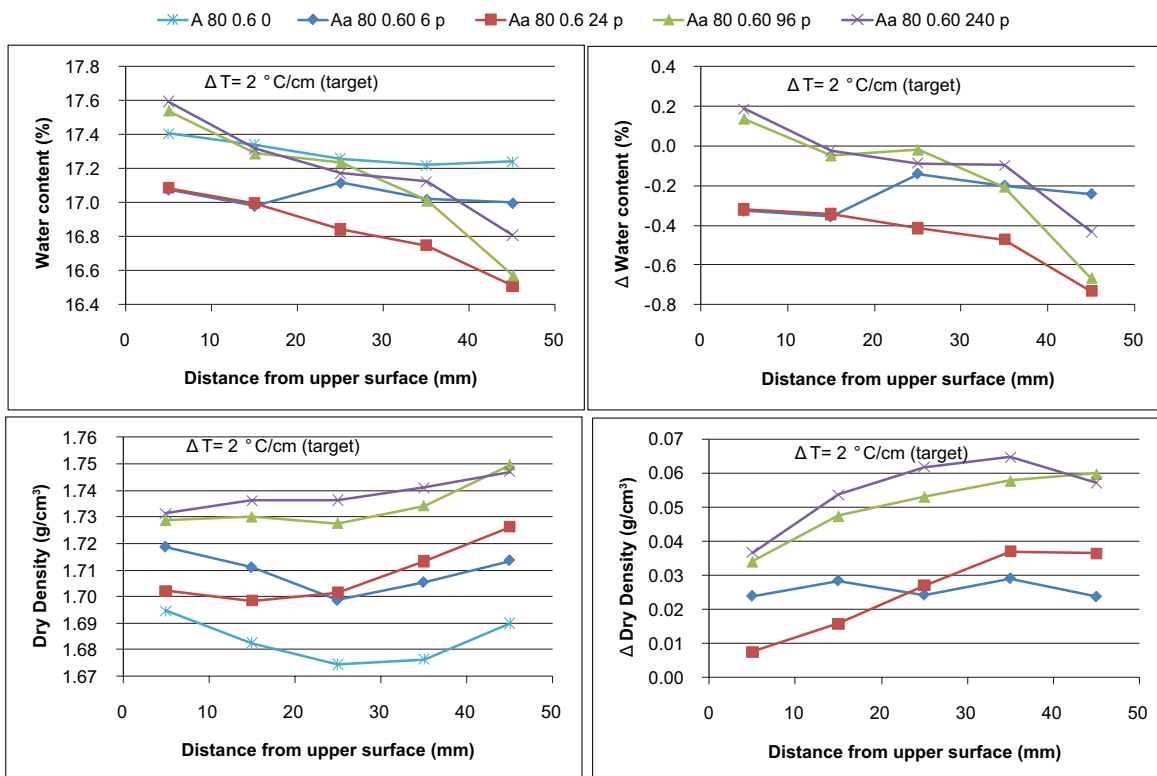
Figure A4-11. *Results from specimen type Aa 50 0.78.*

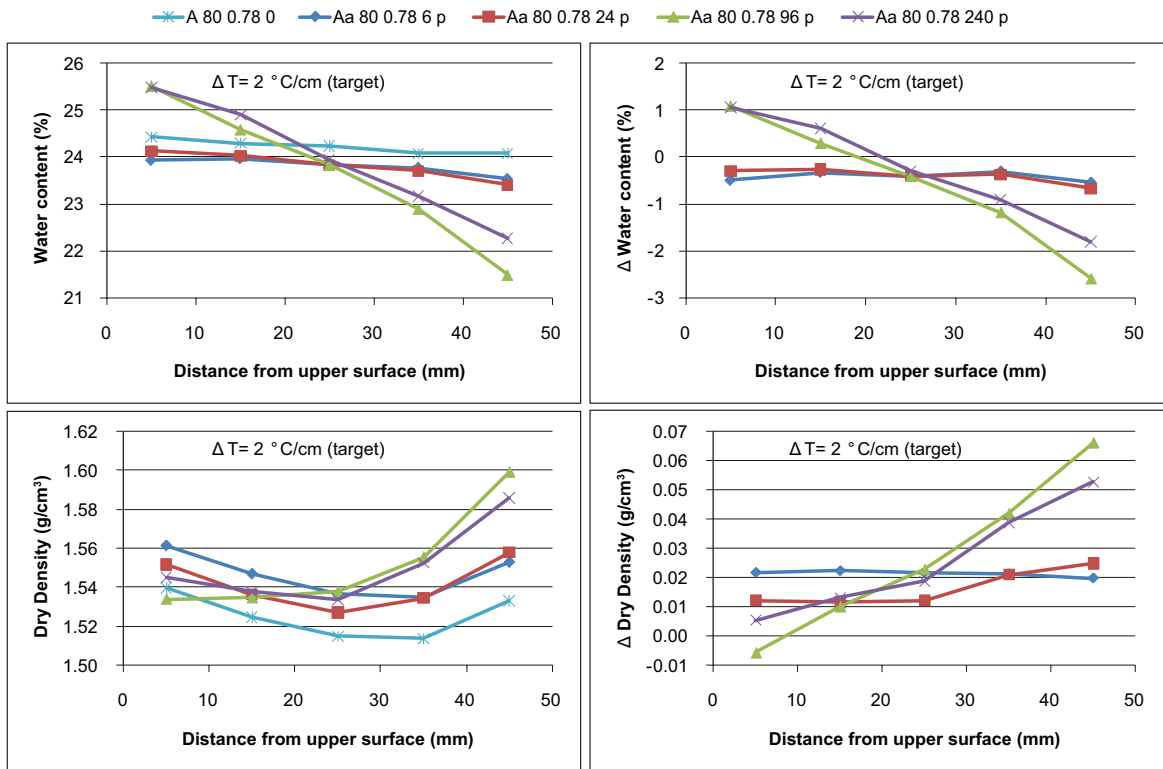**Figure A4-12.** *Results from specimen type Aa 80 0.60.*

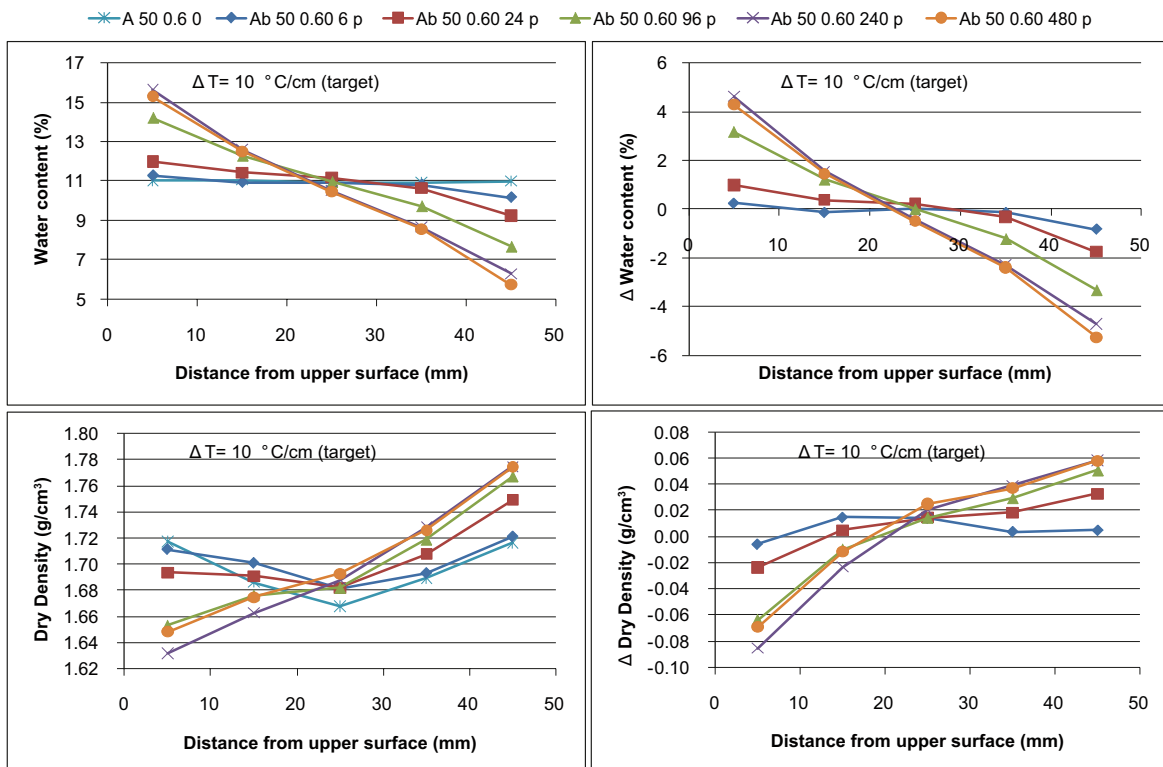**Figure A4-13.** *Results from specimen type Aa 80 0.78.*

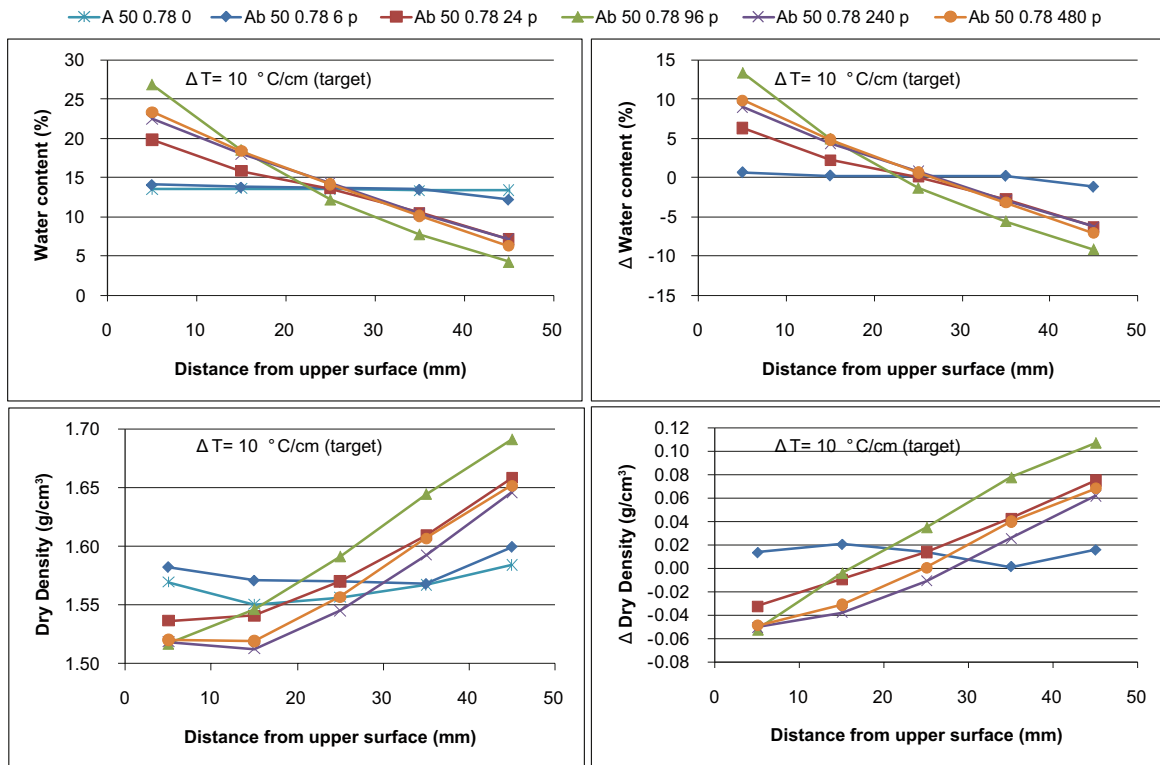**Figure A4-14.** *Results from specimen type Ab 50 0.60.*
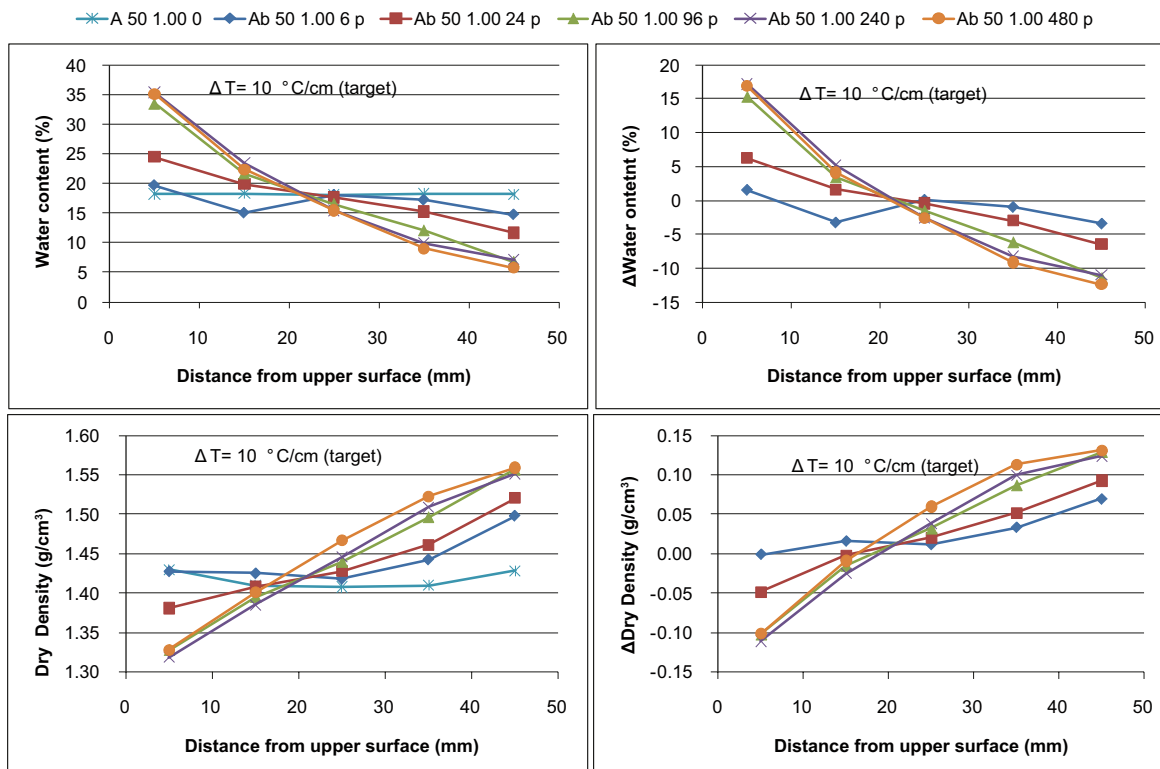
Figure A4-15. *Results from specimen type Ab 50 0.78.*
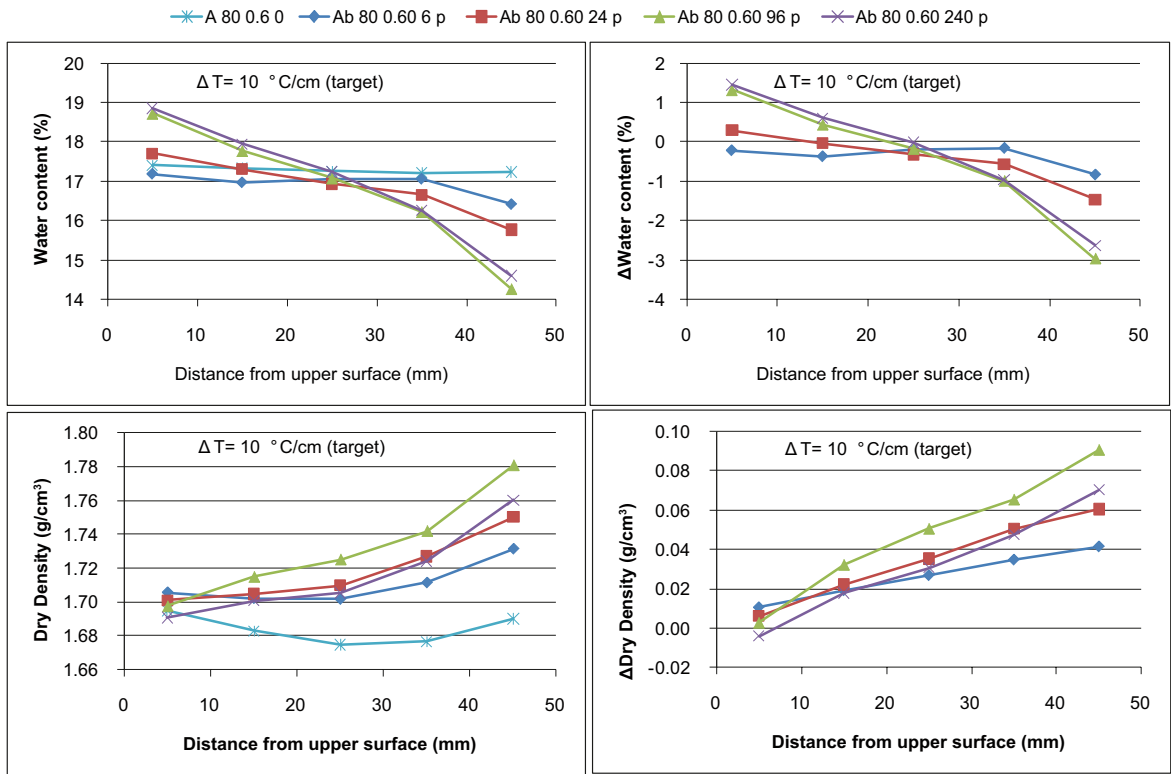

Figure A4-16. *Results from specimen type Ab 50 1.00.*

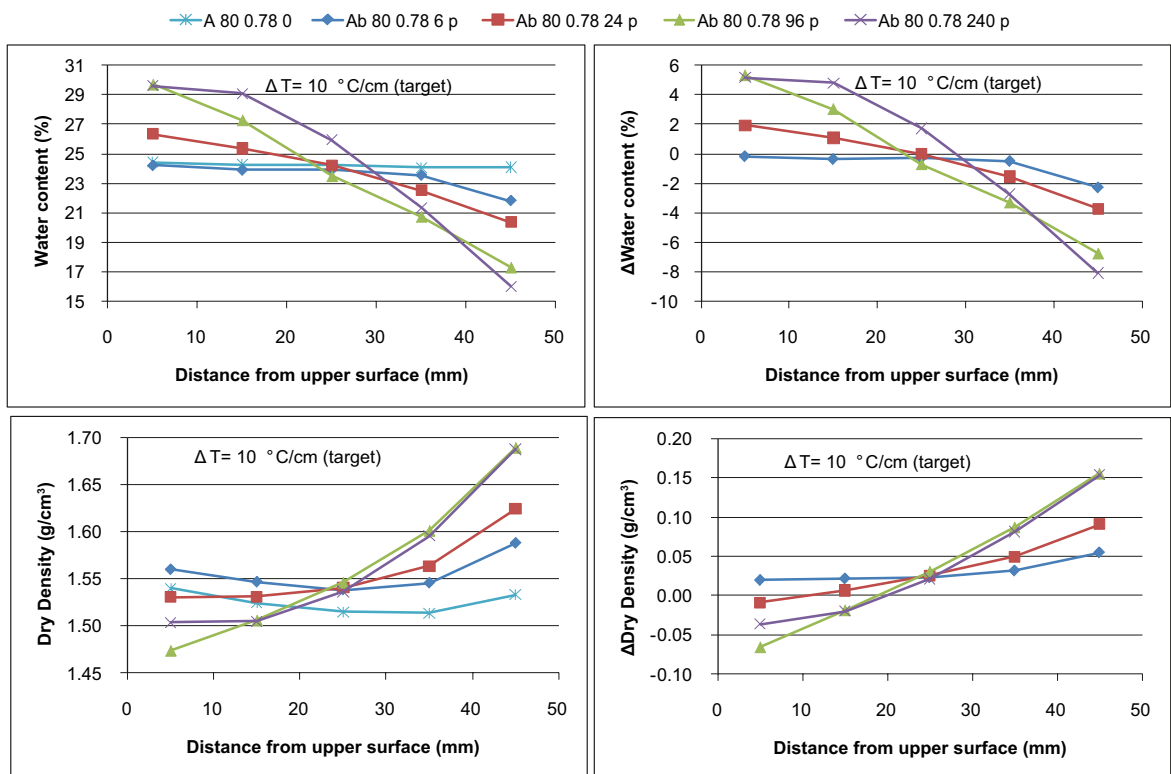**Figure A4-17.** *Results from specimen type Ab 80 0.60.*

Figure A4-18. *Results from specimen type Ab 80 0.78.*

Average values of water content and void ratio, tables

Table A4-1. Final average water contents (%) resulting from tests with 2°C/cm.

Time (h)	$S_r = 50\%$ target e (w (%))			$S_r = 80\%$ target e (w (%))		
	0.6 (10.8)	0.78 (14.0)	1 (18.0)	0.6 (17.3)	0.78 (22.4)	1 (28.8)
0	10.98	13.45		17.29	24.22	
6	10.78	13.97		17.04	23.80	
24	10.96	13.97		16.83	23.79	
96	10.80	13.94		17.18	23.70	
240	10.84	12.66		17.21	24.10	

Table A4-2. Final average water contents (%) resulting from tests with 10°C/cm.

Time (h)	$S_r = 50\%$ target e (w (%))			$S_r = 80\%$ target e (w (%))		
	0.6 (10.8)	0.78 (14.0)	1 (18.0)	0.6 (17.3)	0.78 (22.4)	1 (28.8)
6	10.82	13.42	17.64	16.94	23.46	
24	10.97	13.30	18.42	16.87	23.35	
96	10.82	14.40	19.03	16.98	23.55	
240	11.21	14.10	19.51	16.97	24.18	
480	10.36	14.32	18.20			

Table A4-3. Final average void ratios resulting from tests with 2°C/cm.

Time (h)	$S_r = 50\%$			$S_r = 80\%$		
	e = 0.6	e = 0.78	e = 1	e = 0.6	e = 0.78	e = 1
0	0.64	0.78		0.65	0.82	
6	0.63	0.79		0.63	0.80	
24	0.64	0.78		0.63	0.80	
96	0.63	0.78		0.60	0.79	
240	0.63	0.74		0.60	0.80	

Table A4-4. Final average void ratios resulting from tests with 10°C/cm.

Time (h)	$S_r = 50\%$			$S_r = 80\%$		
	e = 0.6	e = 0.78	e = 1	e = 0.6	e = 0.78	e = 1
6	0.63	0.76	0.93	0.63	0.79	
24	0.63	0.76	0.94	0.62	0.78	
96	0.63	0.75	0.95	0.61	0.78	
240	0.65	0.77	0.96	0.62	0.78	
480	0.63	0.77	0.93			

Reference tests for temperature measurements

In some reference tests the temperature was measured by Pt100 sensors at the end surfaces of the specimens, in addition to the temperature measurements by thermocouples for the regulation. The target of the temperature gradients used was the same as in the test program, i.e. 2°C/cm and 10°C/cm. Specimens with different water contents were used.

Table A4-5. Temperature measurements with Pt100 sensors at the bottom and top of specimens exposed to temperature gradient 2°C/cm.

Test No	average w of specimen	T (bottom)	T (top)	ΔT per cm	T (average)
	%	°C	°C	°C/cm	°C
1	11	37.0	26.7	2.1	31.9
2	11	36.9	26.8	2.0	31.8
3	14	37.5	26.6	2.2	32.0
4	14	37.6	26.6	2.2	32.1
5	17	37.1	26.7	2.1	31.9
6	17	37.2	26.5	2.1	31.9
Average		37.2	26.7	2.1	31.9

Table A4-6. Temperature measurements with Pt100 sensors at the bottom and top of specimens exposed to temperature gradient 10°C/cm.

Test No	w	Pt100 (bottom)	Pt100 (top)	ΔT per cm	T (average)
	%	%	%	°C/cm	°C
7	11	79.8	31.2	9.7	55.5
8	11	79.8	31.2	9.7	55.5
9	17	77.1	32.2	9.0	54.6
10	17	77.0	32.3	8.9	54.6
11	17	76.9	32.2	8.9	54.6
12	18	76.8	33.1	8.7	55.0
13	18	79.3	33.6	9.1	56.4
Average		78.1	32.3	9.2	55.2